Investigation of Asphaltene-Metal Interactions

by

Amit Rudrake

A thesis submitted to the Department of Chemical Engineering

in conformity with the requirements for

the degree of Master of Science (Engineering)

Queen's University

Kingston, Ontario, Canada

February, 2008

Abstract

Asphaltenes are the most polar fraction of petroleum that can precipitate due to changes in pressure, temperature and composition which may be encountered during petroleum production and transportation. The precipitated asphaltenes can subsequently deposit on the surfaces of production/transportation pipelines and clog the pipeline partially or completely. Why asphaltenes deposit on a metal surface remains a poorly understood topic. This thesis investigates asphaltene-metal interactions through physical and chemical characterization of the adsorption behaviour of asphaltenes on metal surfaces.

A relatively novel technique called quartz crystal microbalance (QCM) was employed to study the kinetics of asphaltene adsorption and the data analyzed to estimate the adsorption isotherm. The X-ray photoelectron spectroscopy (XPS) technique was employed to determine the functional groups in bulk asphaltene and adsorbed asphaltene. The asphaltene adsorption experiments on metal surfaces were carried out in toluene medium at dilute concentration ranging 10-1500 ppm. A mathematical model was developed to analyze the XPS data, which was subsequently assessed to estimate the fractional coverage and thickness of adsorbed asphaltene. The isotherms generated from QCM and XPS experiments were compared and analyzed to estimate the free energy.

Three different asphaltene samples were investigated – one sample was derived from Cold Lake bitumen and two others were supplied by DBR-Oilphase (a Schlumberger company) and termed as MD and HO2 asphaltenes. Most extensive experimentations and

analyses were carried out for Cold Lake asphaltenes. The same procedure was applied for the other asphaltene samples. The kinetic analyses of Cold Lake and MD asphaltenes indicated that the adsorption process is diffusion controlled at initial times but follows a first-order kinetic rate law at longer times. MD asphaltenes exhibited higher equilibrium adsorbed amounts than Cold Lake asphaltenes. The XPS spectral analysis for MD and Cold Lake asphaltene revealed presence of carboxylic, thiophenic, thiol, pyridinic and pyrrolic type species. All adsorption isotherms could be described by follows Langmuir (type-I) isotherm. The estimated thickness of adsorbed asphaltene varied between 8 and 12 nm.

Acknowledgements

I would like to express my sincere gratitude to my supervisor Dr. Kunal Karan for his continuous support, criticism, encouragement and invaluable assistance throughout the course of this study. His criticism has always challenged and brought the best out of me. His enthusiasm towards the work, knowledge and friendly nature has inspired and shaped me in different ways.

I would like to thank Dr. Hugh Horton for his extended help in carrying out the experiments, giving me the right direction when needed the most, offering me expertise and insights in the area of surface chemistry and kindly granting access to research instruments in his lab. I would also like to thank Dr. Abdel Kharrat from DBR-Oilphase Schlumberger for valuable technical discussions and supplying the asphaltene samples for performing the experiments.

The financial support from DBR-Oilphase Schlumberger and Natural Science and Engineering Council of Canada (NSERC) is highly acknowledged. I would like to thank faculty members, staff and graduate students in the department of chemical engineering and chemistry for their help throughout my graduate study.

Finally, I wholeheartedly thank my family for their support, confidence and love without which this work would have never been completed.

Table of Contents

Abstract ii

Acknowledgements iv

List of Figures x

List of Tables xiv

Nomenclature xvi

Chapter 1 1

1.1 Introduction 1

1.2 Objectives 5

1.3 Thesis Structure 6

Chapter 2 Literature Review 8

2.1 Petroleum classification 8

2.2 Brief description of Asphaltenes 9

2.2.1 State of asphaltene in petroleum 10

2.2.2 Structure of Asphaltenes 13

2.2.3 Asphaltene molar mass and self-association tendency of asphaltenes 16

2.2.4 Asphaltene size and shape 17

2.3 Adsorption of Asphaltenes 17

2.3.1 Adsorption of asphaltenes on Liquid-Liquid interface 18

2.3.2 Adsorption of asphaltenes on mineral surfaces 19

2.3.3 Adsorption of asphaltenes on metal surface 21

2.3.4 Adsorption of Amphiphilic Molecules on Asphaltene Particles 22
2.4 Characterization of adsorbed asphaltenes and deposits 23
2.5 Summary 26
Chapter 3 Experimental and Theory 27
3.1 Materials and Sample Preparation 27
3.1.1 Materials 27
3.1.2 Asphaltene Extraction 28
3.1.3 Asphaltene Solution Preparation 30
3.1.4 Surface Preparation or pre-cleanup step 31
3.2 QCM Experiment 31
3.2.1 Quartz Crystal Microbalance (QCM) Theory 31
3.2.2 QCM and Flow cell apparatus 35
3.2.3 Experimental Set-up and Procedure 37
3.3 X-Ray photoelectron spectroscopy (XPS) Experiments 39
3.3.1 XPS Theory 39
3.3.2 XPS instrumentation 42
3.3.3 Experimental Protocol 44
3.4 Gold surface characterization by AFM 45
Chapter 4 Results and Discussion 47
4.1 Summary of Experimental Runs 47
4.2 A QCM and XPS Investigation of Cold Lake Asphaltene Adsorption 48
4.2.1 Asphaltene Adsorption Kinetics 49

4.2.2 XPS Spectral Analysis 52
4.2.2.1 Survey Spectra 52
4.2.2.2 Peak intensity data 53
4.2.2.3 Carbon Spectra 54
4.2.2.4 Oxygen Spectra 56
4.2.2.5 Sulfur Spectra 57
4.2.2.6 Nitrogen Spectra 59
4.2.3 Analysis of XPS data for estimation of adsorbed asphaltene surface coverage 60
4.2.4 Adsorption isotherm analysis 63
4.2.5 Investigation of Thickness and Orientation of Adsorbed Asphaltene 68
4.2.6 Summary and further discussion 72
4.3 A QCM and XPS study of MD Asphaltene and Comparison with Cold Lake Asphaltene 73
4.3.1 Adsorption Isotherm 74
4.3.2 XPS Analysis 77
4.3.3 Adsorption isotherm analysis 79
4.3.4 Thickness of adsorbed asphaltene 81
4.3.5 Summary 82
4.4 XPS Study of Heavy Oil 2 (HO2) Asphaltene and Sub-Fraction 82
4.4.1 XPS analysis of heavy oil asphaltene and sub-fraction 83
4.4.1.1 Carbon 1s Spectra 83
4.4.1.2 Oxygen 1s Spectra 85

4.4.1.3 Sulfur 2p Spectra 86
4.4.2 Summary 88
4.5 Asphaltene Adsorption on Stainless Steel Surface 88
4.5.1 Cold Lake asphaltene adsorption kinetics on stainless steel surface 88
4.5.2 XPS Spectral Analysis 90
4.5.2.1 Carbon Spectra 90
4.5.2.2 Oxygen Spectra 92
4.5.2.3 Sulfur Spectra 93
4.5.2.4 Nitrogen Spectra 95
Chapter 5 96
5.1 Conclusions 96
5.2 Recommendations 98
References 100
Appendix A 107
Troubleshooting the base line drift problem of QCM experimental 107
Set-up 107
Base line drift problem of QCM 107
Trouble shooting strategy 110
Investigation of effect of ambient conditions on RQCM electronics 111
Examination of any effect related to reversal of flow line direction on frequency response 113
Static Experiments 114

Examination of effect of O-ring swelling on frequency response 115
Appendix B 118
XPS Peak fit Parameters for Cold Lake asphaltene adsorption on Gold Surface 118
Appendix C 121
Kinetic data for MD Asphaltene Adsorption on Gold Surface 121
Appendix D 124
XPS spectra for MD asphaltene and peak fit parameters 124
Appendix E 130
Peak fit Parameters for Heavy Oil 2 Asphaltene Adsorbed on Gold Surface 130
Appendix F 131
Peak fit parameters for Cold Lake asphaltene on Stainless Steel surface 131

List of Figures

Figure 1.1 Proposed Asphaltene Deposition Mechanism (Karan *et al.,* 2001). 3

Figure 3.1 Schematic representation of experimental procedure for asphaltene extraction. 29

Figure 3.2 The principle of operation of QCM 32

Figure 3.3 Pictures of a standard one-inch QCM sensor crystal 35

Figure 3.4 Cut-out view of QCM probe with flow cell and crystal installed 36

Figure 3.5 QCM experimental setup with flow cell 37

Figure 3.6 High resolution valance band spectra for the gold surface from the spectrometer employed in present study. 42

Figure 3.7 XPS instrumentation (Johnson *et al*., 1998) 43

Figure 3.8 AFM images of cleaned gold sample (blank) employed for XPS and QCM study (2.5 × 2.5 micron) 45

Figure 3.9 The AFM image of control QCM sample at high resolution of 500 nm. 46

Figure 4.1 (a) Asphaltene adsorption kinetics on gold surface. The dotted line presents fit for equation (4.1). (b) Mass of asphaltene adsorbed as a function of square root of time. 50

Figure 4.2 Survey spectra for blank gold surface and C_7 bulk asphaltene 52

Figure 4.3 C 1s XPS spectra for blank sample, adsorbed and bulk asphaltenes on gold surface. The inset graph presents peak fit for the blank sample 54

Figure 4.4 O 1s XPS spectra for blank sample, adsorbed and bulk asphaltenes on gold

surface. The inset graph presents peak fit at 50 PPM 56

Figure 4.5 S 2p XPS spectra for blank sample, adsorbed and bulk asphaltene on gold surface. The inset graph presents peak fit at 50 PPM. 58

Figure 4.6 Nitrogen (N 1s) XPS spectra for bulk asphaltene with peak fitted features. ... 60

Figure 4.7 Schematic depiction of XPS carbon intensity from blank, bulk and adsorbed asphaltene samples on gold surface..... 61

Figure 4.8 Fractional coverage data of absorbed asphaltene estimated by QCM and XPS techniques. The dotted lines represent Langmuir fit. 65

Figure 4.9 Asphaltene nano-aggregate dimensions..... 69

Figure 4.10 The equilibrium mass adsorption data for Cold Lake and MD asphaltenes .. 74

Figure 4.11 The change in resistance with frequency shift for Cold Lake and MD asphaltene at concentration of 1000 ppm 76

Figure 4.12 Fractional coverage data of absorbed MD asphaltene estimated by QCM and XPS techniques. The dotted lines represent Langmuir fit. 80

Figure 4.13 C 1s XPS spectra for C7, F7 and F3 asphaltene adsorbed on gold surface at 500 ppm. The inset table presents the data of peak intensity. 84

Figure 4.14 O 1s XPS spectra for C7, F7 and F3 asphaltene adsorbed on gold surface at 500 PPM. The inset table presents the data of peak intensity. 85

Figure 4.15 S 2p XPS spectra for C7, F7 and F3 asphaltene adsorbed on gold surface at 500 PPM. The inset table presents the data of peak intensity. 87

Figure 4.16 Kinetics of asphaltene adsorption on stainless steel surface..... 89

Figure 4.17 C 1s XPS spectra for Cold Lake asphaltene adsorbed on stainless steel

surface, bulk Cold Lake asphaltene (C7) and blank stainless steel surface. 91

Figure 4.18 O 1s XPS spectra for Cold Lake asphaltene adsorbed and bulk (C7) and blank stainless steel surface and inset graph presents the peak fitted feature at 500 ppm. 92

Figure 4.19 S 2p XPS spectra for blank stainless steel surface, adsorbed Cold Lake and bulk asphaltene sample. The inset graph presents the peak fitted features at 50 ppm 94

Figure A.1 Delta Frequency response for QCM exposed to air followed by toluene [25 ^{o}C; Toluene flow rate in the flow cell of 1 ml/min; gold surface]. 108

Figure A.2 Delta Frequency response for QCM exposed to toluene for three different runs on gold surface. 109

Figure A.3 Delta frequency data for toluene medium and temperature data of room for investigation of any temperature effect on frequency response……..... 111

Figure A.4 Delta frequency data for toluene medium and pressure data of room for investigation of any pressure effect on frequency response. 112

Figure A.5 Delta Frequency response for QCM exposed to toluene after direction of flow reversal 113

Figure A.6 Delta Frequency response for QCM exposed to toluene under static flow conditions. 115

Figure A.7 Delta Frequency responses for QCM exposed to toluene after soaking the flow cell O-ring for a week in toluene 116

Figure C. 1 Kinetic data of MD asphaltene adsorption on Gold surface at 25^{o}C. 121

Figure C.2 Kinetic data of MD asphaltene adsorption fitted to equation 4.1, the dotted line shows the fit 122

Figure D.1 C 1s XPS spectra for blank, adsorbed and bulk MD asphaltene on gold surface 124

Figure D.2 O 1s XPS spectra for blank, adsorbed and bulk MD asphaltene on gold surface 125

Figure D.3 S 2p XPS spectra for blank, adsorbed and bulk MD asphaltene on gold surface 127

List of Tables

Table 3.1 Chemicals and materials used in the experiments 27

Table 3.2 Key auxiliary equipment specifications 38

Table 4.1 The list of experiments performed 48

Table 4.2 Asphaltene adsorption data on gold surface 51

Table 4.3 The peak intensity data for blank, adsorbed and bulk asphaltene Cold Lake sample 53

Table 4.4 Free energy of adsorption from QCM and XPS data 68

Table 4.5 Estimated thickness for Cold Lake asphaltene adsorbed on gold surface 71

Table 4.6 Relative intensity ratio of MD to Cold Lake asphaltene 78

Table 4.7 Free energy of adsorption for MD from QCM and XPS data 81

Table 4.8 Thickness data of adsorbed MD asphaltene on gold surface 81

Table B.1 Peak fitted parameters of C 1s for blank, adsorbed and bulk Cold Lake asphaltene on gold 118

Table B.2 Peak fitted parameters of O 1s for blank, adsorbed and bulk Cold Lake asphaltene on gold 119

Table B.3 Peak fitted parameters of S 2p for blank, adsorbed and bulk Cold Lake asphaltene on gold 120

Table B.4 Peak fitted parameters of N 1s for bulk asphaltene 120

Table C. 1 MD asphaltene adsorption data on gold surface 123

Table D.1 Peak fitted parameters of C 1s for blank, adsorbed and bulk MD asphaltene on

gold surface 127

Table D.2 Peak fitted parameters of O 1s for blank, adsorbed and bulk MD asphaltene on gold surface……128

Table D.3 Peak fitted parameters of S 2p for adsorbed asphaltene on gold..... 129

Table E. 1 Peak fit parameters for adsorbed heavy oil asphaltene and its sub-fraction at 500 ppm on gold surface 130

Table F. 1 Peak fit parameters of Carbon 1s for adsorbed Cold Lake asphaltene, bulk and blank samples on stainless steel surface..... 131

Table F. 2 Peak fit parameters of Oxygen 1s for adsorbed Cold Lake asphaltene, bulk and blank samples on stainless steel surface..... 132

Table F. 3 Peak fit parameters of Sulfur 2p for adsorbed Cold Lake asphaltene, bulk and blank samples on stainless steel surface..... 133

Nomenclature

A	Adsorbate
B	Adsorbent
BE	Binding Energy [eV]
c_0	Adsorbate concentration in the bulk [ppm]
C_A	Bulk concentration of solute in the medium [ppm]
C_{AB},	Surface concentration of adsorbed solute [μg/cm^2]
m_{eq}	Surface concentration of adsorbed solute at equilibrium [μg/cm^2]
C_{BS}	Surface concentration
C_f	Sensitivity factor for the crystal [Hz μg $^{-1}$cm^2]
C_{max}	Maximum surface coverage concentration [μg/cm^2]
C_P	Pressure sensitivity of the QCM crystal [kPa/Hz]
C_S	Concentration of solvent [ppm]
D	Dissipation factor
E	Energy of Photon [eV]
f^E	Equilibrium frequency [Hz]
$f(t)$	Frequency respone with respect to time [Hz]
I_{Ct}	Total C 1s signal intensity from covered and uncovered surface
I_{C1}	C 1s signal intensity from adsorbed asphaltene film of thickness (t)
I_{C2}	C 1s signal intensity from under-layer of uncovered surface

I_{C3}	C 1s signal intensity from under-layer of asphaltene-covered surface
I_{CO}	C 1s signal intensity of blank sample
I_{CBulk}	C 1s signal intensity of bulk asphaltene sample
I_{Gt}	Total Au 4f signal intensity from uncovered and covered surface
I_{G1}	Au 4f signal intensity through adsorbed asphaltene film
I_{G2}	Au 4f signal intensity from the blank sample
K	Adsorption equilibrium constant
KE	Kinetic Energy [eV]
K^{ad}	Rate constant of the adsorption
k_{ads}	Langmuir adsorption rate constant [s^{-1}]
k_B	Boltzmann's constant [1.3807×10^{-23} J/K]
k_{des}	Langmuir desorption rate constant [s^{-1}]
K_{eq}	Adsorption equilibrium constant
K_L	Langmuir equilibrium constant [s^{-1}]
L_D	Decay length [m]
m	mass per unit area [mg/m^2]
Q	Volumetric flow rate [ml/min]
R	Universal gas constant [J/Kmol]
R_m	Motional resistance [ohm]
S	Charging Effect [eV]
T	Temperature [K]
t	Thickness [nm]

t_m	Lag time [min]
h	plank constant (6.62 x 10^{-34} J s)
θ	Surface coverage [degrees]
Φ	Work Function [eV]
τ	Characteristic time [min or s]
μ	Solvent viscosity [Pa-s]
μ_q	Shear modulus of quartz [GPa]
ρ_q	Density of quartz [mg/m^3]
λ	Inelastic mean free path length [nm]
ξ	Time [min]
υ	Frequency of radiation (Hz)
ΔG_{ads}	Energy of adsorption [mJ/m^2]

Chapter 1

Introduction

1.1 Introduction

The non-conventional sources of petroleum such as Oilsands in Alberta and crude oil in deep sea reservoirs are being increasingly explored and exploited as the conventional crude oil reserve continue to deplete. These non-conventional petroleum sources require specialized pre-processing and refining steps to produce useful petroleum fractions. For instance, the high viscosity of heavy oils renders it difficult to be transported and processed. Usually transportation/processing of heavy oils and oil extracted from oil sands undergoes a change in overall composition as a result of addition of diluents to reduce its viscosity. On the other hand, during the production/transportation process a crude oil from deep sea reservoir can undergo changes in temperature, pressure and composition. These changes can cause precipitation of the heaviest fraction of crude oil, called the asphaltenes. The effect of composition change, and by inference, pressure change on asphaltene precipitation is generally believed to be stronger than the effect of temperature (Hammami *et al.*, 2000). Once precipitated, the asphaltenes may deposit on the pipeline surface and other process unit surface and, in adverse situation, can severely clog the pipelines. Therefore, understanding the mechanism of asphaltene deposition is a critical step in combating asphaltene deposition problem.

Asphaltenes are a solubility class of compound, defined as the fraction of petroleum that is insoluble in low molecular weight normal paraffins such as pentane or heptane, but soluble in aromatics such as benzene or toluene (Francisco and Speight, 1984; Institute of Petroleum, 1982). Asphaltene extracted using n-pentane is known as C5-Asphaltene and with n-heptane is known as C7-Asphaltenes. Asphaltenes from different sources may have different physical and chemical characteristics which can be attributed to the nature of the source material and subtle regional variations in maturation conditions serves to differentiate one crude oil (and hence one asphaltene) from another (Speight *et al.,* 1991).

Asphaltene deposition can occur through several sequential and parallel steps including precipitation, flocculation, and transportation of the flocculated asphaltenes to the surface, and finally adhesion of the asphaltenes to the surface, followed by subsequent cohesion of precipitated/flocculated asphlatenes with asphaltene-covered surface. Precipitation of asphaltenes involves the formation of a solid phase or a dense liquid due to a change in thermodynamic equilibrium among the crude oil components. Deposition, on the other hand, involves the attachment or sticking of this solid or dense liquid phase to the surface. The precipitation of asphaltene does not necessarily lead to deposition. Although the precipitation and the deposition represent different process the two terms are used interchangeably in the literature (Karan *et al.*, 2003). A majority of the studies so far have focused on the different aspects of the precipitation and flocculation of asphaltenes. However, asphaltene deposition and, in particular asphaltene-metal interaction remains a poorly understood topic. Only recently have studies focused on asphaltene deposition begun to appear in open literature (Papadimitriou *et al.,* 2007

Shedid *et al.,* 2006; Alboudwarej *et al*., 2005).

The figure 1.1 shows a possible mechanism for asphaltene deposition on pipeline surface.

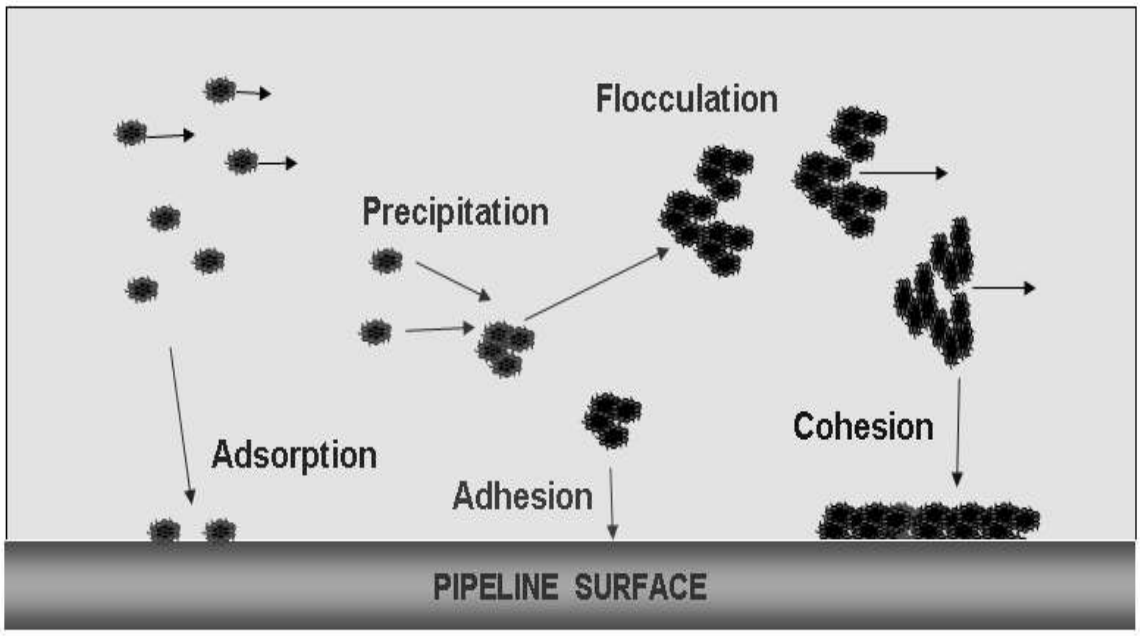

Figure 1.1 Proposed Asphaltene Deposition Mechanism (Karan *et al.,* 2001).

As stated earlier, a change in the process parameters such as temperature, pressure and composition causes the precipitation of asphaltenes. The precipitated asphaltenes, due to attractive forces, can form a bigger floc whereas some particles may be transported and adhere to the pipeline surface. The formation of a layer of precipitated asphaltenes on a bare surface occurs via adhesion and can be called as deposition. The multilayer formation can easily occur by cohesion (attraction between adsorbed/adhered asphaltene and precipitated/flocculated asphaltene). It is also possible that the asphaltene molecules or nano-aggregates (Andreatta *et al.*, 2005) of asphaltenes can attach directly to a surface

via the process of adsorption. However, in reality, the deposition mechanism may be very complicated and many aspects of the process are not well understood.

The question of scientific importance are – why do asphaltenes adhere/deposit to a surface? What types of asphaltene subspecies are responsible for the metal-asphaltene interaction? From the operational point of view, the questions facing the design /operation engineers are - whether asphaltene deposition will occur during the production/transportation? how fast would the deposition occur?, and, what are the best coating material for mitigating the deposition? Conducting deposition experiments under controlled conditions is difficult and extraction of meaningful deposition parameters is even more complicated. On the other hand, the answers to these fundamental questions regarding the asphaltene-metal interaction can be explored via adsorption studies.

Prior studies on asphaltene adsorption can be categorized as one of the following - adsorption on hydrocarbon-water interface, adsorption on non-metallic surfaces and adsorption on metallic surfaces. Adsorption of asphaltenes on liquid-liquid interfaces has been studied by several investigators (Acevedo *et al.*, 1995; Jeribi *et al*., 2002; Ramos *et al*., 2001) to understand the role of asphaltenes in stabilizing the oil-water emulsion. Adsorption of asphaltenes on non-metallic surfaces such as minerals has been extensively studied to investigate the wettability changes of minerals, which affects the fluid permeability within the reservoir porous media (Acevedo *et al*., 2002; Marczewski *et al*., 2002; Ramos *et al*., 2001; Gonzalez *et al*., 1991; Jaroniec and Madey, 1988; Pernyeszi *et al.*, 1998). On the other hand, the adsorption of asphaltenes on metal surfaces has been

studied by only a few investigators (Alboudwarej *et al*., 2005; Ekholm *et al.*, 2002; Xie *et al*., 2005;) with an overall objective of understanding what leads to asphaltene deposition in pipelines. While others limited their investigation of equilibrium behaviour of asphaltenes obtained from one petroleum source only, Alboudwarej *et al*., 2005 studied the equilibrium behaviour for adsorption of two different kinds of asphaltenes (different sources) on metal surfaces. It is generally accepted that the asphaltenes obtained from different petroleum sources may exhibit different behavior.

Furthermore, there has been very little work done in characterizing the chemical nature of species interacting with the metal surfaces. Identifying what functional groups are responsible for asphaltene affinity for metals can help find suitable surfactant or pre-coating material to mitigate the asphaltene deposition problem. In a very recent study (Abdallah *et al*., 2007), XPS (X-Ray photoelectron spectroscopy) was employed to characterize the functional groups of adsorbed asphaltene. The functional groups found were carboxylic, thiophenic, pyridinic, pyrrolic type. However, the study focuses on asphaltene obtained from one source and does not explore the effect of change in concentration.

1.2 Objectives

The broader objective is to investigate the asphaltene-metal interaction and, in particular, to study the kinetic and equilibrium behavior of asphaltene adsorption as well as the nature of interacting chemical species. The specific objectives are divided into the

following tasks:

- Measurement of the asphaltene adsorption kinetics on gold and stainless steel surface using QCM (Quartz crystal microbalance)
- Determination of asphaltene adsorption isotherm and free energy of adsorption.
- Physical characterization of adsorbed asphaltenes in terms of the estimation and comparison of fractional coverage and thickness of adsorbed asphaltene using QCM and XPS analyses
- Chemical characterization of asphaltenes (obtained from different sources) by XPS in terms of the type of carbon, oxygen, sulfur, and nitrogen functional groups.

1.3 Thesis Structure

In this section, a brief description of the thesis structure is presented wherein the key points covered in each chapter is described.

Chapter 2 presents the literature review on the various relevant topics covered in this study. These include summary of current understanding of petroleum classification and structure, molar mass, and self-association of asphaltenes. A review of prior literature on the topics of direct relevance to the experimental work conducted in this study, i.e. asphaltene adsorption and chemical/physical characterization of asphaltenes and asphaltenic deposits, is presented in detail.

In chapter 3, the experimental protocol and the theory relevant to the methods employed in this study is presented. The materials and sample preparation methods (i.e asphaltene extraction, solution preparation and pre-clean up step of metal surface) is first presented. The theory, instrumentation and protocol for QCM and XPS experimentations are presented in details.

Chapter 4 focuses on the analysis of experimental data and discussion of results. Results for experiments carried out with asphaltenes from three different sources – asphaltene derived from Cold Lake Bitumen and two asphaltene samples (called MD and HO2) supplied by Schlumberger (Edmonton, Canada) – is discussed. The most extensive experimentation was carried out with Cold Lake asphaltene and allowed for the improvement of experimental protocol and the development of the method for data analysis. A mathematical model developed based on XPS data to estimate the fractional coverage and thickness of adsorbed asphaltene is discussed. Adsorption isotherms generated from QCM and XPS data are also compared. The QCM and XPS results obtained for MD asphaltene are discussed. Finally the MD asphaltene results were compared with Cold Lake asphaltene and analyzed. Finally, the XPS experiments on Heavy oil 2 and its sub-fraction sample are discussed.

Chapter 5 presents conclusions of the study and recommendation for future work.

Chapter 2

Literature Review

This chapter presents a brief review on petroleum classification and physical/ chemical characterization of asphaltenes. A review of literature on asphaltene adsorption, which is a topic central to this thesis, is presented in detail. Asphaltene adsorption on different interfaces such as gas-liquid, liquid-liquid, liquid-solid is discussed. Finally, a review on the characterization of functional groups of adsorbed asphaltenes using X-Ray Photoelectron Spectroscopy (XPS) is presented.

2.1 Petroleum classification

Petroleum or crude oil is a complex mixture of hydrocarbon, hetero-atoms such as sulphur, oxygen and nitrogen as well as compounds containing metallic constituents particularly vanadium, nickel, iron and copper (Speight *et al*., 1991). The complexity of petroleum further increases due to the fact that its composition can vary not only with the location and the age of oil field but also with the depth of individual wells (Speight *et al*., 1991). Since petroleum comprises hundreds of molecular species, a simpler means of describing petroleum is in terms of four major fractions (based on their solubility and polarity) - *s*aturates, *a*romatics, *r*esins and *a*sphaltenes; know as SARA fractions (Speight *et al*., 1991). Of the four fractions, saturates can readily be differentiated from other fractions by virtue of the difference in their polarity due to an absence of π bonds. The

remainder of the oil is composed of aromatics and heteroatomic compounds of varying degree of condensation, alkyl substitution and functionalism, which constitute a compositional continuum with respect to molecular weight and polarity (Altgelt *et al*., 1994). Based on this classification method, asphaltenes are the heaviest and most polar fraction of petroleum. The asphaltenes and resins have similar molecular structure but as a result of solubility based fractionation scheme employed, resins are less polar, less aromatic and have lower molar mass than asphaltenes.

2.2 Brief description of Asphaltenes

As a solubility class compound, asphaltenes are most commonly defined as the fraction of petroleum that is insoluble in low molecular weight paraffins but soluble in aromatics such as Toluene or Benzene. It has been argued that asphaltenes extracted using *n*-heptane as a precipitant (known as C7-Asphaltenes) are "real" asphaltenes and those extracted using pentane (know as C5-Asphaltenes) are composed of both asphaltenes and resins (Speight *et al*., 1991). The molecular weight, polarity and aromaticity of precipitated asphaltenes generally increase with an increase in carbon number of *n*-alkane precipitant. The amount of precipitant (paraffin) required to initiate the precipitation process increases with increase in carbon number of *n*-alkane. On the other hand, the amount of asphaltene extracted upon the addition of excess precipitant (paraffin) has been found to decrease with an increase in carbon number of *n*-alkane and with temperature (Fuhr *et al*., 1991).

The elemental composition of 57 different asphaltenes from 8 countries was reported by

Speight (1991). He found that carbon and hydrogen contents of asphaltenes do not vary significantly, however, the proportion of hetero-elements, such as oxygen, sulfur and nitrogen, varies significantly - from 0.3 to 4.9% for oxygen; from 0.3 to 10.3% for sulfur; from 0.6 to 3.3% for nitrogen. This observation suggests that the variation of hetero-element content may be the main contributor to the differences in the behavior of asphaltenes. Asphaltenes usually appear brown to black in color and have no definite melting point but decomposes when the temperature exceeds 300-400 °C (Bunger *et al*., 1981).

As the composition of petroleum can vary from one source (location of oil field) to another source, within the source (with the depth in a reservoir) and with time, the asphaltene content in petroleum also varies from 0 to 20 % (Leon *et al*., 1999). Generally, a crude oil with significant amount of asphaltene content do not exhibit any asphaltene related problem (deposition, oil-water emulsion stabilization, wettability changes of minerals) whereas severe asphaltene related problems have been reported for petroleum with low asphaltene content of ~0.2 to 2% (Boer *et al*., 1995). The asphaltenes can cause problems when they become unstable in petroleum and start to precipitate. The stability of asphaltenes is critical and depends not only on the properties of asphaltene but also on how good a solvent the balance of oil is for its asphaltene.

2.2.1 State of asphaltene in petroleum

The state of asphaltene in a petroleum fluid continues to be a topic of debate. This is due mainly to the complex nature of asphaltenes being defined as a solubility class

compounds rather than a pure component. The view that asphaltenes are colloidal system whose dispersion phase is composed of asphaltenes and resins was held for a long time since the original proposition by Nellensteyn *et al*. (1938) and Pfeiffer *et al*., (1940). According to this view, the asphaltene particles are stabilized by resins adsorbed on asphaltene surface (see Figure 2.1). In fact, Koots *et al*., (1998) have pointed out that structural similarities in the asphaltenes and resins facilitated formation of micelles and, consequently stabilization of asphaltenes by resins. It has been thought that the nature and content of asphaltenes together with the nature and content of dispersion medium are the main factors that determine the relative stability of crude oils and related materials (Buckley *et al*., 1996).

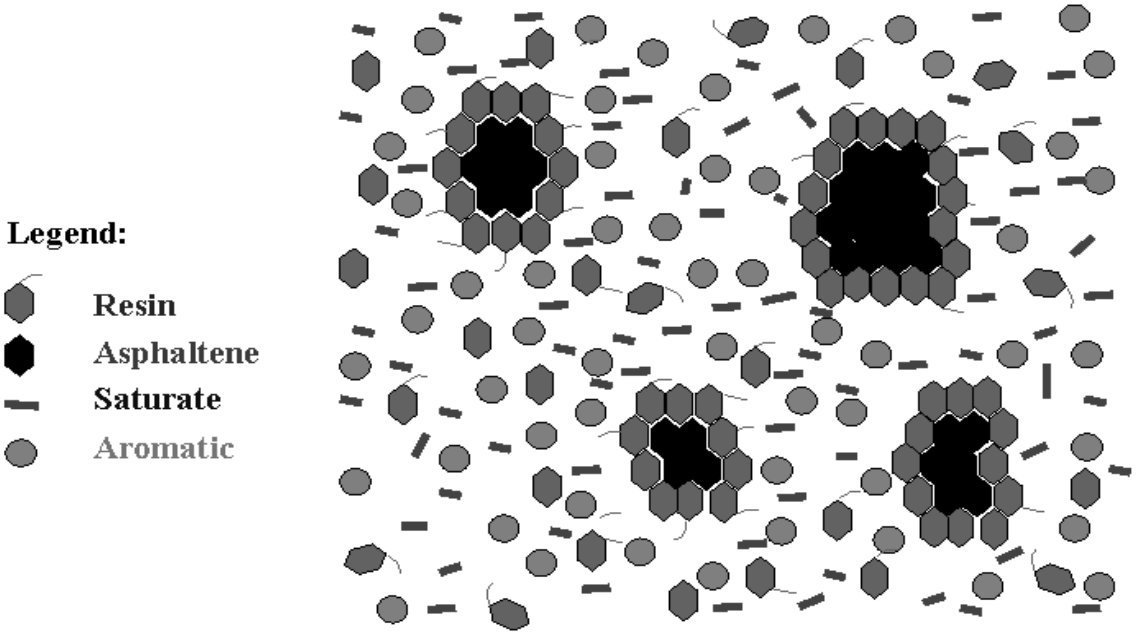

Figure 2.2 Colloidal model of petroleum (adapted from Pfeiffer and Saal)

Leon (1999), based on flocculation onset measurements, found that the composition of the dispersion medium does not play a key role in the asphaltene stability of crude oil. Recently, Ekholm *et al* (2002) studied the interaction between adsorbed asphaltene and resin dissolved in Toluene. They found that resins do not desorb pre-adsorbed asphaltenes from the surface, neither do they adsorb onto the asphaltene adsorbed on the surface. This result contradicts the theory of stabilization effect of resins on asphaltenes. On the contrary, Alboudwarej *et al.* (2005) studied adsorption of asphaltene, resins and asphaltene-resin mixture from their solutions in Toluene. They found a trend of increasing mass saturation adsorption in the order of resins to asphaltene-resin mixture to asphaltenes. They explained the results by suggesting that resins, when co-existing in a liquid mixture, reduce the extent of asphaltene self-association. Consequently, the average molar mass of the asphaltenes are lower and, as such, the mass saturation adsorption level is also lower compared to that for solution containing only asphaltene.

The asphaltenes are also being considered to exist as physically solvated entity (solute) in the oil (solvent). The solubility of the heaviest fraction of a crude oil, the asphaltenes, depends on a delicate balance between this fraction and the lighter fractions of the crude oil. Any unfavourable disturbance, i.e. a change in the thermodynamic conditions of temperature, pressure and composition can cause the precipitation of asphaltenes. A reversal can be attained by taking the system back to the original thermodynamic state. As a result, the asphaltene precipitation is considered to be a thermodynamically reversible process (Hirschberg *et al.*, 1984; Kawanaka *et al.*, 1991).

2.2.2 Structure of Asphaltenes

Due to the complexity of asphaltene molecules, finding the exact structure of asphaltenes has proven to be a daunting task. Numerous techniques has been used to investigate the structure of asphaltenes using physical methods that include infrared spectroscopy (IR), nuclear magnetic resonance (NMR), electron spin resonance (ESR), mass spectroscopy, X-ray, ultra-centrifugation, electron microscopy, small angle neutron scattering, small angle X-ray scattering, quasi-elastic light scattering spectroscopy, vapour pressure osmometry (VPO) and gel permeation chromatography (GPC) as discussed by Auflem *et al*., (2002). Chemical methods involve oxidation and hydrogenation of asphaltenes. Naske *et al*., (2002). Although the complete structure of asphaltene has not yet been completely revealed, some common features have been established. Asphaltenes are now believed to consist of condensed aromatic nuclei that carry alkyl and alicyclic systems with hetero elements (i.e., nitrogen, oxygen and sulfur) scattered throughout in various, including hetrocyclic locations (Speight *et al*., 1991). The aromatic carbon content of asphaltenes is typically in the range of 40 to 60 %, with a corresponding H/C atomic ratio of 1.0-1.2. A large percentage of these aromatic carbon rings are interconnected in the molecular structure and, consequently, the asphaltene molecule appears flat or planar (Auflem *et al*., 2002).

The NMR results indicate that the average number of rings in a single fused ring system is around 7 (Calemma *et al*., 1995). A technique called ruthenium-ion-catalysed oxidation (RICO) was applied by Strausz *et al.* (1992) to probe the structure of

asphaltenes. It was shown that the extent of aromatic condensation is low and that highly condensed pericyclic aromatic structures are present in very low concentrations. In a recent study (Groenzin *et al*., 2000), fluorescence depolarization technique was applied to survey the molecular size of a broad range of asphaltenes and related compounds. It was found that, the variability in asphaltene molecules is huge, some with nitrogen, others with sulfur, some with a big ring system, others with a small ring system, an occasional molecule with a metal, a porphyrin, etc. At the risk of oversimplifying, three idealized asphaltene structures were proposed. These three structures are presented in figure 2.2.

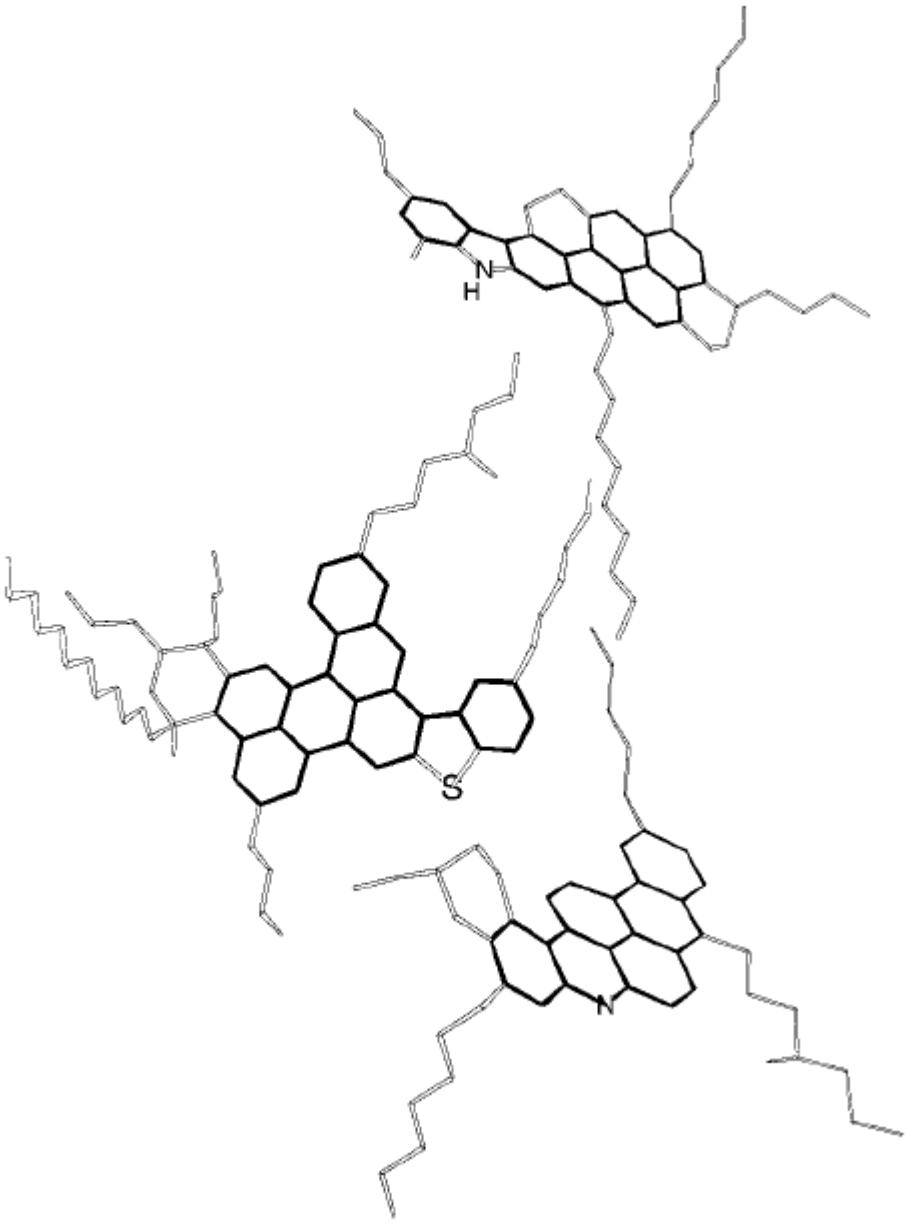

Figure 2.2 Idealized molecular structures for three asphaltenes consistent with overall molecular size, aromatic ring systems, and chemical speciation. The aromatic rings are shown with darker lines (Groenzin *et al*., 2000)

2.2.3 Asphaltene molar mass and self-association tendency of asphaltenes

The molar mass of asphaltenes has been a topic of continued controversy mainly due to its tendency to aggregate or associate even at low concentration. Knowing the molar mass of asphaltene is important, in particular, because it offers an insight into the size of the molecule. The molar mass of asphaltenes has been measured by various techniques such as vapour pressure osmometry (VPO), mass spectrometry (MS), size exclusion chromatography (SEC), and scattering phenomena such as small angle X-ray (SAXS), small angle neutron scattering (SANS). Molecular mass determined by light scattering methods (SAXS, SANS) and fluorescence depolarization technique differ by as much as factor of 10 or more. It has been understood that many of these techniques have measured molar mass of aggregated asphaltenes or micelles than a single asphaltene molecule. Also, it is recognized that the molar mass of asphaltenes depends on the technique and experimental condition (time, concentration and temperature) employed for the measurement.

Size exclusion chromatography has yielded average molecular weights as high as 10,000 amu (Andersen *et al*., 1991). In another study (Miller *et al*., 1998), laser desorption mass spectroscopic results yielded asphaltene molecular weights of 400 amu with a range of roughly 200-600 amu. Fluorescence depolarization measurements indicated the molecular weights of 750 amu with a range of roughly 500-1000 amu (Groenzin *et al*., 2000).

Micellization of asphaltenes in solutions was investigated using micro calorimetric titration procedure (Andersen *et al*., 2000) and the critical micelle concentrations (CMCs) were found to fall within a very narrow range of 3.2–4.9 g/L. A new term critical

nanoaggregate concentration (CNAC) was introduced (Andreatta *et al*., 2005); asphaltene CNACs in toluene occur at roughly 0.1 g/L although the exact concentration depends on specific (crude oil) asphaltene. Asphaltene aggregation has been observed in toluene at a concentration of 50 mg/L (Acevedo *et al*., 1998). Size of aggregates formed were found to increase with solute concentration is solution.

2.2.4 Asphaltene size and shape

The asphaltene particle size and shape varies widely in literature. Ravey et al. (1988) reported that the diameter of disk-like asphaltene entities in tetrahydrofuran for safanya asphaltene fractions is about 13 nm. Rajagopal and Silva (2004) measured the spherical particle size of asphaltenes in toluene by light scattering method and estimated it to be 23 nm even at very low concentration of about 1ppm. The freeze-fracture-transmission-electron-microscopy (FFTEM) technique was employed to study the asphaltene particle diameter in toluene medium and was found to be in the range of 7-9 nm (Acevedo *et al*., 2004). Thus, the survey of the literature indicates that the asphaltene particle diameter varies between 7 and 23 nm. The variation in data is attributed to the difference in solvents, techniques and concentration range employed. The variety of shape of asphaltene has been proposed including thin-disk, spherical, fractal-like, oblate ellpsoid, prolate and discoid (Ravey *et al*., 1998; Acevedo *et al*., 2004; Sirota *et al*., 2005).

2.3 Adsorption of Asphaltenes

Although the focus of this thesis is on studying the adsorption of asphaltenes on metal

surfaces, a review of literature on asphaltene adsorption on various substrates or interfaces is presented. The literature review is presented in three separate sub-sections depending on the adsorbent type: (a) Adsorption of asphaltenes on liquid-liquid and air-liquid interfaces (b) Adsorption of asphaltenes on minerals (c) Adsorption of asphaltenes on metal surfaces. A review on adsorption of amphiphilic molecules on asphaltenes is also discussed.

2.3.1 Adsorption of asphaltenes on Liquid-Liquid interface

The adsorption of asphaltene on oil-water interface leading to emulsion stabilization is a very serious problem encountered in the petroleum industry. The oil-water emulsion may be formed during oil production by natural or artificial contact with water or during spillage in natural waters such as seas, lakes, and rivers (Acevedo *et al*., 2005). Adsorption of asphaltene at the water-oil interface results in a film of elastic or viscous properties which acts as a barrier for the separation of oil and water.

The most common problems encountered are environmental damage, corrosion in the pipelines and therefore, increasing the cost of transportation and refining. Development of strategies to combat emulsion stabilization problems requires deep understanding of the mechanism of adsorption.

The adsorption of asphaltenes at water-toluene interface was studied using ring-detachment and pendant drop method by Acevedo *et al.* (2005). The plot of measured interfacial tension versus concentration indicated features typically observed for stepwise

adsorption isotherm but was attributed to the formation of asphaltene aggregate in the solution. Measurements were reported for asphaltene concentrations ranging 0-4000 ppm. Jeribi *et al*. (2002) studied adsorption kinetics of asphaltenes at oil-water interfaces, the initial diffusion step towards the interface was found to be rapid, followed by a long reorganization and by the progressive building of multilayer. The reorganization process was faster at oil-water interface when compared with that at air-oil interface. Although the above studies indicated multilayer adsorption isotherm, some researchers have reported monolayer adsorption isotherm. Sztukowski *et al*., (2003) studied the adsorption isotherm for oil-water interface using drop volume tensiometer. The results indicated that asphaltenes forms a monolayer on the interface even at concentration as high as 40,000 ppm; the equilibrium adsorption amounts were in the range of 2-10 mg/m^2. The estimated thickness of monolayer ranges from 2 to 9 nm. In another study from the same group (Gafonova *et al*., 2001), the equilibrium adsorption amounts of asphaltene at oil-water interface was found to be in the range of 2-12 mg/m^2 up to concentrations of 45,000 ppm.

2.3.2 Adsorption of asphaltenes on mineral surfaces

The reservoirs of crude oil are found underneath in rock formations. Asphaltenes get adsorbed on minerals and rocks causing a well known problem of wettability change (from water-wet to oil-wet) of minerals, affecting the fluid permeability within the reservoir rocks (Acevedo *et al*., 1999). Several investigators have studied adsorption of asphaltenes on mineral surfaces such as kaolin, alumina, dolomite, calcite, and Berea sandstone. The adsorption kinetics of asphaltene on silica interface was studied by

Acevedo *et al.* (2002) using spectroscopy technique for a concentration range of 5-3000 mg/L. The kinetic results were adjusted to irreversible second-order adsorption kinetics, where adsorption rate constant, *k,* was strongly dependent on concentration. The stepwise trends were observed for adsorption isotherms of asphaltenes which were related to aggregation state of asphaltenes. Adsorption of asphaltenes on glass and silica surface was studied using photo thermal surface deformation spectroscopy and spectroscopy technique respectively (Acevedo *et al*., 1998, 2000). A stepwise or multilayer adsorption isotherm was obtained. On the other hand, Langmuir type adsorption isotherm was observed (Gonzalez *et al*., 1991) with maximum adsorption amounts of 1-4 mg/m^2.

Interestingly, Marczewski *et al*. (2002) studied adsorption of asphaltenes on soils arguing it to be one of the important problems, though largely underestimated, in environment protection of Lublin region. The adsorption study for different kinds of soil involved using spectroscopy technique wherein the asphaltene content of solution before and after adsorption was measured. The adsorption isotherms were found to have Freundlich characteristics with slope coefficients or/and inflections characteristics for lateral interactions, as well multiple steps that may be related to surface phase reorientation, multilayer formation or hemi-micelle formation.

In a recent study, Lopez-Linares *et al* (2006) reported adsorption of Quinolin-65 and Violanthrone-79 as model molecules to simulate the adsorption behavior of the C7-Athabasca asphaltene from toluene solution over macro porous solid surfaces such as

Kaolin. Thermodynamic and kinetic experiments were carried out using chromatography and spectroscopy techniques and Kaolin as an adsorbent, and the results indicated the adsorption was governed by the presence of aromatic framework, hetroatoms such as N, O, and to lesser extent S and a minor dependence on molecular weight.

2.3.3 Adsorption of asphaltenes on metal surface

The adsorption of asphaltenes on metal surface is the main focus of the study undertaken in this thesis. The adsorption of asphaltenes has direct relevance to the well known asphaltene deposition problem. However there have been very limited studies of asphaltene adsorption on metal surfaces. The adsorption isotherm for Athabasca and Cold Lake C7-Asphaltenes on stainless steel, iron, and aluminium was investigated by Alboudwarej (2003) using UV-Spectroscopy. The effects of resins, temperature and *n*-heptane to toluene ratio were also examined. The adsorption of asphaltenes and resins in toluene followed Langmuir type isotherm. The saturation adsorptions of the asphaltenes on metals (0.25-2.7 mg/m^2) were of the same order of magnitude as the adsorption of asphaltenes on minerals. However the saturation adsorptions were less than the monolayer surface coverage observed on water-in-hydrocarbon emulsion interfaces (2-12 mg/m^2), indicating that there are a limited number of adsorption sites on the metals. In another study (Ekholm *et al*., 2002), the adsorption of asphaltenes and resins on gold surface was studied using quartz crystal microbalance with dissipation measurement (QCM-D). In toluene, the adsorption amount of asphaltenes was found to be 0.2 to 8.2 mg/m^2 for concentration range of 50-10000 ppm. The amounts of adsorbed asphaltenes

were larger than that observed for resins (0.2 – 2.3 mg/m^2). The adsorbed amount is also higher than those observed for typical non-associating polymers, indicating aggregate adsorption. The comparison of above studies indicate significant difference in adsorption amount, however one need to note that concentration range, asphaltene type and metal surface are different.

In a previous study from our laboratory (Xie, 2006 and Xie and Karan, 2005), asphaltene adsorption from toluene, toluene-heptane and toluene-pentane solutions were investigated using a quartz crystal microbalance in a flow-cell system. The adsorption isotherm analysis of asphaltene in toluene followed Langmuir adsorption isotherm with saturation amounts of 4-10 mg/m^2. For toluene-heptane and toluene-pentane solutions, the kinetics of adsorption was slow and equilibrium adsorption levels were not achieved even after 700 min. Asymptotic analyses indicated that initial adsorption process is controlled by the diffusion of asphaltenes from the bulk solution to the adsorption surface. A thermodynamic framework to describe asphaltene adsorption on metal surfaces in terms of Lifshitz-van der Waal (LW) and acid-base (AB) free energy interactions was proposed. The LW and AB components of the surface tension parameters of asphaltenes and metal surfaces were determined from contact angle measurements. It was predicted that asphaltenes will adsorb preferentially in the following order Au > SS > Al.

2.3.4 Adsorption of Amphiphilic Molecules on Asphaltene Particles

One of the proposed remedies to mitigate asphaltene deposition problem is the use of amphiphiles (surfactant), they stabilize and /or solubilize asphaltenes in oil. This

stabilizing effect of amphiphiles on asphaltenes depends on the ability of amphiphiles to get adsorbed on asphaltene surface. Since the chemical composition of oil around the world varies significantly, (and hence asphaltenes) choice of additive is important criterion.

The adsorption of amphiphilic molecules on asphaltene particles was studied by Ostlund *et al*., (2004) using spectroscopy technique. The adsorbed amount of amphiphilic molecules was in the range of $0–2\times10^{-4}$ mol/g of asphaltenes. Furthermore, the amphiphilic molecules containing acidic functional groups appear to be a good choice, if the stability of asphaltene molecules to be achieved. In another study (Leon *et al*., 1999), adsorption isotherms of alkylbenzene-derived amphiphiles were determined experimentally and correlated with their activity as stabilizers of asphaltenes. The isotherms of these amphiphiles indicate an adsorption process in two steps: in the first step, the amphiphiles are adsorbed by the interactions with the surface of the asphaltene particles; in the second step, the interactions between adsorbed amphiphiles become predominant and the formation of aggregates on the surface begins. The adsorbed amounts were in the range of 0–0.007mol/g of asphaltenes.

2.4 Characterization of adsorbed asphaltenes and deposits

Although adsorption isotherm and kinetics of asphaltene adsorption are important steps in the understanding of the deposition mechanism, it is equally important to characterize the species/functional groups of adsorbed asphaltene and asphaltenes. It is believed that the interfacial activity and ability to create surface charge at the interface is a consequence of

the presence of functional groups in the asphaltene molecule (Marczewski *et al*., 2002). Therefore, it can be proposed that functional groups/species of adsorbed asphaltenes play a critical role in changing the surface characteristics from hydrophilic to hydrophobic.

In a very recent study (Abdallah *et al*., 2007), X-ray photoelectron spectroscopy (XPS) was used to characterize a single layer of adsorbed asphaltene on a stainless steel surface. The deposits were generated by immersing a stainless steel disc into a dilute asphaltene solution (100 ppm) made of either toluene or dichloromethane as the solvent. The toluene solution allowed for a better control of the adsorbed asphaltene layer and less atmospheric oxygen contamination. The analyses of asphaltene layer for C 1s, S 2p3/2, N 1s and O 1s photoemission peaks indicated the presence of different types of functional groups including carboxylic, pyrrolic, pyridininc, thiophenic and sulfite, with slight differences in their binding energies.

In another study (Ostlund *et al*., 2004), the functional groups of fractionated asphaltene were characterized. Distinct differences in the content of certain functional groups were observed between two asphaltene sub-fractions. The sub-fractions that contained the smallest and least aromatic asphaltenes was found to contain a high concentration of carboxylic carbons, while the sub-fraction that consisted of the largest, most aromatic and highly unstable asphaltenes did not. However it may be worth to note here that only functional groups from carbon (C 1s) peak were analyzed for two different asphaltene sub-fractions.

In a very interesting study, Cosultchi *et al*. (2003) analyzed the organic deposits adhering

to the internal surface of the tubing wall (stainless steel) of an oilwell by means of X-ray photoelectron spectroscopy, X-Ray diffraction and atomic absorption spectroscopy. The high resolution spectra of C 1s indicated presence of C-C bonds as in hydrocarbon like species and Fe bonded to carbonyl groups and organic polymer species at 288.2 and 285.9 eV respectively. The high resolution spectra of O 1s showed presence of iron and aluminium oxide, whereas for Nitrogen (N 1s) aromatic amines, cyclic amines, aminobenzene sulphonic compounds (which was used as corrosion inhibitor). The S 2p core level spectra indicated organic sulphides, $BaSO_4$ (a mineral normally used in the drilling mud composition) and iron oxides. This indicates that the deposits adhered to the steel surface is structurally formed by two inhomogeneous layers and their compositions are result of a complex process of interaction of organic and mineral compounds as well as steel corrosion products.

Fourier transform infrared spectroscopy (FTIR) and X-ray absorption spectroscopy (XAS) were used (Bantignies *et al*., 1998) to characterize the absorption phenomenon of asphaltenes on kaolinite, at the microscopic level, in the presence and absence of water. When kaolinite is wetted by asphaltenes in the presence of water, infrared spectroscopy results show that the OH surface of the kaolinite is sensitive to contact with asphaltenes. The XAS results indicate that OH are linked to aluminum atoms in the kaolinite, on the other hand, the Si environment of the kaolinite remains insensitive to the contact (Si atoms are not linked to OH groups). Furthermore, only the grain surfaces containing Al–OH linkages are sensitive to asphaltene contact. Only these sheets generate preferential

specific interaction with asphaltenes.

2.5 Summary

From the review of literature, it can be summarized that although carbon and hydrogen are main constituents of asphaltenes, the structure and composition of asphaltene varies from one source to another. Although several studies have investigated asphaltene adsorption on oil-water interface and on mineral surfaces, studies on asphaltene adsorption on metal surfaces is limited and the nature of asphaltene-metal interaction is not fully understood. Furthermore, chemical speciation of adsorbed asphaltenes on metal surfaces has not been fully investigated, as well the energy of interaction is not known.

Chapter 3

Experimental and Theory

This chapter describes experimental techniques employed and their underlying theory. A detailed description of material and sample preparation involving asphaltene extraction and solution preparation is first presented. Next, the QCM theory, experimental set up and protocols is described. Similarly XPS theory, instrumentation and protocols are discussed. Relevant theory/instrumentation and protocols for QCM and XPS experiments are described.

3.1 Materials and Sample Preparation

3.1.1 Materials

The major chemicals and materials used in this study are listed in Table 3.1

Table 3.1 Chemicals and materials used in the experiments

Material	Source	Purpose	Grade
Toluene	Fisher Scientific Inc., Canada	Adsorbent Cleaning	Certified A.C.S
Toluene-Extra Dry	Fisher Scientific Inc., Canada	Solvent	
n-Heptane	Fisher Scientific Inc., Canada	Precipitant	Reagent
Bitumen	Imperial Oil Resources Limited, Canada	For extraction of asphaltenes	n/a
MD Asphaltene	DBR Oilphase, Schlumberger, Canada	Adsorbate- Sample	n/a

HO2-C_7 Asphaltene	DBR Oilphase, Schlumberger, Canada	Adsorbate- Sample	n/a
HO2-C_6 Asphaltene	DBR Oilphase, Schlumberger, Canada	Adsorbate- Sample	n/a
HO2-F_7 Asphaltene	DBR Oilphase, Schlumberger, Canada	Adsorbate- Sample	n/a
HO2-F_3 Asphaltene	DBR Oilphase, Schlumberger, Canada	Adsorbate- Sample	n/a
Deionized Water	Chem. Eng. Department, Queens University	Adsorbent Cleaning	n/a
Hellmanex® II	HELLMA GmbH & Co. KG	Adsorbent Cleaning	n/a
Anhydrous Ethyl Alcohol	Commercial Alcohols Inc.	Adsorbent Cleaning	n/a
Compressed Nitrogen	Praxair Canada Inc.	Blow dry the adsorbent	>99%
Gold on Mica	George Albert, Germany	Adsorbent-XPS Measurement	n/a
Gold Coated Quartz Crystal	Maxtek, Inc., USA	Adsorbent-QCM Measurement	n/a
304 SS Coated Quartz Crystal	Tangidyne, Corp, USA	Adsorbent-QCM + XPS Measurement	n/a

3.1.2 Asphaltene Extraction

The asphaltene samples from different sources were explored in this study. The specific asphaltene samples were – (i) Cold Lake asphaltenes that were obtained by in-house extraction from Cold Lake Bitumen and.(ii) MD asphaltene and Heavy Oil 2 (HO2) asphaltenes supplied by DBR Oilphase.

The Cold Lake asphaltenes sample was derived from bitumen sample supplied by Imperial Oil Resources Ltd, Calgary, Canada. The bitumen sample was processed by Imperial Oil to be dewatered and inorganic-free. For asphaltene extraction, reagent grade heptane procured from Fisher Scientific Company was used. The asphaltene extraction

procedure is summarized in figure 3.1.

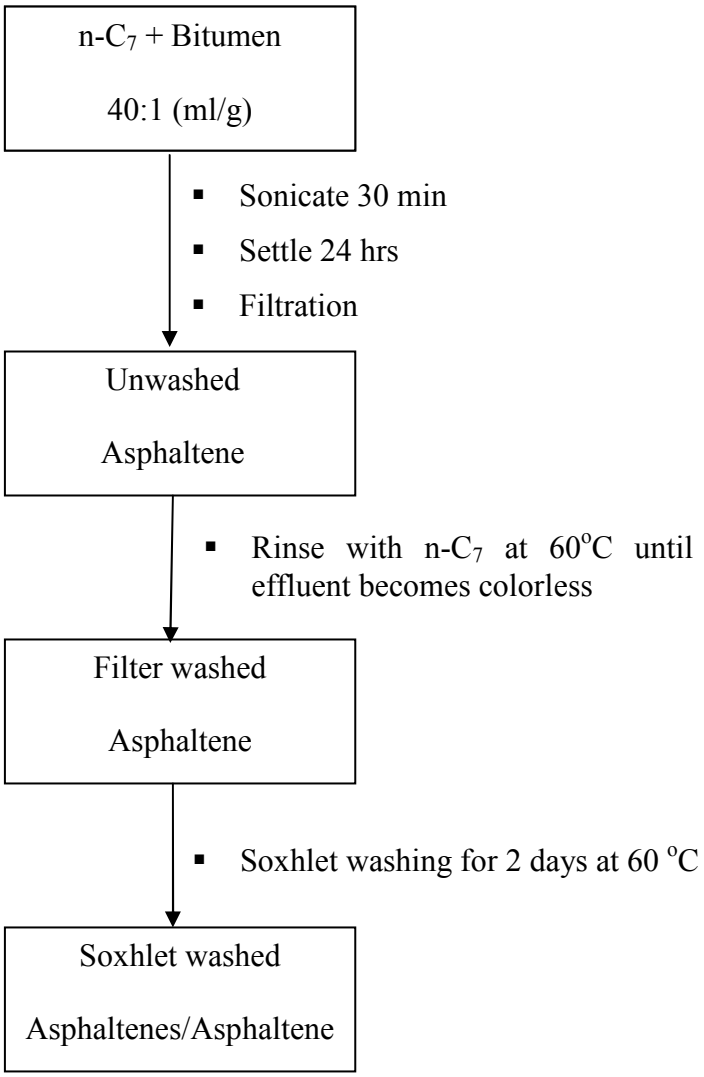

Figure 3.1 Schematic representation of experimental procedure for asphaltene extraction.

First, a known amount of bitumen was mixed with n-heptane at 1:40 ml/gm ratio. After 30 minutes sonication, the mixture is allowed to equilibrate with occasional shaking for 24 hours in the dark. This is followed by filtration under vacuum using 0.2μm white Nylon filter paper (MILLIPORE Corporation GNWP04700). Asphaltenes obtained at this stage are called unwashed asphaltenes. The filtered material, predominantly asphaltenes, was further rinsed with hot n-heptane (heated to 60 ^{o}C) until the effluent from the filter become colorless. The asphaltenes obtained at this stage were called filter washed asphaltenes. The filter washed asphaltene were transferred to Soxhlet apparatus and rinsed with n-heptane at 60 ^{0}C for 2 days with interruption once a day to change the n-heptane and crush the asphaltene sample. The Soxhlet washing ensure any waxes in the asphaltene samples are dissolved out in the filtrate**.** The asphaltenes washed by this method is, hereafter, referred as Soxhlet-washed asphaltenes. The yield of extracted asphaltene was found to be 13.3 ± 0.5% by weight.

3.1.3 Asphaltene Solution Preparation

The asphaltene solutions were prepared in extra dry toluene procured from Fisher Scientific (Canada). The solution preparation involves two steps i.e. preparation of stock solution and dilution to lower designated concentration. The solutions expressed in ppm were prepared by adding known mass of asphaltene in known litre of toluene (mg/L). Toluene was first degassed using a sonicator for 30 min. A known amount of asphaltene was then added to the degassed toluene to prepare stock solution. The mixture was then stirred and sonicated for 30 min. The resulting stock solution was allowed to equilibrate

for 5 days. The stock solution was then diluted to obtain the required concentration of working solution. Once prepared, solutions were sonicated for 20 min per day for 4 days before performing the adsorption experiments. Loss of solvent, if any, was adjusted based on volume.

3.1.4 Surface Preparation or pre-cleanup step

Prior to initiating the adsorption of asphaltenes, the gold and stainless steel surface was subjected to a chemical based pre-treatment step for cleaning. First, the samples were cleaned with toluene by sonication for 15 min followed by exposure to absolute ethanol for 15 min. Then the samples were then rinsed with deionized water. The samples were further cleaned by soaking in 2% Hellmanex® II solution for 40 minutes at 35ºC. Finally, the samples were thoroughly rinsed with deionized water and gently blow-dried under a flow of nitrogen gas.

3.2 QCM Experiment

In this study, a quartz crystal microbalance (QCM) was used to measure the mass of asphaltene adsorbed on metal surface. A general background on the QCM working principle and details of the system employed is presented in the following sub-sections.

3.2.1 Quartz Crystal Microbalance (QCM) Theory

Quartz crystal microbalance is a technique used to measure small change (micrograms) in mass. This technique works on the principle of reverse piezoelectric effect wherein

applied electric charge generates mechanical stress in some materials (notably crystals and certain ceramics). Specifically, in QCM the application of a voltage across these crystals results in a corresponding mechanical strain.

Due to the piezoelectric properties and crystalline orientation of the quartz, the crystal can be made to oscillate at its resonant frequency, f_0, when connected to an external driving oscillator circuit (Czandema *et al*., 1984). In a QCM, the crystal is sandwiched between a pair of metal electrodes (refer figure 3.2). Gold electrodes have most commonly been used in QCM studies; however SS, Cu, Al, Pt and other metals can also be used. The AT-cut crystals are made to oscillate in a shear thickness mode at their resonant frequency, which in most common QCM is 5MHz. Upon excitation by application of alternating voltage, the crystal vibrates at its resonant frequency

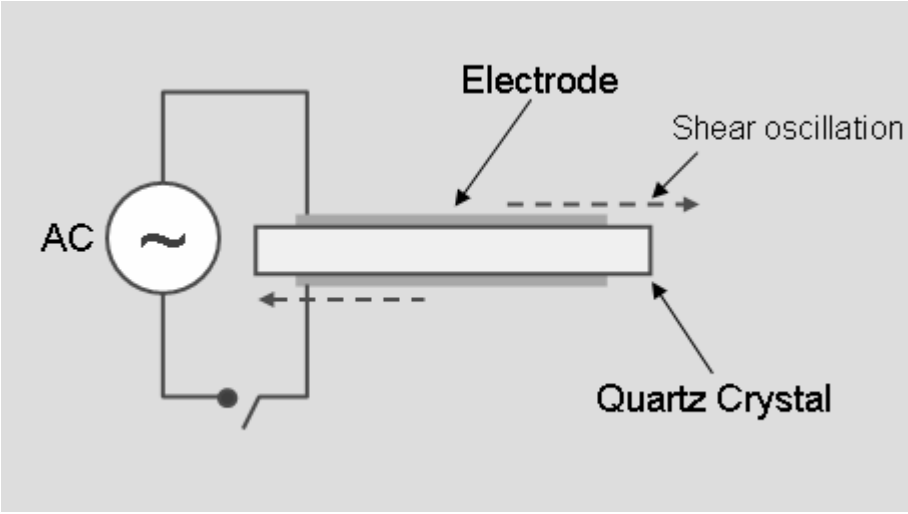

Figure 3.2 The principle of operation of QCM

Any mass added or loaded on the crystal surface causes a drop in the oscillation

frequency of crystal. In 1959, Sauerbrey demonstrated that the mass change per unit area at the QCM electrode surface can be related to the change in the oscillation frequency of the crystal according to the following relation:

$$\Delta f = -C_f \cdot \Delta m \qquad (3.1)$$

where,

Δf = the observed frequency change in Hz,

Δm = the change in mass per unit area in mg/m^2,

$$C_f = \frac{2 f_0^2}{\left(\rho_q \cdot \mu_q\right)^{1/2}}$$

C_f is the sensitivity factor for the crystal (5.66 Hz mg $^{-1}$m^2 for a 5 MHz AT-cut quartz crystal at room temperature) and f_o is the resonant frequency of crystal (5 MHz for crystals employed in this study).

However, the equation 3.1 is valid under the following assumptions:

1. The adsorbed mass is distributed evenly over the crystal.

2. The adsorbed mass is rigidly attached, with no slip or inelastic deformation in the added mass due to the oscillatory motion.

3. Δm is much smaller than the mass of the crystal itself

QCMs have been utilized for past many years as mass sensors in vacuum and gas phase systems. However, QCM was first proven reliable for measurements in the liquid phase

by Nomura and Okuhara (1982). Later, Kanazawa and Gordon (1985) developed a relationship between resonant frequency change Δf and the liquid density-viscosity. Kanazawa's solution for the change in resonant frequency of the crystal due to liquid loading is shown in following equation:

$$\Delta f = -f_0^{3/2}\left(\frac{\rho_L \eta_L}{\pi \rho_q \mu_q}\right)^{1/2} \tag{3.2}$$

where,

f_0 = Resonant frequency of unloaded crystal in *Hz*

ρ_q= Density of quartz = 2.648×10^3 kg/m^3

μ_q= shear modulus of quartz = 2.947×10^{10} *Pa*

ρ_L = density of the liquid in contact with the electrode in kg/m^3

η_L= viscosity of the liquid in contact with the electrode in N · Sec/m^2

For example, when the medium of exposure for crystal is changed from air to water at 25 ^{o}C a frequency drop of 672.7 Hz is predicated using equation 3.2. Although the immersion of liquid to QCM causes a decrease in the resonant frequency, it also dampens the resonant oscillation, resulting into a series resonant resistance, R, of QCM resonator. A Butterworth-Van Dyke equivalent circuit model was developed (Martin *et al.*, 1991) to predict the increase in the series resonant resistance R. Therefore, Δf and ΔR measurements can be used as independent indicators of mass loading and density-viscosity change at the crystal-liquid interface of the QCM resonator.

The factors which can affect the QCM response are surface roughness, pressure and temperature.

3.2.2 QCM and Flow cell apparatus

The QCM utilized in this study was acquired from Maxtek, Inc. The RQCM (Research Quartz Crystal Microbalance) comprises of a 1-inch AT-cut polished quartz crystal of 5 MHz fundamental resonant frequency mounted on a 10 cm (4") Teflon® crystal holder which terminates with a male SMB connector. This quartz crystal acts as a reference oscillator. The SMB connector connects to a base unit that contains a phase lock oscillator circuit. The RQCM has a RS-232 computer interface and Windows-based software which can be used to acquire the data.

The figure 3.3 below shows the pictures of the crystals employed in this study. The left picture shows the front side of the crystal called as sensor electrode and right picture shows rear side called as counter electrode.

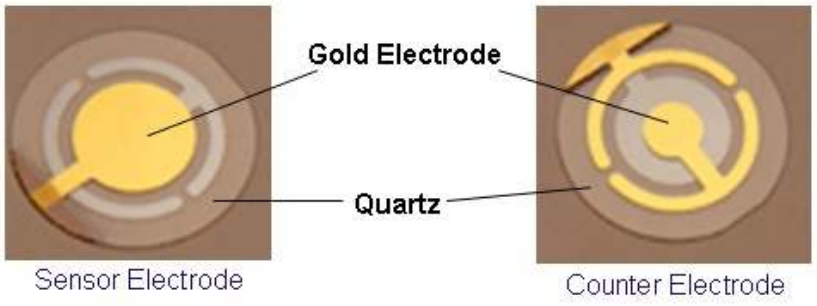

Figure 3.3 Pictures of a standard one-inch QCM sensor crystal

The sensor electrode has a diameter of ½ inch with an extended electrode that wraps

around the edge of the crystal and extends into a semicircle; the counter electrode has a diameter of ¼ inch. The oversized sensor electrode as opposed to counter electrode was chosen to ensure a more consistent deposition across the active area of crystal.

The flow cell (FC-550) made from Kynar was procured from Maxtek. The cut view of QCM probe with flow cell and crystal installed is presented in figure 3.4 below. The crystal is installed in the probe body with the rear electrode facing towards the spring contacts. The flow cell is mounted on the top of the crystal, A Viton O-ring provides a sealing between the cell and the face of the sensor crystal creating a flow chamber of approximately 0.1 ml.

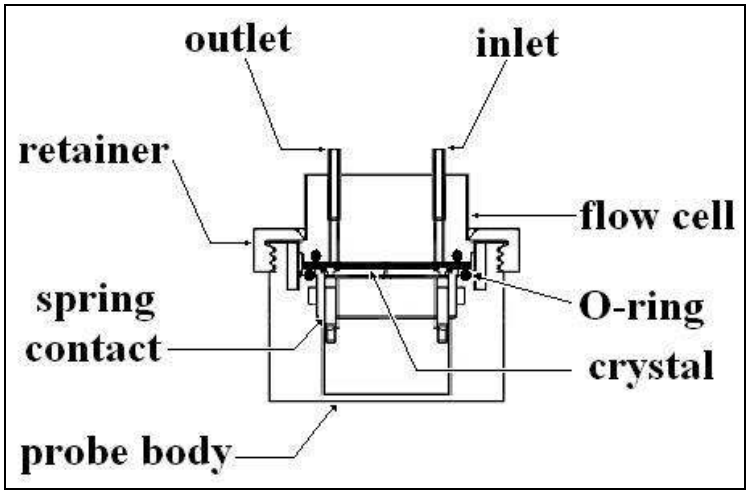

Figure 3.4 Cut-out view of QCM probe with flow cell and crystal installed

The flow cell has stainless steel inlet and outlet tubes which provide the inlet and outlet for liquid allowing the liquid to flow on the crystal surface.

3.2.3 Experimental Set-up and Procedure

The experimental set-up employed in this study was developed previously by Kui Xie as a part of his M.Sc. thesis (Xie, 2006). The schematic diagram of experimental set-up is presented in figure 3.5 below. The experimental set up consists of Quartz Crystal Microbalance instrument (shown as RQCM in figure 4.2) with data acquisition card, flow cell apparatus, temperature controlled water bath, peristaltic pump, 3-way valve and beakers containing testing solution and solvent. The flow cell apparatus is connected to RQCM via a signal cable.

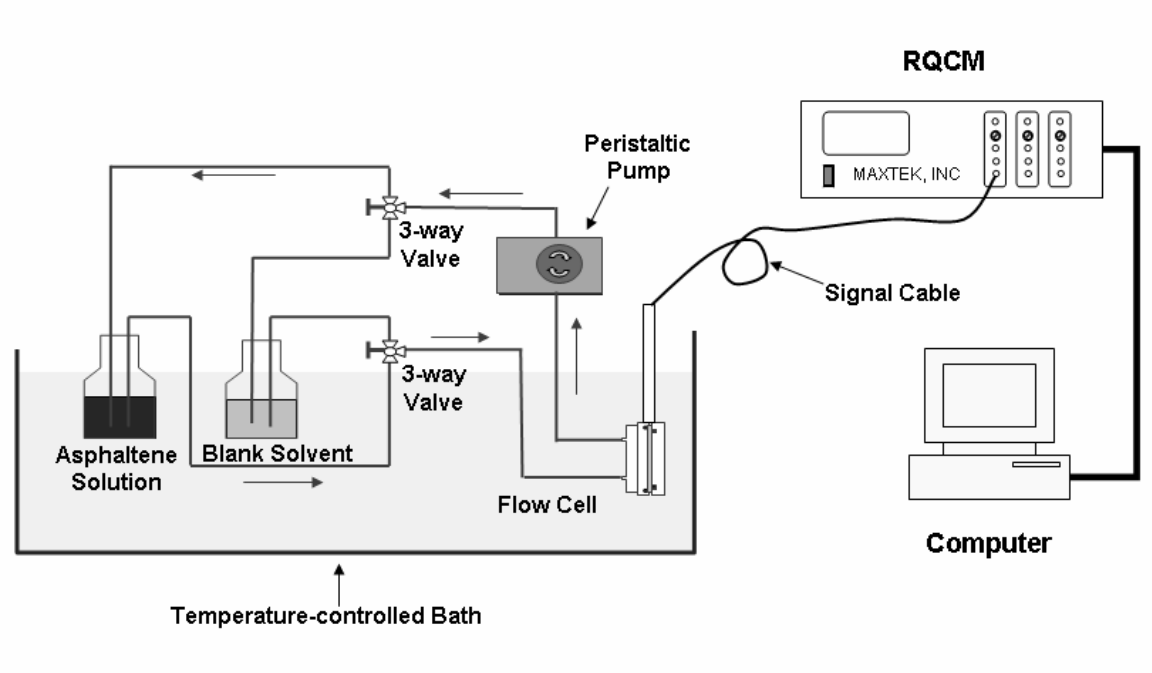

Figure 3.5 QCM experimental setup with flow cell

The development of the experimental protocol involved investigating the effectiveness of flow cell apparatus and achieving a good thermal stability. The QCM is extremely

sensitive mass detector system and the response gets affected due to change of external factors such as temperature and pressure. The use of flow cell apparatus eliminated any temperature difference between crystal and solvent or liquid medium and effect of any stress or pressure due to manual uplifting of the crystal holder assembly. Achieving a good thermal stability of water bath is extremely important and it was found that water bath which has temperature stability of ± 0.2ºC caused frequency variation of less than 1.6 Hz (Xie, 2006). A better temperature controlled water bath was acquired which can achieve stability of ± 0.01ºC and the noise level was reduced to ± 0.25 Hz (Xie, 2006).

The specifications of auxiliary equipment are provided in table 3.2 below.

Table 3.2 Key auxiliary equipment specifications

Equipment Name	Specification	Supplier
Temperature Controlled Bath	Temperature stability: +/- 0.01 ºC Temperature range: -35 - 200 ºC Reservoir Capacity: 28L	VWR International, Canada
Peristaltic Pump	Flow rate:0.7-29 ml/min	Masterflex®, Canada
Sonicator	Model 50D	AQUASONIC, VWR Scientific Products, Canada

The experimental procedure for adsorption studies is described next. The experiments were carried out at room temperature and atmospheric pressure. First, the water bath was set to desired temperature and allowed to attain equilibrium. Next, known quantities of degassed toluene/blank solvent and asphaltene solution were filled in the respective flasks. The flasks were placed in the thermally equilibrated water bath. The quartz crystal + holder system was placed in the bath and allowed to equilibrate (for 8-10 hours). The

system was considered to have reached equilibrium when crystal frequency does not vary more than ± 5 Hz over a one-hour period. Next, degassed toluene/blank solvent was pumped into flow cell and allowed to circulate over the crystal surface. The equilibration was assessed via a criterion similar to that of air. Finally, the asphaltene testing solution was allowed to flow through the flow cell (by changing the valve position) while frequency response is continuously monitored and recorded.

3.3 X-Ray photoelectron spectroscopy (XPS) Experiments

3.3.1 XPS Theory

The X-ray photoelectron spectroscopy (XPS) works on the principle of photoelectric effect discovered in early 1900s (Briggs and Seah, 1990). A photon is term used for a bundle of electromagnetic radiations such as X-rays, ultraviolet light, and visible light that travels at the speed of light. The energy of a photon is given by the Einstein relation

$$E = h\upsilon \tag{3.3}$$

where,

h = plank constant = 6.62×10^{-34} J s

υ = Frequency of radiation (Hz)

The magnitude of frequency of radiation can vary depending upon the type of electromagnetic radiation. In XPS, typically two anodes are used to generate the X-ray's,

aluminum ($h\nu$ = 1486.6 eV) and manganese ($h\nu$ = 1256.6 ev). When a photon gets absorbed by an atom in a molecule, it leads to ionization and, consequently, to the emission of an electron. This effect is known as photoelectric effect and electrons emitted are referred to as photoelectrons.

Albert Einstein (Siegbahn *et al*., 1967) further developed a relationship between energy of photon and energy of emitted electron/photoelectron described as follows:

$$KE = h\nu - BE \tag{3.4}$$

where KE and BE are kinetic energy and binding energy of the photoelectron respectively. Since the value of $h\nu$ is known depending upon Al and Mg anode, the measurement of KE provides the information about the binding energy. Electron binding energy is a measure of energy required to free its electrons from their atomic orbit. The electron binding energy is characteristics of chemical state of an atom. The binding energy of an electron in an orbital varies from one atom to another and with different orbitals within an atom due to electrostatic attraction. An important step in the development of electron spectrometers was the realization that electron binding energies were sensitive to the chemical state of the atom and the technique can be surface sensitive (Brundle *et al*, 1992).

In equation 3.4 the binding energy is referred to with respect to vacuum (free electron) level. However, in solids the binding energies should be with respect to the Fermi level. The Fermi level is the energy associated with top of the valance band. The energy

required for an electron to escape to vacuum is known as work function (Φ). Thus from a practical point of view equation 3.4 can be modified as

$$KE = h\nu - BE - \Phi \qquad (3.5)$$

The value of work function for metals ranges between 1 and 4 eV (Cox *et al*., 1992). Since the samples and spectrometer are in electrical contact with one another, their Fermi energies equilibrate. Thus calibration of spectrometer takes care of work function in equation 3.4. A high resolution valance band spectrum for the gold surface from the XPS spectrometer employed in the present study is presented in figure 3.6 below.

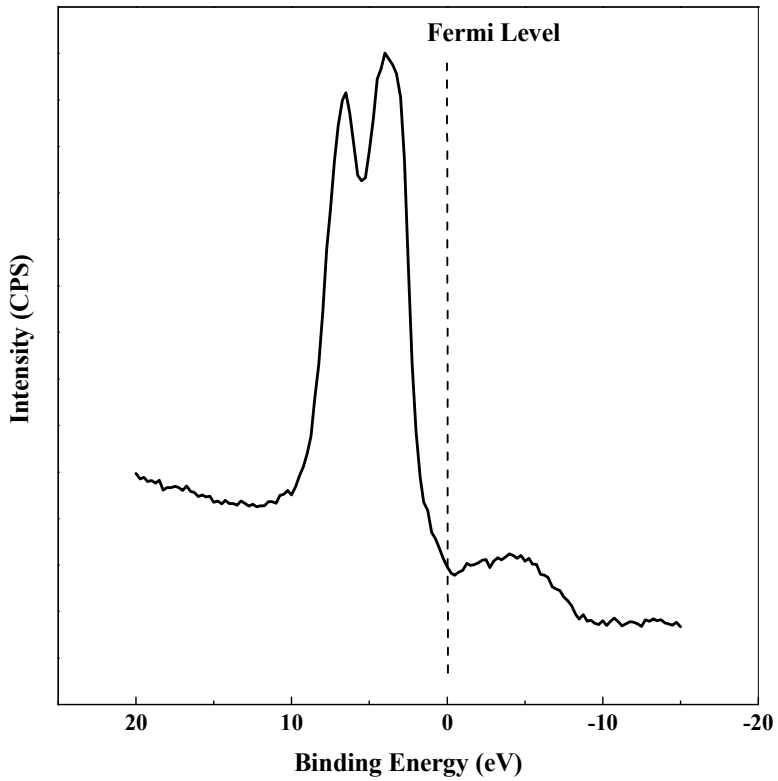

Figure 3.6 High resolution valance band spectra for the gold surface from the spectrometer employed in present study.

For conducting samples, because the electrons within it are free to move in the "sea" of electrons characteristic of metallic bonding, the positive charge does not gets established. On the other hand, for insulating samples, once the photoelectrons are emitted out of the sample surface a positive charge zone gets established on the sample surface.. This effect is known as charging effect (S) and results in a shift of the XPS peak to a higher binding energy. Thus, equation 3.4 now can be written as

$$KE = h\nu - BE - \Phi - S \qquad (3.6)$$

To correct for sample charging, the binding energy of Au 4f peak at 84.0eV, is commonly used as the reference for calibration. The alternate approach is to flood the sample with electrons of sufficient energy to offset the positive charge built up by the holes left by the ejected electrons (Briggs and Seah, 1990). The electron flood gun can be tuned to provide the approximate level of current to push the XPS peaks back to the real position. In the present study, the charging effect is corrected based on Au 4f peak at 84.0eV except for the bulk asphaltene samples which are corrected for C 1s peak.

3.3.2 XPS instrumentation

The key instrumental parts of XPS include a vacuum system, a lens and a hemispherical analyzer. The vacuum system is extremely important part of the XPS system for two reasons. The vacuum system keeps the test surface free of contaminants and allows the

relatively low energy electrons to travel from the surface to the detector without colliding with gas molecules which would cause a loss of kinetic energy. Thus, to obtain reliable and accurate information on the chemical state of the surface requires the experiments to be carried out in vacuum system.

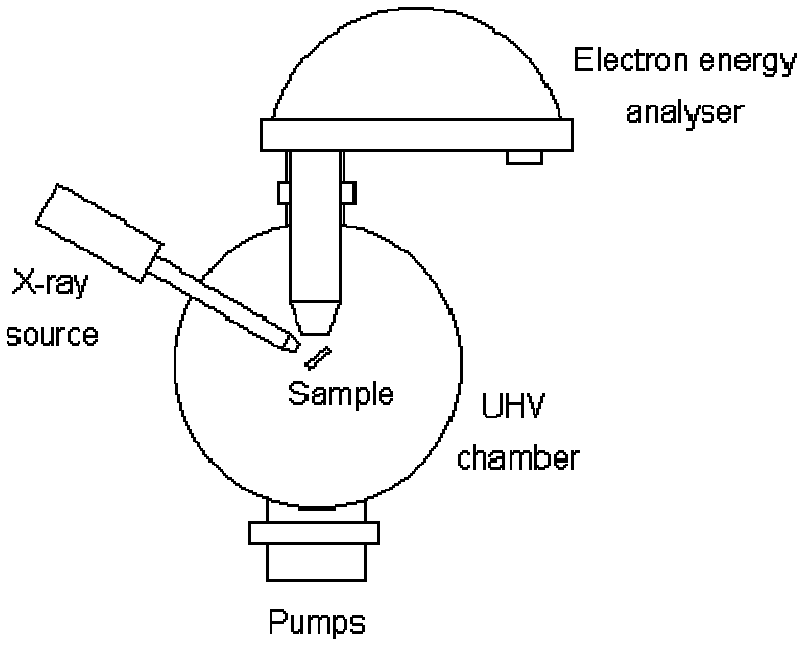

Figure 3.7 XPS instrumentation (Johnson *et al*., 1998)

The photoelectrons ejected from the sample travel through the vacuum system to lens where photoelectrons are focused before entering the analyzer. The XPS instrument employed in this study has concentric hemispherical analyzer (CHA) system. A voltage bias is applied to CHA to produce an electrostatic field. The energy required for an electron to pass through the hemispherical analyzer (CHA) is known as pass energy and is determined by electrostatic field between the two hemispheres. The analyzer was set to

fixed analyzer transmission mode (FAT), where the scan energy was kept constant throughout the scan. Operating the analyzer in the FAT mode produces a spectrum with higher counts at low kinetic energies and lower counts at high kinetic energies (Briggs and Seah 1983).

3.3.3 Experimental Protocol

XPS measurements For preparation of the samples of asphaltenes adsorbed on a gold surface for XPS analyses, the pre-cleaned gold-coated mica substrates were exposed to asphaltene solutions of varying concentrations for a period of 2 days. The samples were removed from the solution and blow dried under gentle flow of nitrogen. For preparation of bulk asphaltene sample, thick slurry of the asphaltene in extra dry toluene was prepared. The pre-cleaned gold-coated mica substrate was immersed in the slurry and then dried under a gentle flow of nitrogen gas. The sample was then transferred into nitrogen filled glass containers prior to being transported to the XPS system. The typical elapsed time between the removal from solution and the transfer into the XPS system ranged 12-15 minutes. XPS measurements were performed using a Thermo Instruments Microlab 310F surface analysis system (Hastings, UK) under ultrahigh vacuum conditions and using a Mg Kα X-ray source (1253.6eV) at 15 kV anode potential and 20 mA emission current. Scans were acquired at fixed analyzer transmission (FAT) mode at a pass energy of 20 eV. Some survey scans were acquired at pass energy of 50 eV. Spectra for all samples except that for bulk were calibrated to the Au 4f peak at 84.0 eV binding energy. For bulk asphaltene sample, Au 4f peak was not visible in the spectra and

as such calibration was performed based on C 1S peak. Minor charging effects were observed ranging 0.4-1.5 eV with a higher magnitude for the bulk asphaltene sample.

3.4 Gold surface characterization by AFM

The physical characteristics of the gold surface such as surface roughness and grain size were assessed using atomic force microscopy (AFM).

The gold crystals used in QCM study were procured from Maxtek, Inc., USA whereas gold coated mica surface was purchased from George Albert, Germany. To assess the extent of difference in microstructural characteristics of the two surfaces, that may produce differences in the experimental results, AFM characterization was carried out. The AFM images of the two samples are presented in Figure 3.8.

Control_XPS **Control _QCM**

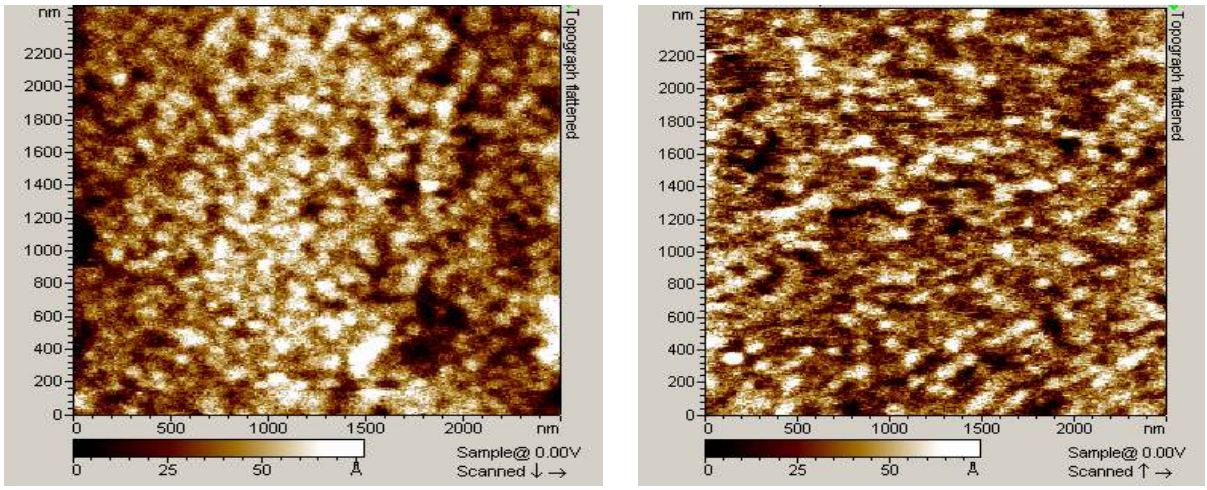

Figure 3.8 AFM images of cleaned gold sample (blank) employed for XPS and QCM study (2.5 × 2.5 micron)

The gold surface was found polycrystalline in nature and the AFM software yielded an average grain size of 80-100 nm and a surface roughness of 7-9 nm. The morphology of the QCM and XPS samples can be considered to be similar and, therefore, any significant differences in experimental results due differences in surface morphology were not anticipated. The figure 3.9 shows the image of control sample of QCM at high resolution (500 nm). The figure 3.9 clearly shows the grain size and structure of grains.

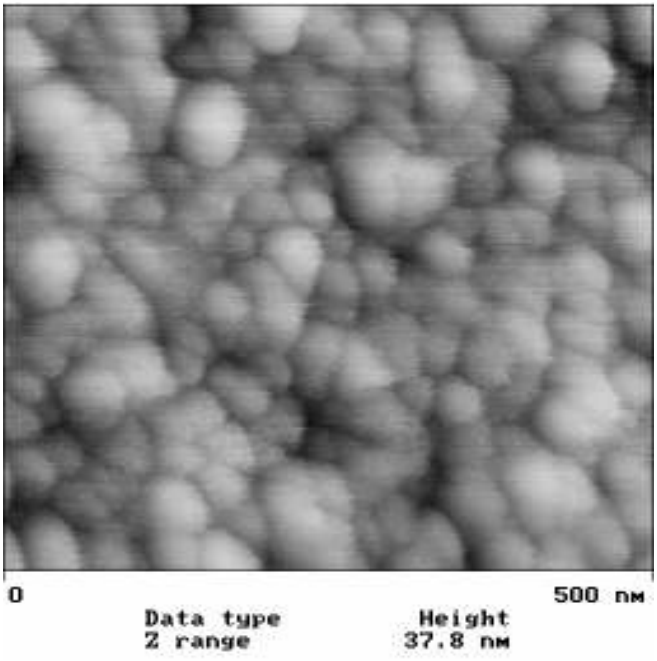

Figure 3.9 The AFM image of control QCM sample at high resolution of 500 nm.

Chapter 4

Results and Discussion

This chapter discusses the results for three asphaltene samples i.e. Cold Lake, MD and Heavy Oil asphaltene and its sub-fraction. A summary of experimental runs is presented in section 4.1. The results and analysis is presented in four sections. Section 4.2 is dedicated to Cold Lake asphaltene. The subsequent sections 4.3 and 4.4 contain the results and analysis for MD and Heavy Oil asphaltene samples. The sub-sections are organized in terms of QCM and XPS results.

4.1 Summary of Experimental Runs

The experiments were performed to meet desired objective stated in Chapter1. The objectives were to investigate the kinetics and equilibrium behavior of adsorption of asphaltenes combined with the chemical and physical characterization of adsorbed asphaltenes. The summary of experiments performed is outlined in table 4.1 below.

The QCM technique was employed to investigate the kinetics of asphaltene adsorption and data was further processed to estimate the isotherm. The XPS technique provides information on the nature of species interacting with metal surface. The obtained data was further analyzed via a mathematical model developed to estimate the isotherm. Finally, the adsorption isotherms generated from QCM and XPS experimentations were

compared and Gibbs free energy for adsorption was estimated.

Table 4.1 The list of experiments performed

Asphaltene	Solvent	Metal Surface	Concentration (PPM)	Technique
Cold Lake	Toluene	Au	0-1500	QCM
		SS		XPS
MD	Toluene	Au	0-1500	QCM
				XPS
HO2-C_7	Toluene	Au	500	XPS
HO2-F_7	Toluene	Au	500	XPS
HO2-F_3	Toluene	Au	500	XPS

For Cold Lake and MD asphaltene sample, both QCM and XPS techniques were employed. For Heavy Oil 2 (HO2) sample only XPS technique was employed to distinguish any key difference in functional group of Heavy Oil asphaltene and sub-fraction samples.

The repeat runs were also conducted to check the reproducibility of the experiments. The results and discussion on asphaltene samples of Cold Lake, MD and Heavy oil follow in the next sections.

4.2 A QCM and XPS Investigation of Cold Lake Asphaltene Adsorption

Adsorption experiments were carried out by first extracting asphaltenes from Cold Lake bitumen and then preparing asphaltene solutions of desired concentrations following a

procedure described in Chapter 3. In this section, first, the results and analysis of the kinetic data for asphaltene adsorption using the QCM flow cell system is presented. Next, XPS spectral analysis of asphlatene adsorbed samples (prepared in separate batch experiments) for Carbon 1s, Oxygen 1s, Sulfur 2p and nitrogen 1s are presented. Next, a mathematical model developed to analyze XPS data for the estimation of fractional coverage is presented. A comparison of adsorption isotherms generated from QCM and XPS measurements was done. Finally, an analysis of the XPS and QCM data to investigate the orientation of adsorbed asphaltene is presented.

4.2.1 Asphaltene Adsorption Kinetics

The time evolution of the mass of asphaltene adsorbed on the gold surface was monitored using a quartz crystal microbalance. The results for asphaltene adsorption with concentrations ranging from 50-1500 ppm are shown in Figure 4.1. The adsorption kinetics exhibit a rapid initial response followed by a slower approach to equilibrium. As shown in Figure 4.1, the initial response shows a linear trend when plotted against the square root of the elapsed time, ζ, which is indicative of a diffusion controlled process (Weber *et al*., 1963). At longer timescales, the data was found to follow first-order kinetics, and for $\zeta > 10$ minutes, the data could be adequately fitted to an equation of the following form:

$$m = m_{eq} + (m_0 - m_{eq})e^{-\zeta/\tau} \tag{4.1}$$

where, m_0 is the initial mass, m_{eq} is the mass adsorbed after the system had reached equilibrium and τ is the characteristic time (Jeribi *et al*, 2002).

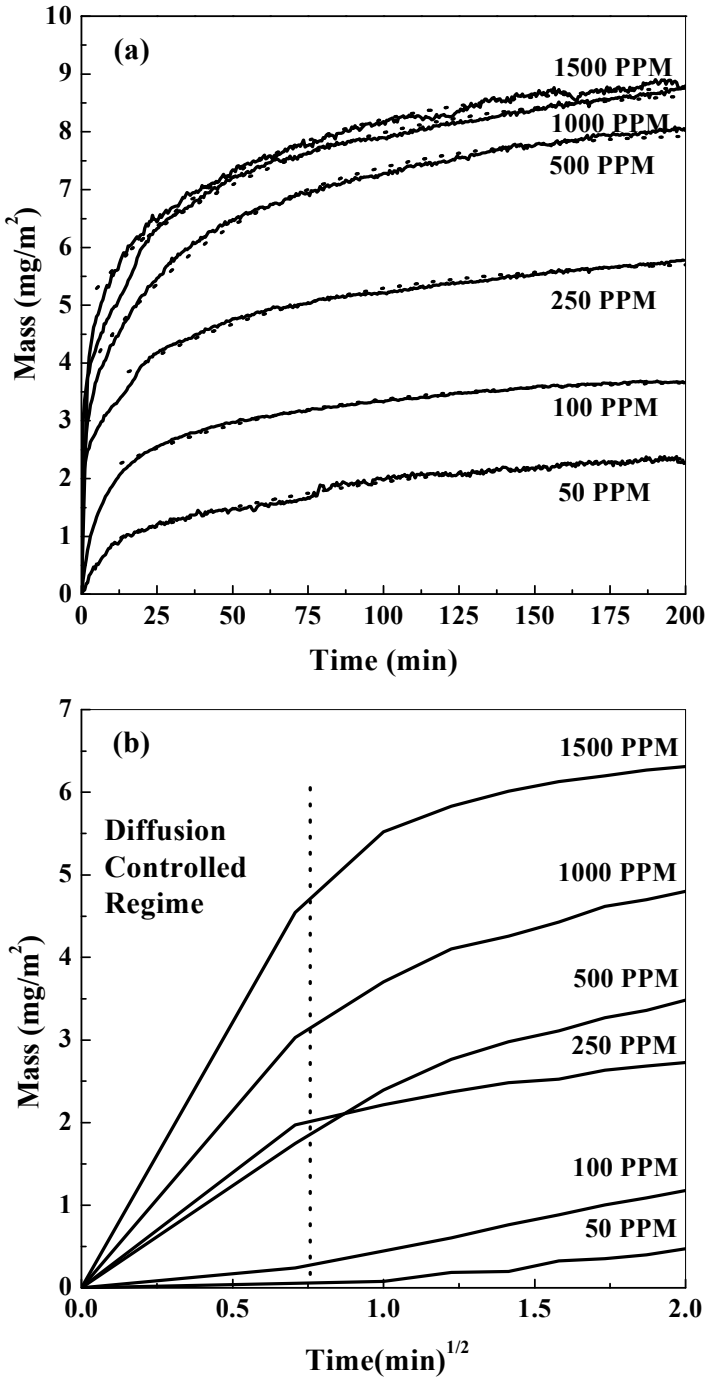

Figure 4.1 (a) Asphaltene adsorption kinetics on gold surface. The dotted line presents fit for equation (4.1). (b) Mass of asphaltene adsorbed as a function of square root of time.

Since equation (4.1) is valid for ξ (time) >10 minutes, m_0 the apparent initial mass adsorbed and does not have any significance with respect to the real initial mass of adsorbed asphaltene. For each plot, the three parameters - m_0, m_{eq}, and τ - were fit to the data using regression analysis. The increasing trend of m_{eq} and m_o was anticipated with increase in concentration whereas for characteristic time (τ) no specific trend was found. The fit to the kinetic data is shown as dashed lines in the Figure 4.1 (a). As can be observed, the quality of fit is satisfactory and is supported with error bounds on the fit parameters in table 4.2. The values for the mass adsorbed at equilibrium, m_{eq} reported in Table 4.2 were used to generate adsorption isotherms as discussed below.

Table 4.2 Asphaltene adsorption data on gold surface

Concentration (PPM)	m_{eq} (mg/m^2)	m_o (mg/m^2)	τ (min)
50	2.56 ± 0.02	0.74 ± 0.01	92.8 ± 2.50
100	3.73 ± 0.02	1.92 ± 0.01	61.5 ± 0.92
250	5.78 ± 0.01	3.31 ± 0.03	62.8 ± 1.26
500	8.01 ± 0.01	3.73 ± 0.03	52.1± 0.73
1000	8.86 ± 0.01	4.95 ± 0.02	55.8± 0.82
1500	9.93 ± 0.02	6.35 ± 0.01	77.1± 0.78

4.2.2 XPS Spectral Analysis

XPS measurements allow a comparison between the spectra of bulk asphaltene and that adsorbed from solution. The presence or absence of various functional groups in the adsorbed asphaltene as compared to that in the bulk asphaltene should indicate the role of such functional groups on asphaltene-metal interactions.

4.2.2.1 Survey Spectra

Survey spectra of all samples indicated the presence of X-ray or X-ray induced Auger transitions corresponding only to Au, C, S, N and O in all samples. Figure 4.3 presents survey spectra for blank gold sample and bulk asphaltene sample.

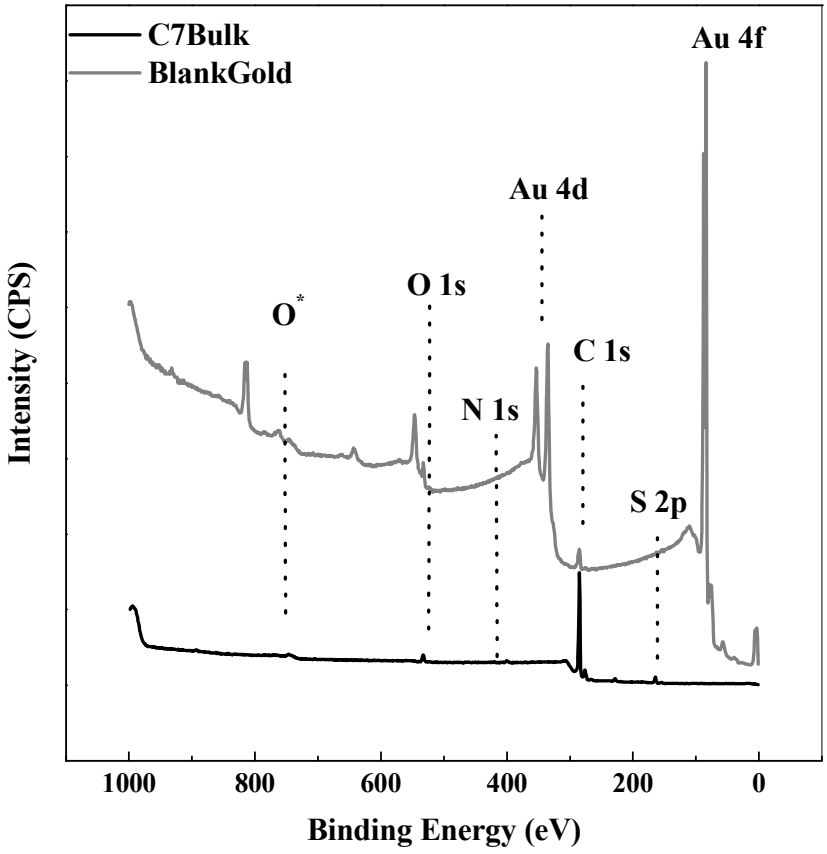

Figure 4.2 Survey spectra for blank gold surface and C_7 bulk asphaltene

The blank gold surface spectra contained weak signals in the C 1s and O 1s regions, consistent with residual surface contamination that could not be removed by solution cleaning. Attempts were made to remove these species by flame-annealing the blank sample. Although this strongly reduced the signal in the C 1s region, it also led to a substantial signal for silicon oxide and a significant reduction in the intensity of gold signal. For consistency sake and to allow for comparison of XPS and QCM data on equal basis, pre-cleaning step without flame annealing was adopted for all experiments.

4.2.2.2 Peak intensity data

The peak for carbon, oxygen sulfur and nitrogen elements were analyzed and presented in detail in subsequent sections. A summary of the data is presented in table 4.3 below.

Table 4.3 The peak intensity data for blank, adsorbed and bulk asphaltene Cold Lake sample

Concentration (PPM)	Carbon Peak Intensity (CPS.eV)		Oxygen Peak Intensity (CPS.eV)		Sulfur Peak Intensity (CPS.eV)		Nitrogen Peak Intensity (CPS.eV)	
	Main Peak (C-H)	Sub Peak (C-O and C=O)	C-O Peak	C=O Peak	Thio-phenic	Thiol	Pyrrolic	Pyridinic
Blank	48.1	67.2	31.9	9.4	0.0	2.0	0.0*	
50	192.8	59.3	20.4	12.1	5.4	6.1	4.2*	
100	202.1	53.6	23.2	10.2	6.1	2.5	4.9*	
250	226.1	46.9	20.5	8.8	8.2	2.2	5.9*	
500	274.5	22.6	22.6	7.9	8.2	0.0	2.1	3.2
1000	327.5	15.1	13.3	5.7	10.4	0.0	1.4	3.6
1500	320.4	12.6	16.7	7.5	8.4	0.0	3.5	2.1
Bulk (C7)	360.7	11.9	18.1	4.3	13.2	0.0	3.3	1.5

***** The two peaks were not discernable

The peak intensity data is referred subsequently with carbon, oxygen, sulfur and nitrogen spectral analysis discussion.

4.2.2.3 Carbon Spectra

The C 1s spectra for bulk asphaltene, the blank gold substrate surface and the Au substrate exposed to solutions of varying asphaltene concentrations are shown in Figure below.

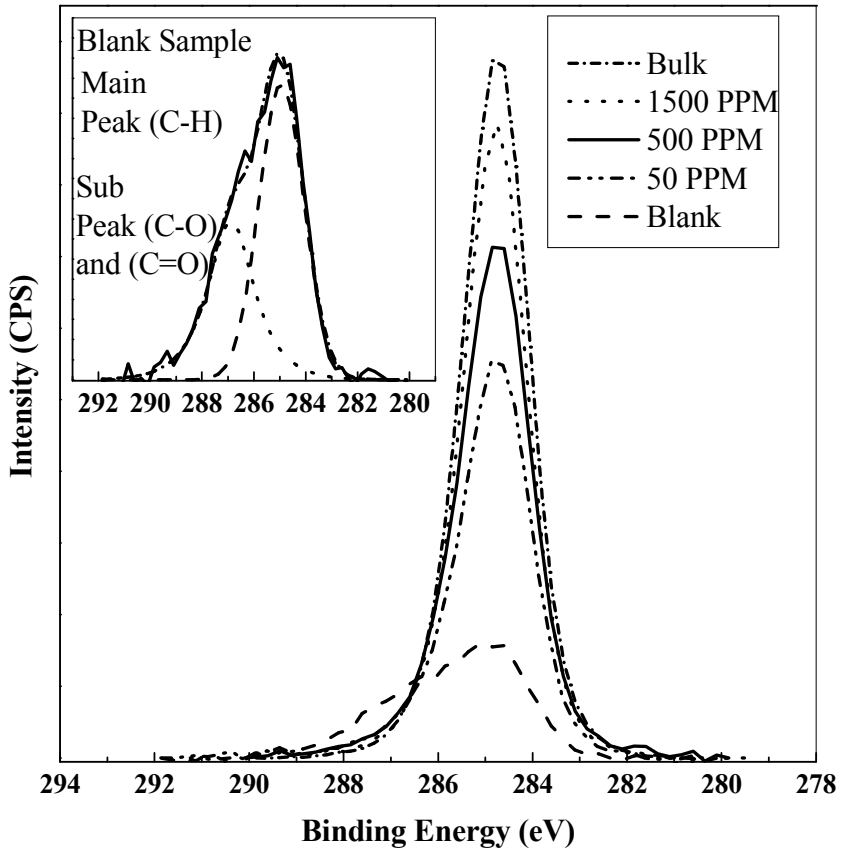

Figure 4.3 C 1s XPS spectra for blank sample, adsorbed and bulk asphaltenes on gold surface. The inset graph presents peak fit for the blank sample

Two peaks were fit to the C 1s spectrum of the Au substrate at 284.8 and 286.3 eV binding energies, respectively. The former peak, which may be attributed to C in an aliphatic or aromatic C-H environment, grows in intensity with increasing asphaltene concentration. The latter peak at 286.3 eV is consistent with C in a C-O environment, and this peak is attenuated as the coverage of asphaltene is increased, although traces of it may still be observed in the bulk asphaltene sample. Table 4.3 outlines the intensity data obtained at each concentration. The peak fitted parameters are presented in Appendix (B). Ostlund *et al*. (2004), used XPS to study asphaltene sub-fractions F10/90 and F40/60, which was extracted using a mixture of methylchloride (a polar solvent) and n-pentane (a flocculant), and found that the F 40/60 fraction had response associated with the main carbon peak (C-H) only whereas F10/90 had response corresponding to the C-O environment specified as carboxylic group containing ketonic and non-ketonic oxygen atom. This indicates that asphaltenes are a mixture of molecules of which some are oxygen devoid while others contain significant levels of oxygen. Here**,** the intensity of the signal at 286.3 eV decreased with an increasing amount of adsorbed asphaltene. Thus, although some of the C-O signal response may be originating from the asphaltene themselves, the trend of decreasing intensity with asphaltene concentration indicates that the material response for C-O response is present predominantly on the blank sample surface and is a result of the pre-treatment step. The source of asphaltene and fractionation procedures used by Abdallah *et al*. (2007) were similar to those used in present study; however, they attributed the C-O signal to adsorbed asphaltene without considering the possibility that the signal could arise from the remnants of chemical

species from the pre-cleanup step.

4.2.2.4 Oxygen Spectra

The O 1s spectra for bulk asphaltene, the blank gold substrate surface and the Au substrate exposed to solutions of varying asphaltene concentrations are shown in Figure 4.4 below

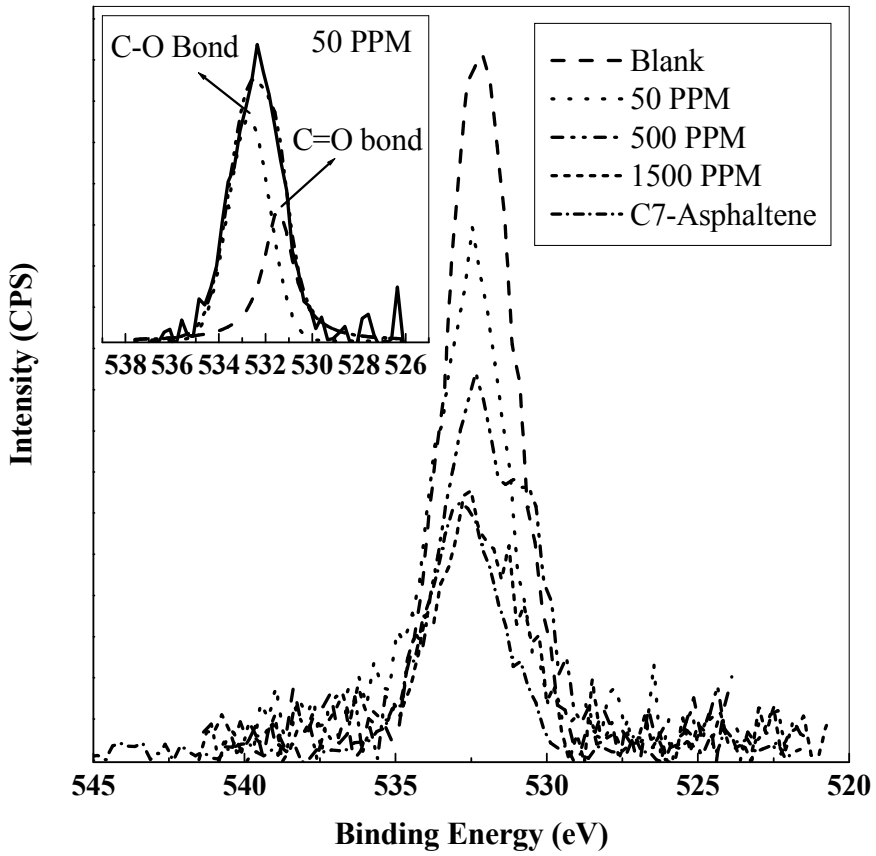

Figure 4.4 O 1s XPS spectra for blank sample, adsorbed and bulk asphaltenes on gold surface. The inset graph presents peak fit at 50 PPM

The blank sample has the highest O 1s signal intensity, which decreases with an increase

in asphaltene solution concentration. This is consistent with the C 1s observations discussed above that the asphaltene is deficient in O-containing species. The peak fitted feature for O 1s spectra is presented as an inset in figure 4.4. The binding energy at 533 eV can be attributed to C-O environment and low binding energy peak 531.5 eV as C=O environment (Beamson *et al*., 1992). It may also be worth to note that the FWHM for bulk asphaltene at 531.3 and 532.9 eV were 2.73 and 2.53 eV, respectively whereas for the blank and adsorbed samples the FWHM were around 2 eV. This implies that C-O and C=O environment are more ordered in bulk asphaltene sample as compared to adsorbed and blank sample. The relative intensity of C - O to C = O are listed in Table 4.3 and the peak fitted parameters are presented in Appendix (B). The relative intensity was highest for the bulk asphaltene indicating that it predominately contains C-O environment. The relative intensity was found to decrease with decreasing asphaltene concentration (or surface coverage). However, the blank sample exhibited a high relative intensity (3.37), which is attributed to material left after pre-clean-up process. This complicates a conclusive assessment of preferential adsorption of certain type of molecules (C-O environment rich). The oxygen intensity data is presented in Table 4.3.

4.2.2.5 Sulfur Spectra

The S 2p spectra for bulk asphaltene, the blank gold substrate surface and the Au substrate exposed to solutions of varying asphaltene concentrations are shown in Figure 4.5

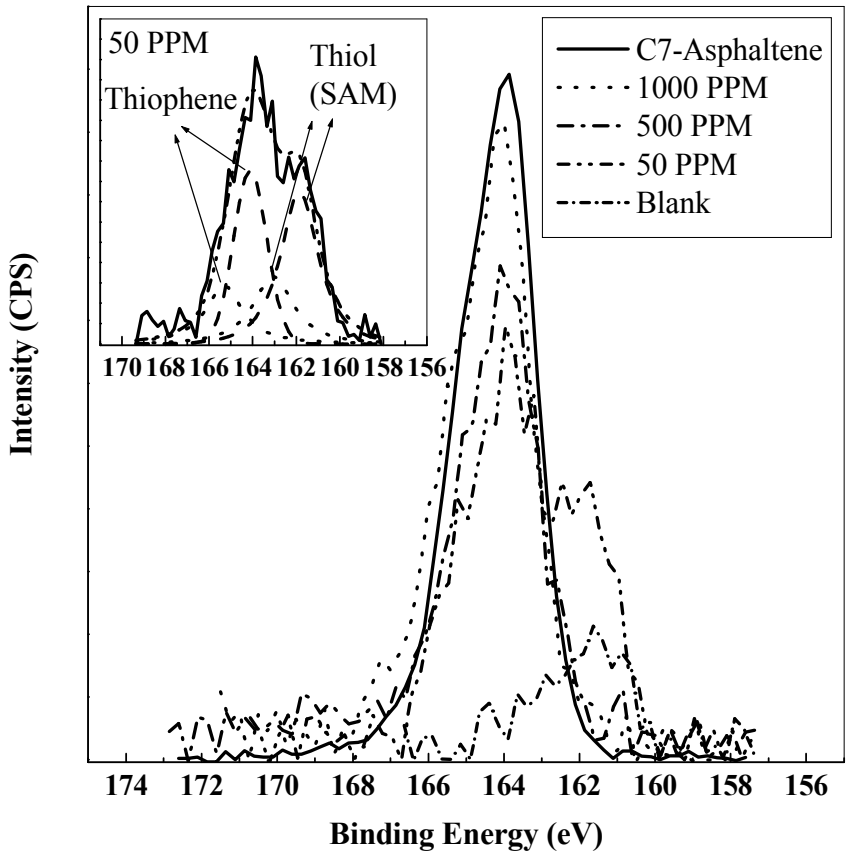

Figure 4.5 S 2p XPS spectra for blank sample, adsorbed and bulk asphaltene on gold surface. The inset graph presents peak fit at 50 PPM.

The $2p_{3/2}$ and $2p_{1/2}$ components of the spectra were peak fitted with a 2:1 relative intensity that is separated in energy by 1.2 eV. Except on the bare Au substrate, a strong S $2p_{1/2.3/2}$ pair of peaks is observed at binding energies of 164.0 and 165.2 eV, consistent with the presence of thiophenic sulfur (Siskin *et al*, 2006). A second pair of peaks appears at 161.8 and 163.0 eV binding energy. The peak fitted features are shown as an inset to figure 4.5 and the parameters are presented in Appendix (B). As can be seen from the Figure 4.5, the relative intensity of the 161.8/163.0 eV pair was largest for the sample

with asphaltene adsorbed from the 50 ppm solution and decreases with an increasing asphaltene concentration, not being discernable beyond 250 ppm. The peak intensity data is presented in Table 4.3. This relatively lower binding energy species is consistent with S being in an environment associated with a more polarizable and electron-donating Au environment, these binding energies corresponds well with literature (Laiho *et al*., 2003) values for dodecanethiol SAMs on Au. Presumably, the thiophenic sulfur from asphaltene may form an Au-S bond on the surface. The decrease in observed peak intensity with an increasing concentration is attributed to the attenuation of the S 2p photoelectrons by the overlying asphaltene layer of increasing thickness.

4.2.2.6 Nitrogen Spectra

The N 1s spectra for bulk asphaltene sample are presented in Figure 4.6. Two peaks may be fit to the curve at binding energies characteristics of pyridinic (398.7 eV) and pyrrolic (400.2 eV) type nitrogen (Kelemen *et al*, 1994). The peak fitted parameters are presented in Appendix (B). The relative intensities of these two peaks were found to be 2.2. For the adsorbed asphaltene samples from solutions of lower concentration the signal to noise ratio in nitrogen spectrum was low making quantitative peak fit very difficult. Since the nitrogen content in the bulk asphaltene itself is ~1 % and given the low cross section of the N1s transitioning, it can be anticipated that at dilute asphaltene concentrations (<1500 PPM) adsorbed asphaltene would likely have low intensity of the nitrogen signal because small amounts of adsorbed asphaltenes.

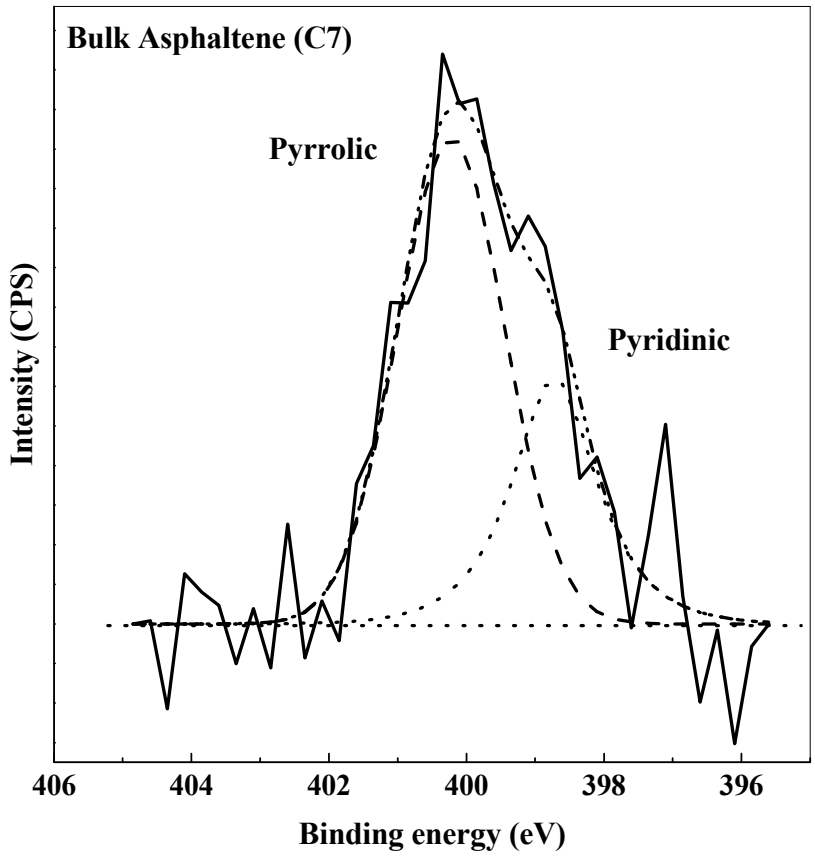

Figure 4.6 Nitrogen (N 1s) XPS spectra for bulk asphaltene with peak fitted features.

4.2.3 Analysis of XPS data for estimation of adsorbed asphaltene surface coverage

In this section, the development of a simple model to estimate surface coverage of adsorbed asphaltene from XPS data analysis is presented. The surface coverage estimated is compared with the surface coverage obtained from the QCM data analysis. For surface coverage estimation from XPS data analysis, the main C 1s peak at 284.8 eV is considered. The basic elements of the model used for surface coverage is shown

schematically in Figure 4.7.

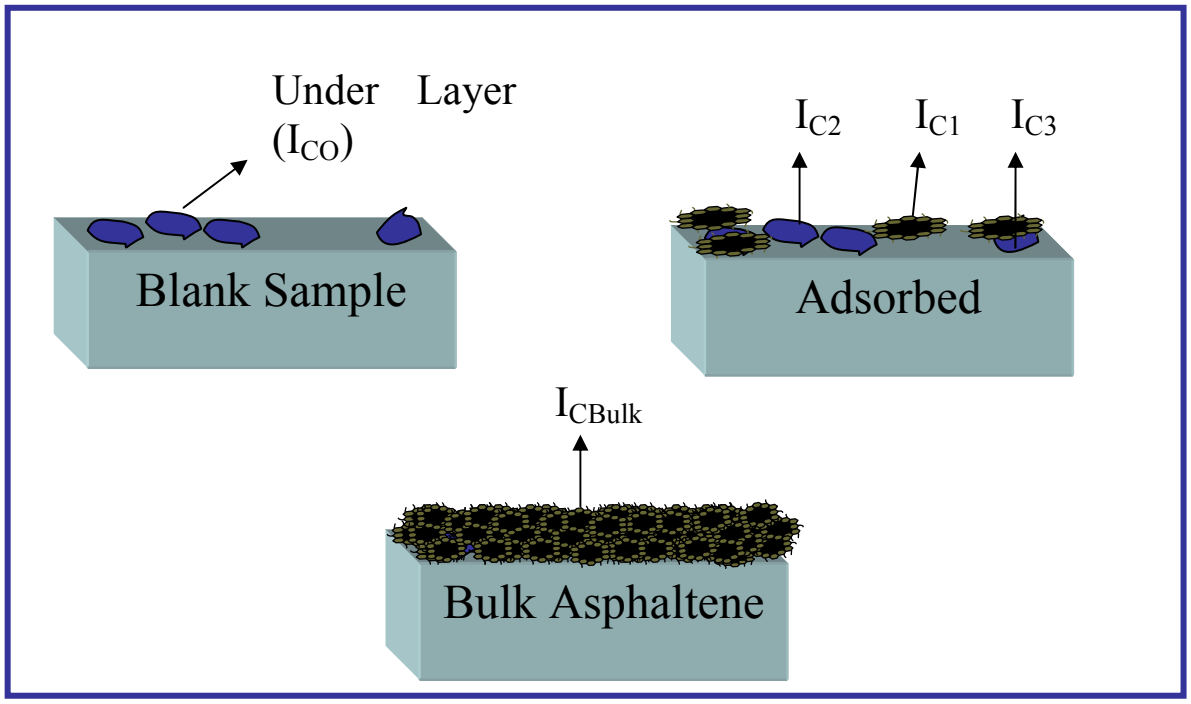

Figure 4.7 Schematic depiction of XPS carbon intensity from blank, bulk and adsorbed asphaltene samples on gold surface

The carbon intensity response for the adsorbed asphaltene sample can be considered to be the sum of responses from the adsorbed asphaltene layer (IC_1 in figure 4.7), the uncovered under-layer (C_2), and the asphaltene-covered under-layer (C_3). The under-layer is essentially modeled as an ultra-thin layer of residual matter adhering the gold surface that is left after the pre-cleaning step. Three key assumptions are made in the analyses: (i) the adsorbed asphaltene molecules have same carbon characteristics as the molecules in the bulk sample (ii) the blank sample is considered to be completely covered with an under-layer which mainly consists of carbon and oxygen as supported by the

corresponding XPS spectra, and, (iii) the adsorbed asphaltene layer is of uniform thickness '*t*', which is greater than 3 nm. It may also be worth to note that although the experimental protocol and scanning parameter were kept constant from one sample to another, the variation in the intensity ranging 10-15 % was observed due to instrumental artifacts. Accordingly, the total carbon intensity can be expressed as:

$$I_{Ct} = I_{C1} + I_{C2} + I_{C3} \tag{4.2}$$

where,

I_{Ct} = Total C 1s signal intensity from covered and uncovered surface

$I_{C1} = \theta I_{CBulk}$ = C 1s signal intensity from adsorbed asphaltene film of thickness (t)

$I_{C2} = (1-\theta) I_{CO}$ = C 1s signal intensity from under-layer of uncovered surface

$I_{C3} = I_{CO}\theta(e^{-t/\lambda})$ = C 1s signal intensity from under-layer of asphaltene-covered surface.

and,

θ = Fractional coverage of adsorbed asphaltene

I_{CO} = C 1s signal intensity of blank sample

I_{CBulk} = C 1s signal intensity of bulk asphaltene sample

λ = Inelastic mean free path length of C 1s photoelectrons

= 0.3 nm

Thus, equation (4.2) can be expressed in terms of experimentally measured parameters

I_{Ct}, I_{CBulk}, and I_{CO} and two unknowns – the surface coverage (θ) and asphaltene layer thickness (t).

$$I_{Ct} = \theta I_{CBulk} + (1-\theta) I_{CO} + I_{CO}\theta(e^{-t/\lambda}) \tag{4.3}$$

An implication of the adsorbed asphaltene layer being greater than 3nm is that the carbon intensity for the adsorbed asphaltene film (I_{C1}) is independent of variation in asphaltene layer thickness (if any). More importantly, it can be computed that at a thickness (t) equal to 3 nm, the term $e^{-t/\lambda}$ is a small number (4.54×10^{-5}). Accordingly, the contribution from the under-layer carbon covered by asphaltene can be neglected. Thus, equation 3 may be rearranged as follows:

$$\theta = \left(\frac{I_{Ct} - I_{CO}}{I_{CBulk} - I_{CO}} \right) \tag{4.4}$$

The surface coverage estimated using equation (4.4) was utilized to create an adsorption isotherm shown in Figure 4.8.

4.2.4 Adsorption isotherm analysis

Fractional coverage as a function of asphaltene concentration was chosen to compare the adsorption isotherms estimated from XPS data with those from QCM data. From the QCM data, the equilibrium fractional coverage at any asphaltene concentration was defined as

$$\theta = C_{AB} / C_{\max} \tag{4.5}$$

where C_{AB} (= m_{eq}) was determined by fitting adsorption data using equation (4.1) as discussed earlier, and C_{max} was obtained by fitting the mass adsorption data to the

following Langmuir isotherm expression:

$$\frac{C_A}{C_{AB}} = \frac{C_A}{C_{\max}} + \frac{1}{K_{eq} C_{\max}} \tag{4.6}$$

where, C_{AB} and C_A are surface concentration of adsorbed solute and bulk concentration of solute in the medium, respectively and have units of mg/m^2,and ppm, K_{eq} is the equilibrium constant for asphaltene adsorption on gold surface. It should be noted that an implicit assumption in using equation (4.5) is that the thickness of the adsorbed layer does not change with the amount of asphaltene adsorbed. The asphaltene fractional coverage as a function of asphaltene concentration for both XPS and QCM data as well as Langmuir isotherm fit to the data is presented in Figure below.

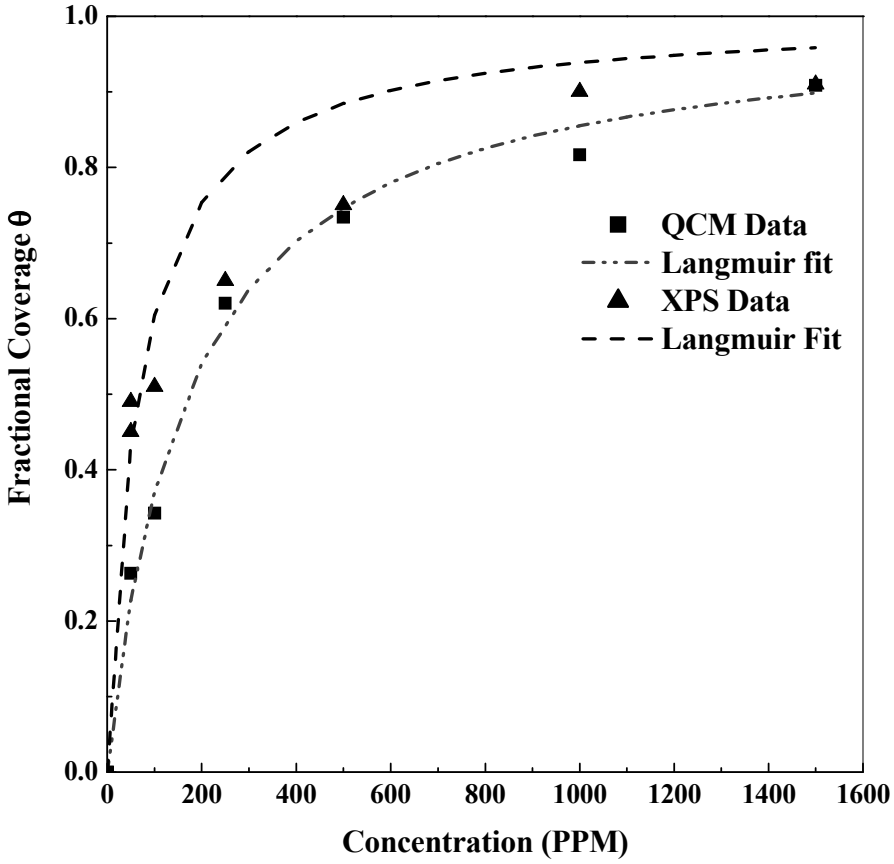

Figure 4.8 Fractional coverage data of absorbed asphaltene estimated by QCM and XPS techniques. The dotted lines represent Langmuir fit.

It can be noted that the XPS derived fractional coverage estimates are higher than those obtained from QCM measurements. The difference is especially large at lower asphaltene concentration. For XPS data, the high fractional coverage at low concentrations is likely overestimated and is attributed to the assumption, employed in data analysis, of blank gold surface being fully covered by carbon-rich under-layer. The XPS data analysis assumed that the blank gold surface was fully covered by carbon-rich under-layer and

that the surface coverage by asphaltene results in a decrease in the response of this layer proportional to the surface coverage. If, however, the blank surface is only partially covered with the carbon-rich layer, and if at low concentrations, the asphaltenes adsorb mainly on gold surface not covered by the carbon-rich under-layer, then no reduction in carbon intensity from the under-layer should result. However, the model does not consider this and, accordingly, it overestimates the surface coverage. That the blank gold surface is only partially covered by carbon-rich under-layer is also supported by indirect evidence as discussed later in the 'Summary and further discussion' section.

For the QCM data, since the fractional coverage data was estimated after fitting the mass adsorption data with Langmuir form, the good fit is not surprising. The QCM and XPS fractional coverage data was fitted with Langmuir isotherm of the following form

$$\theta = \frac{K_{eq} C_A}{1 + K_{eq} C_A} \tag{4.7}$$

The adsorption parameter (K_{eq}) was extracted from Langmuir model to compare the free energy from QCM to XPS data. The Gibbs energy of adsorption ΔG_{ads} can be calculated from the following equation (Adamson *et al*., 1997):

$$\Delta G_{ads} = -RT \ln K \tag{4.8}$$

where, ΔG_{ads} is free energy of adsorption (kJ/mol), R is the universal gas constant (0.008314 kJ/mol·K), T is the temperature (in Kelvin), and K is adsorption equilibrium constant (non-dimensional quantity). To determine free energy we first need to convert K_{eq} obtained from the isotherm data to K. This conversion, although simple, requires a

fundamental proposition regarding the adsorbate-adsorbent interaction. For instance, if it is assumed that the adsorption of A (adsorbate) on the adsorbent (B) can be represented by the following reaction:

$$A + B \longleftrightarrow AB \tag{4.9}$$

the equilibrium constant K can be expressed as:

$$K = \frac{C_{AB}}{C_A C_B} \tag{4.10}$$

where, C_{AB} (= m_{eq}) is surface concentration of adsorbed solute, and C_A is bulk concentration of solute in the medium, C_B is concentration of adsorbent. Regardless of the debate regarding the use of gravimetric versus molar concentration for C_A as discussed by Liu (2006), one major problem with the description of equation (4.9) is that the effect and or the interaction of solvent has not been considered. A better description of the system such as that employed in our study is that the adsorbate sites are covered by solvent molecule (S) which is exchanged by adsorbent (B) upon adsorption. The adsorption mechanism can thus be represented as (Hiemenz *et al*., 1997):

$$BS + A \longleftrightarrow AB + S \tag{4.11}$$

and, the equilibrium constant (*K*) can accordingly be expressed as:

$$K = \frac{C_{AB} C_S}{C_A C_{BS}} \tag{4.12}$$

where, C_{BS} is the surface concentration of adsorbed solvent and the other variables have been previously defined. The equation 12 can further be simplified to relate *K* and K_{eq} as follows:

$$K_{eq} = \frac{C_{AB}}{C_A C_{BS}} = \frac{K}{C_S} \tag{4.13}$$

In the above equation, C_S is concentration of solvent, for present study toluene was used as solvent, C_S = 862270 ppm^{-1} (equivalent to mg/l) can be used based on density of toluene. In the present study, the K_{eq} was converted to K via equation 4.13 and the free energy data of adsorption determined from both XPS and QCM generated data were found to be approximately -21 kJ/mol. The results are tabulated in Table 4.4.

Table 4.4 Free energy of adsorption from QCM and XPS data

Metal	Asphaltene Type	C_{max} (mg/m^2)	K_{eq} PPM^{-1}	K	ΔG (kJ/mol)	Technique
Gold	Cold-Lake	10.1	0.0153	13192	-23.5 ± 0.1	XPS
			0.0059	5087	-21.1 ± 0.1	QCM

The estimated free energy value of - 21 kJ/mol is on the high end of the expected range of values of physisorption (0 to −20 kJ/mol).

4.2.5 Investigation of Thickness and Orientation of Adsorbed Asphaltene

The thickness of adsorbed asphaltene layer can offer insight into asphaltene's physical state. For instance, the thickness can be related to one of the characteristic dimensions of the asphaltene entity which can further allow inference regarding its orientation at the adsorbent surface. The shape of asphaltene has been argued to be thin disk, spherical, fractal-like, oblate ellipsoids, prolate and discoid (Ravey *et al*., 1998; Acevedo *et al*., 2004; Sirota *et al*., 2005). Furthermore, it has been argued by Mullins group (Andreatta *et al*, 2005) and others (Mullins *et al*, 2007; Sztukowski *et al*, 2003) that asphaltenes even in

dilute solutions (100 ppm) exist in an associated state as nano-aggregates or micelles. The term nano-aggregate was introduced because the aggregation number was found to be in the order of 5 with dimension of aggregate in the nano scale. Many argue that "micelle' is the terminology that is preferred to be used for the one phase that is separated from a second phase by surfactant. The nano-aggregate model assumes asphaltenes to be made up of stacked layer of 5-6 macromolecules, each made of 3 or more condensed ring. Thus, one of the dimensions of the nano-aggregate can be estimated to be equal to 6 times the C-C π–bond distance, i.e. 6 x 0.143 = 0.86 nm or nearly 1 nm. The schematics of asphaltene nano-aggregate dimensions in horizontal and vertical position are shown in figure 4.9 below. Indeed, if the asphaltenes adsorb such that it does not interact face-to-face with the surface due either to preferential interaction of ends groups or to steric inhibition, the observed thickness may be more than 0.86 nm.

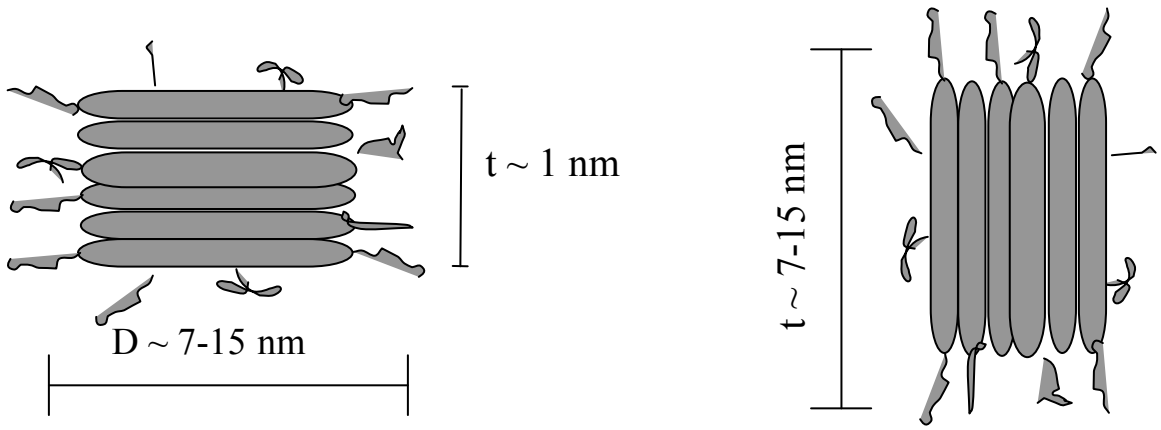

Figure 4.9 Asphaltene nano-aggregate dimensions

In this work, the thickness of adsorbed asphaltene sample was estimated from XPS data by analysis of the substrate Au 4f signal intensity of adsorbed asphaltene samples. The

total Au 4f signal is the sum of intensity through adsorbed asphaltene film and gold intensity from any uncovered surface. It is assumed that the inelastic mean free path length (λ) is independent of material it is interacting with.

$$I_{Gt} = I_{G1} + I_{G2} \tag{4.14}$$

where,

I_{Gt} = the total Au 4f signal intensity from uncovered and covered surfaces

$I_{G1} = \theta I_{G0} e^{\frac{-t}{\lambda}}$ = Au 4f signal intensity through adsorbed asphaltene film

$I_{G2} = (1-\theta) I_{Go}$ = Au 4f signal intensity from the blank sample.

and,

θ = fractional coverage of adsorbed asphaltene

I_{GO} = Gold intensity of blank sample

t = the thickness/depth of the adsorbed asphaltene (nm)

λ = inelastic mean free path length for the Au 4f photoelectrons = 2.02 nm

Thus, equation (4.14) can be rearranged after substituting appropriate expressions for I_{G1} and I_{G2}, the thickness of the adsorbed asphaltene can be estimated as

$$t = \ln\left[\frac{I_{Gt} - (1-\theta) I_{Go}}{\theta I_{Go}}\right] \times (-\lambda) \tag{4.15}$$

The thickness of adsorbed asphaltene at full surface coverage was also estimated from QCM to be equal to 9 nm using the value of computed maximum surface concentration (C_{max}) of 1.09 μg/cm^2. For the calculation, the density of asphaltene was assumed to be 1200 kg/m^3 (Alboudwarej *et al*, 2005). The adsorbed asphaltene thickness estimated from XPS and QCM data are presented in Table 4**.** 5

Table 4.5 Estimated thickness for Cold Lake asphaltene adsorbed on gold surface

Concentration (PPM)	XPS	QCM
	Thickness (nm)	Thickness (nm)
50	5.7	9
100	6.5	
250	6.8	
500	6.6	
1000	7.8	
1500	7.9	

The thickness of adsorbed asphaltene film was determined to vary over 6-9 nm which compares well with those reported in the literature (Sztukowski *et al*, 2003; Toulhoat *et al,* 1994). Toulhoat *et al* reported thicknesses ranging from 10-20 nm as measured by AFM on a mica surface. The Sztukowski *et al* estimated the thickness of asphaltene adsorbed on the oil water interface to range from 2-9 nm. By contrast, the thickness of adsorbed asphaltene on glass surface measured by ellipsometry technique was found to vary over the much wider range of 20-298 nm (Labrador *et al*., 2007). The difference in estimated thickness from the present study and that in literature may be due to the nature of the adsorbent, the concentration range, the measurement techniques employed and the nature of asphaltene itself.

The asphaltene particle diameter in toluene studied by freeze fracture-transmission electron microcopy (FFTEM) were in the range of 7-9 nm (Acevedo *et al*., 2004) studied by small angle neutron scattering (SANS) were in the range of 6-20 nm (Ravey *et al*., 1988) while light scattering techniques have suggested the average asphaltene particle

size to be 23 nm (Rajagopal *et al*., 2004). Therefore, considering the estimated thickness of adsorbed asphaltenes thickness of 6-9 nm, the calculated thickness from asphaltene nano-aggregate model of ~1nm, and the average particle diameter of adsorbed asphaltene reported in the literature ranging 6-20 nm, it is proposed that the adsorbed asphaltenes exist as nanoaggregate that are oriented vertically at the surface.

4.2.6 Summary and further discussion

Analysis of the C 1s and O 1s XPS spectra from the blank sample (asphaltene free) indicated that the Au surface is covered with a carbon-rich under-layer material with carbon present in C-O environment and an aliphatic or aromatic C-H environment. The analysis of the S 2p of blank sample also indicates that the surface also has small amount of material with sulfur-containing thiol species similar to that observed for a dodecanethiol SAM on an Au surface. These materials likely cover the surface partially, leaving some clean gold sites. It is proposed that the adsorption first takes place at clean sites followed by an over-layer formation on contaminated sites. This proposition is consistent with the observations for peak intensities for C-O environment and S 2p. It can be noted from C-O peak intensity data in Table 4.3 that for concentrations up to 250 ppm the peak intensity is reduced by less than 30% although nearly 60% of surface is covered. Also, from the S 2p peak intensity data the presence of sulfide is noticeable up to 250 ppm and very low intensity is observed at the next higher concentration examined. The presence of sulfide at low concentrations can be explained if it is considered that the asphaltenes adsorb on clean gold sites at these concentrations and the sulfur in the

asphaltene has the potential to form a bond with the metal. At higher concentration, the asphaltene also adsorbs on the carbon-rich underlayer where sulfur does not have an ability to form bond with the metal. Further, at high concentrations, response from any sulfur-metal bond formed as a result of asphaltene adsorption on clean metal is attenuated by thick layer of asphaltene coverage on the adjacent sites. Although it is hypothesized that the blank gold surface is partially covered with an underlayer, it is not possible to estimate the surface coverage of the underlayer.

4.3 A QCM and XPS study of MD Asphaltene and Comparison with Cold Lake Asphaltene

The experimental and data analysis approach applied for Cold Lake asphaltene using QCM and XPS technique was also used to investigate the MD asphaltene sample. The MD asphaltene sample was supplied by Schlumberger (DBR-Oilphase). The MD sample is known to be asphaltene derived from a crude oil that is known to have asphaltene deposition problem (Kharrat, 2007).

The kinetics of MD asphaltene adsorption followed a behavior similar to that for Cold Lake asphaltene (Figure 4.1). The kinetic results and analysis for MD asphaltene sample is presented in Appendix (C). The important part of this study was to understand differences, if any, between Cold Lake and MD asphaltene adsorption behaviour. Therefore, the isotherms of both the asphaltene samples were first compared. Next, a comparison of XPS data in terms of carbon, oxygen, sulfur and nitrogen elements is

presented. The isotherm analysis and thickness estimation was carried out with similar approach as briefly described in Cold Lake asphaltene study.

4.3.1 Adsorption Isotherm

The kinetic data for MD asphaltene adsorption on gold surface is presented in Appendix (C). The equilibrium mass of asphaltene adsorbed was estimated based on equation 4.1 using a similar approach as that employed for Cold Lake asphaltene. The following Figure 4.10 presents comparison of Cold Lake and MD asphaltene adsorption data.

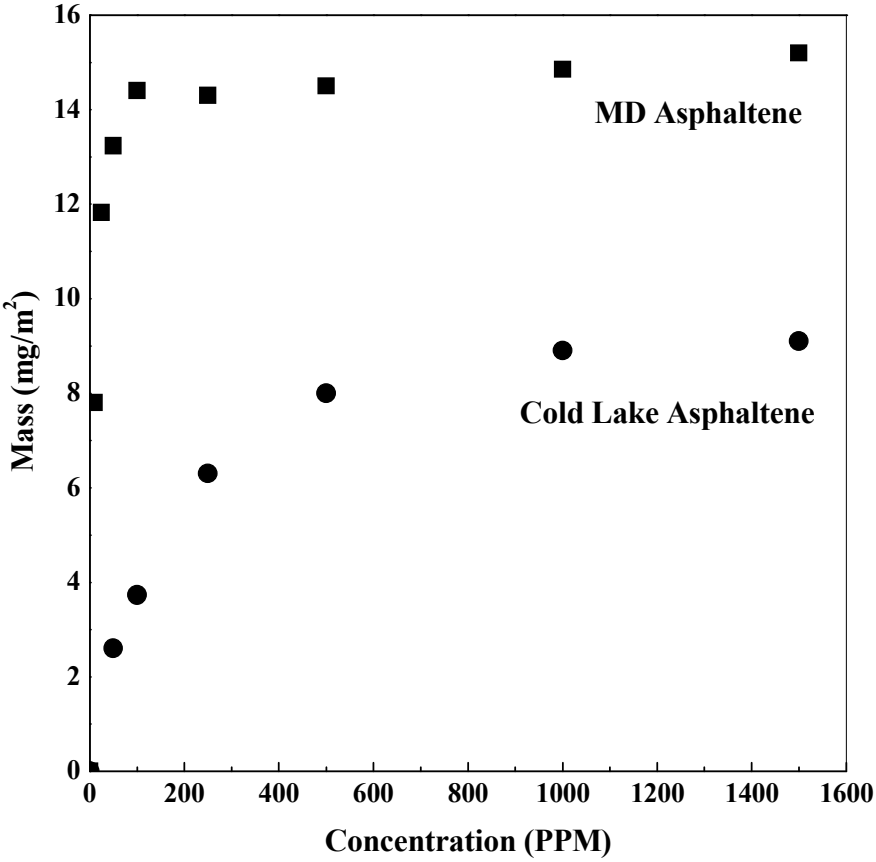

Figure 4.10 The equilibrium mass adsorption data for Cold Lake and MD asphaltenes

It is interesting to note that the equilibrium mass adsorption for MD asphaltenes was higher than that for Cold Lake asphaltenes. The estimated mass may actually be different from true mass, it may be possible that MD asphaltenes are loosely adsorbed or the adsorbed layer behaves as a viscoelastic film. Now, the mass of asphaltene adsorbed was estimated using Sauerbrey equation (3.1) which assumes that adsorbed film formed is rigid. Many films show viscoelastic behavior, which can cause significant differences in the sensor response compared to a corresponding rigid layer (Zhang *et al*., 2002). Viscoelastic losses can be correlated to motional resistance (R_m) measurements that are accessible in some QCM systems such as RQCM employed in this study. For a truly rigid film exposed to a liquid of non-varying viscosity-density, the motional resistance change measured by the RQCM should be zero. On the other hand, the motional resistance change for a viscoelastic film is non-zero. A higher increase in motional resistance indicates a film that is more loosely bound to the surface. The ratio of the resistance change to the frequency shift ($\Delta R_m/\Delta f$) can be used as a criterion to evaluate the relative influence of viscoelastic and mass loading effects (Lucklum *et al*., 1998). Therefore, the measured change in resistance with frequency shift was plotted (Figure 4.11) for Cold Lake and MD asphaltene at 1000 ppm.

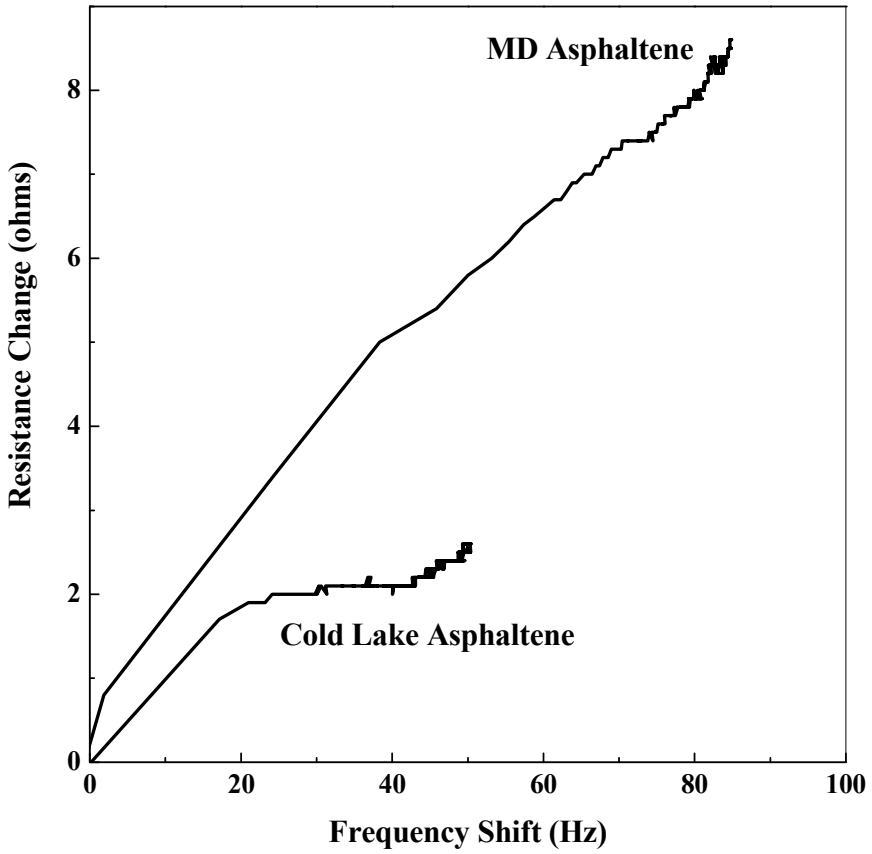

Figure 4.11 The change in resistance with frequency shift for Cold Lake and MD asphaltene at concentration of 1000 ppm

The figure 4.11 shows that change in resistance increases continuously with frequency shift for MD asphaltene whereas for Cold Lake asphaltene resistance change increases until 2 ohms with frequency shift and then reaches a plateau. The ratio of $\Delta R / \Delta f$ for MD asphaltene was 0.1 whereas for Cold Lake asphaltene 0.05. This implies an increased viscoelastic or damping contribution to the frequency measurements for MD asphaltene over Cold Lake asphaltene. Thus, the Sauerbrey equation (3.1) is not strictly valid and its

usage for mass change estimation from measured frequency change for viscoelastic films results in an overestimation of adsorption amount (Aung *et al*., 2007). The quantification of the overestimation requires independent mass measurement using a different technique. In one study (Glasmastar *et al*., 2001), surface plasmon resonance (SPR) technique was used to measure the mass of adsorbed viscoelastic film and compared with the estimated mass from QCM. It was shown that for thin (<25 nm) but very dissipative films, ($\Delta D/\Delta f$)~0.2×10^{-6} Hz^{-1} the mass or thickness can be underestimated by the factor of 2. Based on the experimental measurements of Fig 4.11 and the analyses presented in the literature, the differences in adsorption amount for MD and Cold Lake asphaltenes can be partially attributed to the overestimation of the mass data. Other factors such as chemical composition or molecular mass variation may also play a role in the observed higher mass adsorbed. For example, if the MD asphaltenes contains a larger number of condensed rings, the diameter of the nano-aggregate (refer to Figure 4.9) will not change appreciably but the mass of the MD asphaltene nano-aggregate can easily seen to be larger than the mass of the Cold Lake asphaltene nano-aggregate.

4.3.2 XPS Analysis

The high resolution spectrum for MD asphaltene sample was acquired for C 1s, O 1s, S 2p, N 1s and Au 4f under similar conditions as that of Cold Lake asphaltene. The spectra, peak fitted features and parameters are presented in Appendix (D). There was no distinct difference in peaks (for carbon, oxygen, sulfur and nitrogen) were observed compared with Cold Lake sample and Peak fitting was done in similar fashion as well. The intensity

ratio of MD asphaltene to Cold Lake asphaltene is presented in the following table 4.6. Although it can be anticipated, based on higher amounts of mass adsorbed, that MD asphaltene will show higher intensity ratio over Cold Lake asphaltene, the ratio will provide an insight on differences in the interaction of asphaltene.

Table 4.6 Relative intensity ratio of MD to Cold Lake asphaltene

Concentration (PPM)	Relative Carbon Peak Intensity		Relative Oxygen Peak Intensity		Relative Sulfur Peak Intensity	
	Main Peak (C-H)	Sub Peak (C-O and C=O)	C-O environment	C=O environment	Thiophenic	Thiol
50	1.5	0.8	0.7	1.1	1.2	0.6
100	1.5	0.5	0.5	1.1	1.4	0.7
250	1.4	1.0	0.6	1.1	1.1	1.2
500	1.2	1.1	0.6	0.9	1.1	0.0
1000	1.1	1.2	0.9	0.9	1.0	0.0
1500	1.2	1.1	0.5	0.8	1.0	0.0
Bulk (C7)	1.2	0.0	0.4	1.4	1.0	0.0

It is interesting to note that over the 50-250 ppm range, the intensity ratio of MD asphaltene to Cold Lake asphaltene for main carbon and thiopheinc species was on the higher side in the range of 1.5-1.1. This high intensity ratio was attributed to high surface coverage, the surface coverage for MD asphaltene in the concentration range of 50-250 ppm varied from 0.6-0.75 whereas for Cold Lake asphaltene it is significantly lower ranging 0.45-0.55. At concentrations above 250 ppm the surface coverage almost reaches

unity (> 0.8) and the intensity ratio of MD asphaltene over Cold Lake asphaltene reaches the ratio similar to that for the bulk asphaltenes. Although based on high mass adsorption one would expect the high intensity ratio for main C-H peak and thiophenic peak to increase, it should be noted that intensity is not sensitive enough to the thickness (based on equation 4.3). Lower C-O ratio at low concentrations (50-250) is consistent with higher coverage for MD asphaltene which masks CO in the underlayer.

4.3.3 Adsorption isotherm analysis

The fractional coverage for MD asphaltene was estimated based on XPS data from equation 4.4. For comparison purpose, the fractional coverage was also estimated based on mass adsorption data of QCM using equation 4.5. The fractional coverage data estimated is presented in Figure 4.12 below.

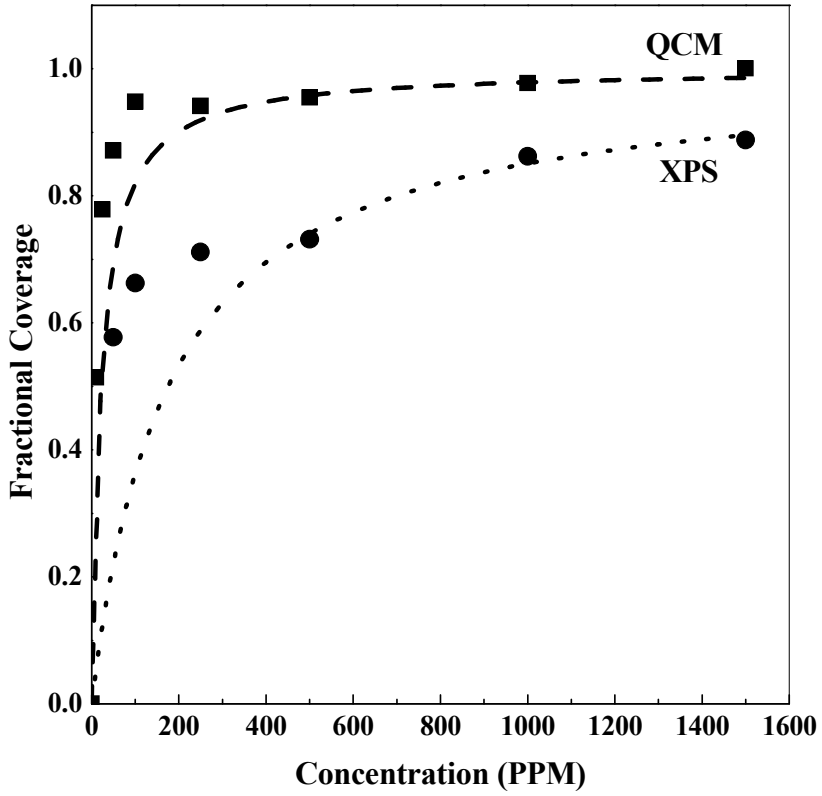

Figure 4.12 Fractional coverage data of absorbed MD asphaltene estimated by QCM and XPS techniques. The dotted lines represent Langmuir fit.

Surprisingly the fractional coverage data estimated from QCM was on higher side compared to XPS and is in contrast with data estimated for Cold Lake asphaltene (figure 4.7). As explained before the MD asphaltenes may adsorb loosely thereby over estimate the adsorption amount and fractional coverage.

The isotherm analysis was carried out as described in section 4.2.4 and data fit well with Langmuir isotherm (type-I). The free energy was estimated from equation 4.8 and is reported in table 4.7.

Table 4.7 Free energy of adsorption for MD from QCM and XPS data

Metal	Asphaltene Type	C_{max} (mg/m^2)	K_{eq} PPM^{-1}	K	ΔG (kJ/mol)	Technique
Gold	MD	15.2	0.006	4914	-21.1 ± 0.1	XPS
			0.046	39319	-26.2 ± 0.1	QCM

Again the free energy value estimated from QCM and XPS data matches well and is higher side of typical physisorption value (0 to −20 kJ/mol).

4.3.4 Thickness of adsorbed asphaltene

The thickness of adsorbed asphaltene was estimated based on XPS and QCM data with equation 4.15 as described in detail in section 4.2.5. The estimated values are reported in the following table 4.8

Table 4.8 Thickness data of adsorbed MD asphaltene on gold surface

	XPS	QCM
Asphaltene Sample	Thickness (nm)	Thickness (nm)
MD Asphaltene	7-8	12
Cold Lake Asphaltene	6-8	9

The thickness estimated from QCM for MD asphaltene was 12 nm and from XPS data 7-8 nm. It must be noted that viscoelasticity was not taken into account in estimation of thickness from QCM. This may have caused the higher estimation of thickness. Regardless, the estimated thickness from XPS data for Cold Lake and MD asphaltene matches well. Based on thickness data it can be concluded that MD asphaltene molecule orient vertically when adsorbed.

4.3.5 Summary

Interestingly, the equilibrium mass adsorbed estimated based on QCM data was found to be significantly higher with MD asphaltene compared with Cold Lake asphaltene. This difference can be attributed to the higher association state of asphaltenes, over estimation resulted due to possibility of asphaltenes adsorbed loosely on metal surface and any variation in the chemical nature of asphaltenes. The XPS data revealed more adsorption of aromatic or aliphatic carbon containing species of MD asphaltenes compared with Cold Lake asphaltenes. This could also be partly responsible for higher amounts of MD asphaltene adsorption. The MD asphaltenes follow a Langmuir (type-I) isotherm. The free energy estimated based on QCM and XPS data match well and was found to be -21.1 to -26.2 ±0.1 kJ/mol. The thickness of adsorbed asphaltene varied between 7-12 nm indicating the asphaltenes are oriented vertically when adsorbed.

4.4 XPS Study of Heavy Oil 2 (HO2) Asphaltene and Sub-Fraction

To investigate if specific species were preferentially adsorbed on gold surface, XPS analysis of asphaltene and its two sub-fractions adsorbed were carried out. The sub-fractionation was based on polarity and solubility. The Heavy Oil 2 asphaltene and sub-fraction samples were supplied by DBR Schlumberger, who did not provide details of the procedure because of proprietary nature of the separation technique. The HO2 asphaltene was fractionated into seven subfractions named F1, F2, F3 to F7. The F1 asphaltene

subfraction sample was known to be most polar and the polarity of asphaltene sample decreased from F1 to F7. The asphaltene subfractions used in this study were F3 and F7 asphaltene and F3 asphaltene was known to be more polar than F7 asphaltene. The asphaltene adsorbed samples were prepared by allowing adsorption on gold surface from their respective solution at 500 ppm.

4.4.1 XPS analysis of heavy oil asphaltene and sub-fraction

The high resolution XPS scan was acquired for C 1s, O 1s, S 2p, N 1s and Au 4f for asphaltene and sub-fraction sample of Heavy Oil 2. The scanning parameters were kept the same that of cold lake asphaltene sample. The peak fit parameters are presented in appendix (E). The N 1s spectra were not presented below as noise to signal ratio was high making the quantification difficult.

4.4.1.1 Carbon 1s Spectra

The C 1s spectra are presented in figure 4.12 below for C7, F7 and F3 asphaltene adsorbed at 500 PPM on gold surface. The intensity data is also included as an inset table.

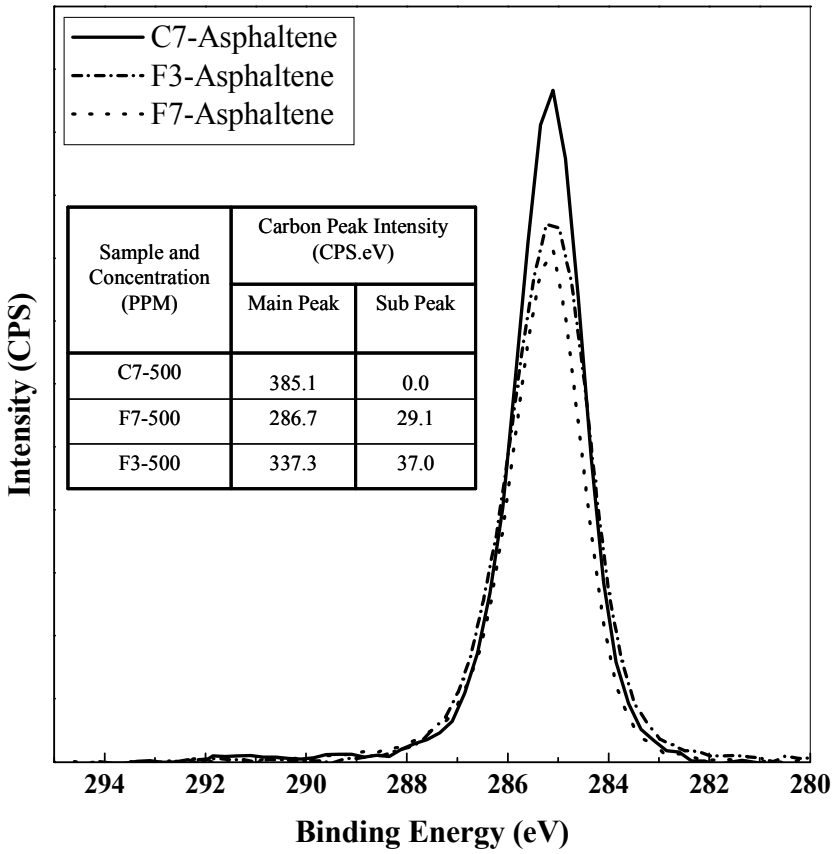

Sample and Concentration (PPM)	Carbon Peak Intensity (CPS.eV)	
	Main Peak	Sub Peak
C7-500	385.1	0.0
F7-500	286.7	29.1
F3-500	337.3	37.0

Figure 4.13 C 1s XPS spectra for C7, F7 and F3 asphaltene adsorbed on gold surface at 500 ppm. The inset table presents the data of peak intensity.

The C 1s peaks were curve resolved into main peak and sub peak in similar fashion as that of MD and Cold Lake asphaltene. It could be argued that C 1s peak was resolved with single main peak regardless it may be safe to conclude that there were no distinct differences in functional group were observed over the carbon 1s region. The C7-Asphaltene shows higher intensity followed by F3 and F7 asphaltenes indicating the variation in content of aromatic and aliphatic carbon containing species. The F3

asphaltene was known to be more polar than F7 asphaltene. The F3 asphaltene may have shown higher affinity towards the gold surface and resulted into higher surface coverage. Therefore, F3 asphaltene have shown higher intensity compared with F7 asphaltene.

4.4.1.2 Oxygen 1s Spectra

The O 1s spectra for C7, F7 and F3 asphaltene adsorbed at 500 PPM on gold surface are presented in figure 4.13 below. The intensity data is also included as an inset table.

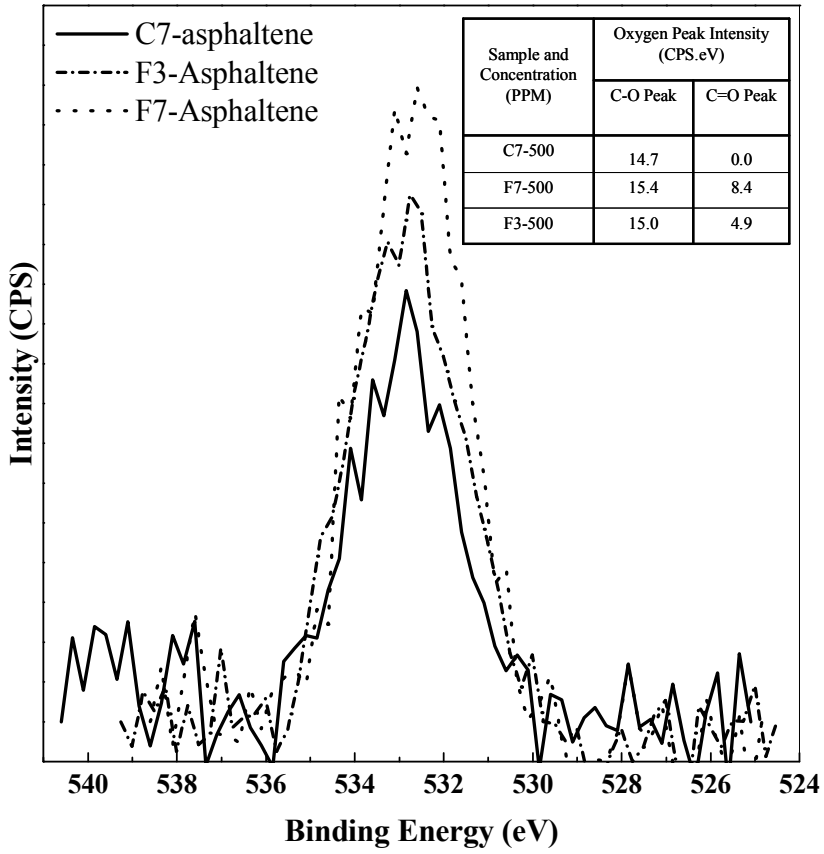

Sample and Concentration (PPM)	Oxygen Peak Intensity (CPS.eV)	
	C-O Peak	C=O Peak
C7-500	14.7	0.0
F7-500	15.4	8.4
F3-500	15.0	4.9

Figure 4.14 O 1s XPS spectra for C7, F7 and F3 asphaltene adsorbed on gold surface at 500 PPM. The inset table presents the data of peak intensity.

The oxygen O 1s peak was resolved into two peaks at binding energy 531.5 and 533 eV is similar way as that of Cold Lake and MD asphaltene sample. The C7 asphaltene peak was curve resolved into single peak whereas the F3 and F7 asphaltenes were curve resolved into two. There were no distinct differences in functional group were observed except the variation in the intensity. The C7-Asphaltene showed lowest intensity whereas F7 showed highest intensity. This variation in intensity was anticipated based on the differences in surface coverage, which is correlated to the main carbon peak data.

4.4.1.3 Sulfur 2p Spectra

The S 2p spectra for C7, F7 and F3 asphaltene adsorbed at 500 PPM on gold surface are presented in figure 4.14 below. The intensity data is also included as an inset table.

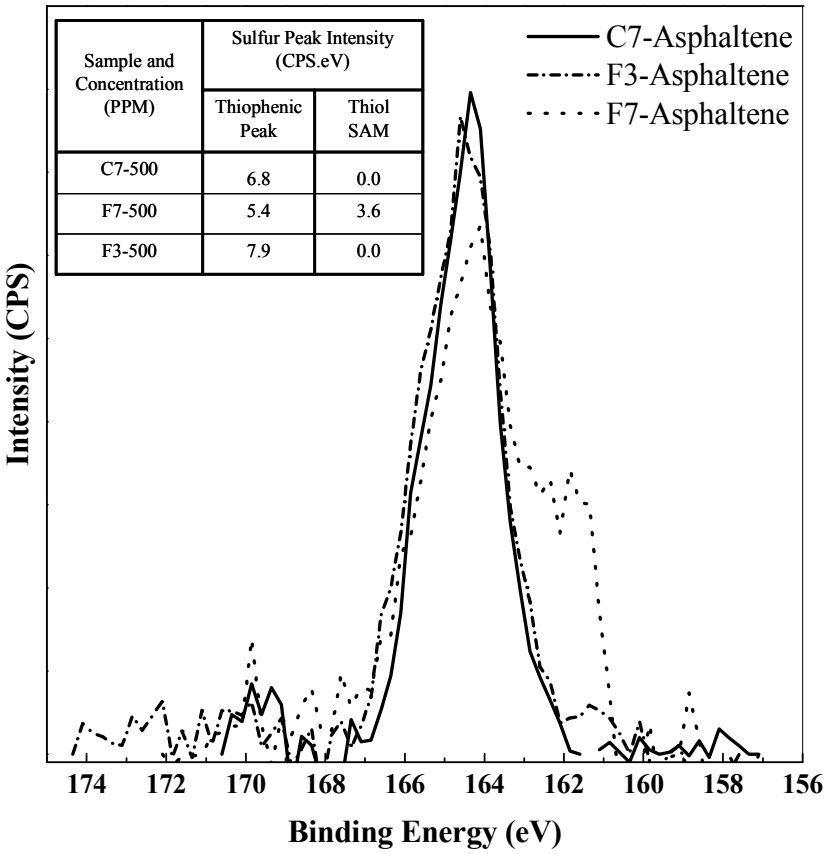

Figure 4.15 S 2p XPS spectra for C7, F7 and F3 asphaltene adsorbed on gold surface at 500 PPM. The inset table presents the data of peak intensity.

The sulfur 2p peaks were curve resolved into similar fashion as that of MD and Cold Lake asphaltene. The F7 asphaltene showed an additional shoulder in the biding energy region of 160-162 eV. The C7, F7 and F3 asphaltenes indicated presence of thiophenic species whereas an additional shoulder for F7 asphaltene was attributed to thiol species. The XPS analysis of blank gold surface has revealed the presence of thiol species due to any surface contamination. At concentration above 250 ppm surface more than 50 percent of the surface is covered for Cold Lake and MD asphaltene samples and, therefore,

presence of thiol species was not anticipated. The F3 and C7 asphaltene did not show any Thiol species as expected. The presence of thiol species for F7 asphaltene can be related to low surface coverage based on main carbon (C-H) data.

4.4.2 Summary

The adsorbed heavy oil asphaltene - C7, F7 and F3 asphaltene did not reveal any significant differences in functional group. The variations in intensities of the carbon, oxygen and sulfur spectrum were observed indicating the variation in the content of adsorbed species.

4.5 Asphaltene Adsorption on Stainless Steel Surface

A QCM and XPS experiments of Cold Lake asphaltene were also conducted on stainless steel surface. The objective was to see any differences in interaction of asphaltenes with stainless steel and gold surfaces. The stainless steel crystals were supplied by Tangidyne Corporation, USA and variation in composition and heterogeneity among the samples was anticipated. In the following subsections a kinetic study using QCM is reported followed by XPS analysis.

4.5.1 Cold Lake asphaltene adsorption kinetics on stainless steel surface

The QCM experiments were performed with same experimental protocols as mentioned in chapter 3 (3.2.3). Asphaltene solutions in toluene were prepared concentration range of 50-1500 ppm. The stainless steel crystals supplied by Tangidyne Corporation were used

in QCM experiments. The mass adsorption data Vs time estimated based on frequency change is reported in following figure 4.15.

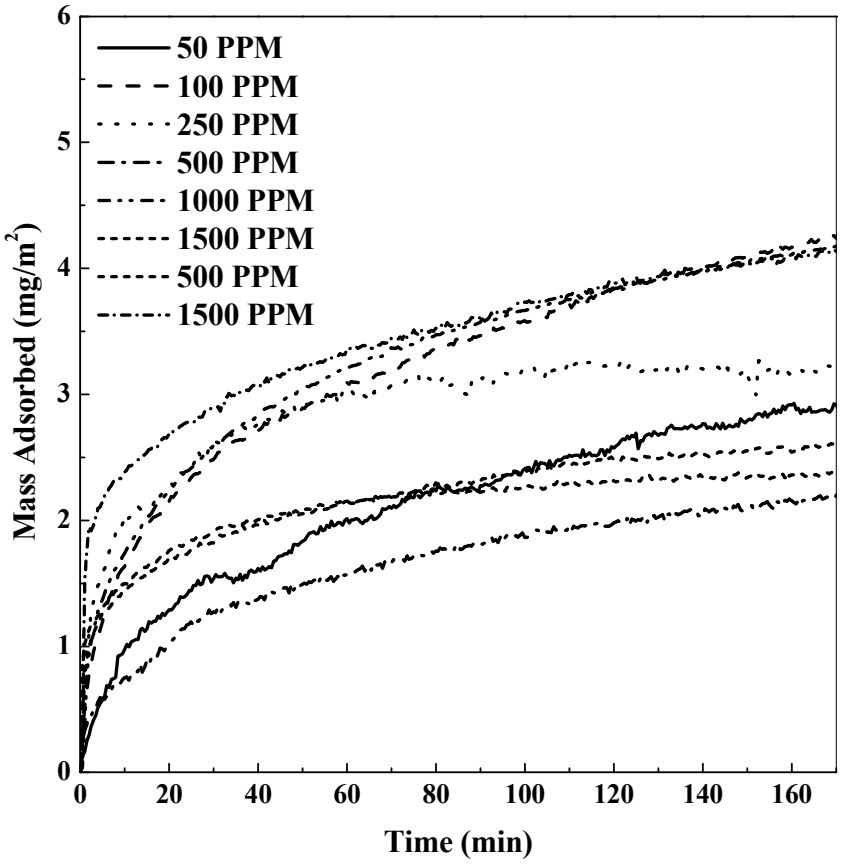

Figure 4.16 Kinetics of asphaltene adsorption on stainless steel surface

The kinetic data showed a similar response as that on the gold surface therefore rapid initial response followed by gradual increase in mass. However, the mass adsorption amount did not increase with an increase in concentration and rather an erratic behaviour was observed. Although the reason for this erratic behaviour is not clearly understood, it

can partially attributed to the surface composition variability of the stainless steel surface. However, more experiments were required to perform to generalize the findings.

4.5.2 XPS Spectral Analysis

The XPS spectra were acquired under the similar parameters as briefly mentioned in chapter 3 (3.3.3). The scan was obtained over carbon, oxygen, nitrogen, sulfur and iron elements. The peak fitted features for these elements are reported in appendix (F). The following subchapters present the detail discussion over these elements.

4.5.2.1 Carbon Spectra

The carbon 1s spectra for asphaltene adsorbed on stainless steel surface, the blank (pre-cleaned) stainless steel surface and bulk asphaltene are presented in fig 4.16. It can be seen that the nature of carbon 1s spectra recorded for Cold Lake asphaltene adsorbed on stainless steel surface show similar features as that of Cold Lake asphaltene, MD asphaltene and Heavy Oil 2 asphaltene adsorbed on gold surface.

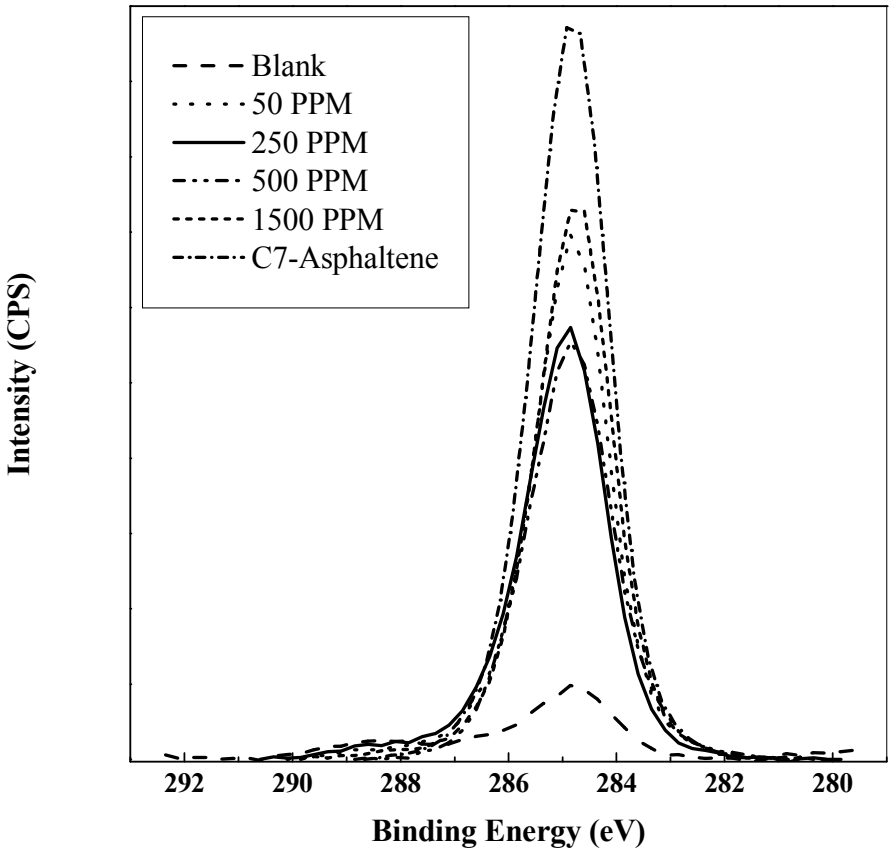

Figure 4.17 C 1s XPS spectra for Cold Lake asphaltene adsorbed on stainless steel surface, bulk Cold Lake asphaltene (C7) and blank stainless steel surface.

The peak fit was carried out in same fashion as shown in Figure 4.3 i.e. main peak and sub peak. The peak fitted features and peak intensity data is presented in Appendix (F). Although the carbon spectra of stainless steel surface did not revealed any differences in bonding of the carbon species when compared with gold surface, the inconsistency of data which was observed in QCM experimental results was also seen with XPS results. The inconsistency in experimental results can be attributed to variability of surface composition or surface characteristics of one surface to another.

4.5.2.2 Oxygen Spectra

The oxygen 1s spectra for Cold Lake asphaltene adsorbed on stainless steel surface from concentration of 50-1500 PPM, the bulk Cold Lake asphaltene (C7) and blank (pre-cleaned) stainless steel surface is shown in figure 4.17 below. Each spectrum was fitted with two sub peaks typical peak fit is shown as an inset to figure 4.17 at 500 PPM.

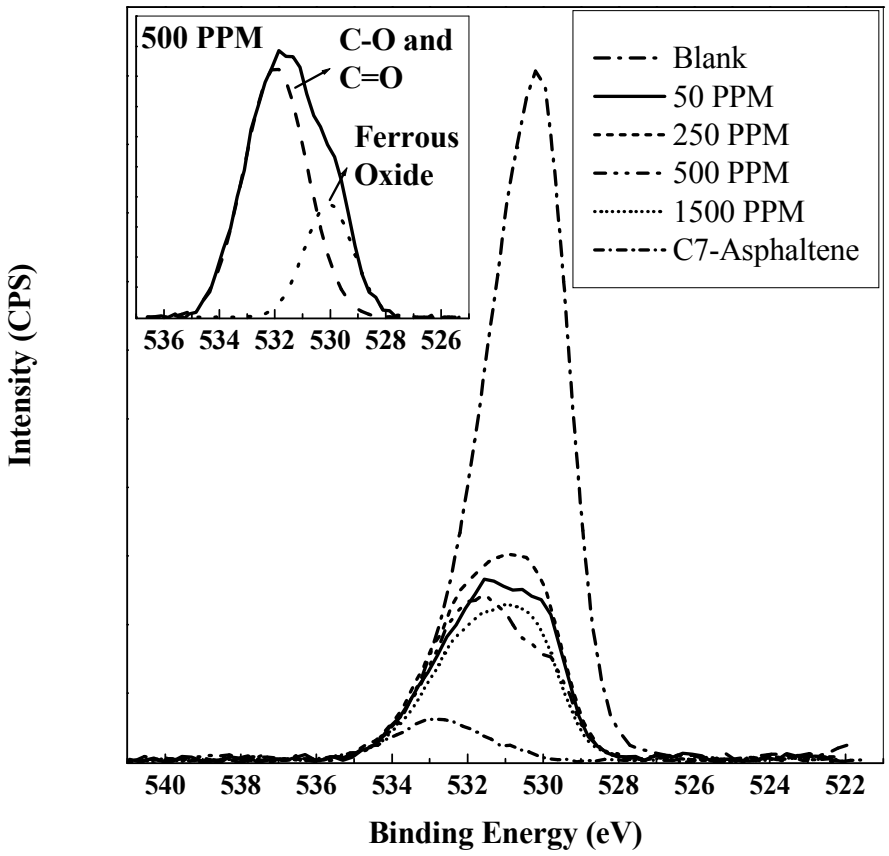

Figure 4.18 O 1s XPS spectra for Cold Lake asphaltene adsorbed and bulk (C7) and blank stainless steel surface and inset graph presents the peak fitted feature at 500 ppm.

The sub peak at lower binding energy (530 eV) corresponds to the ferrous oxide film and sub peak at higher binding energy (531.8 eV) can be attributed to the carbon single and double bond with oxygen atom. Oxygen peak intensity was observed highest for blank sample and decreased for adsorbed asphaltene sample and was lowest for bulk asphaltene sample. The inconsistency of trend in adsorbed asphaltene sample as observed for carbon peak intensity was expected.

4.5.2.3 Sulfur Spectra

The sulfur 2p spectra for adsorbed Cold Lake asphaltene, the bulk Cold Lake asphaltene (C7) and blank (pre-cleaned) stainless steel surface is shown in figure 4.18 below. The XPS 2p spectra made up of $Sp_{3/2}$ and $2p_{1/2}$ was peak fitted with 2:1 relative intensity separated in energy by 1.2 eV. The $Sp_{3/2}$ peak position at 164.1 and 166 eV corresponds to thiophenic and sulfoxide forms (Siskin *et al*., 2006). The inset to the figure 4.18 presents the peak fitted features at 50 PPM.

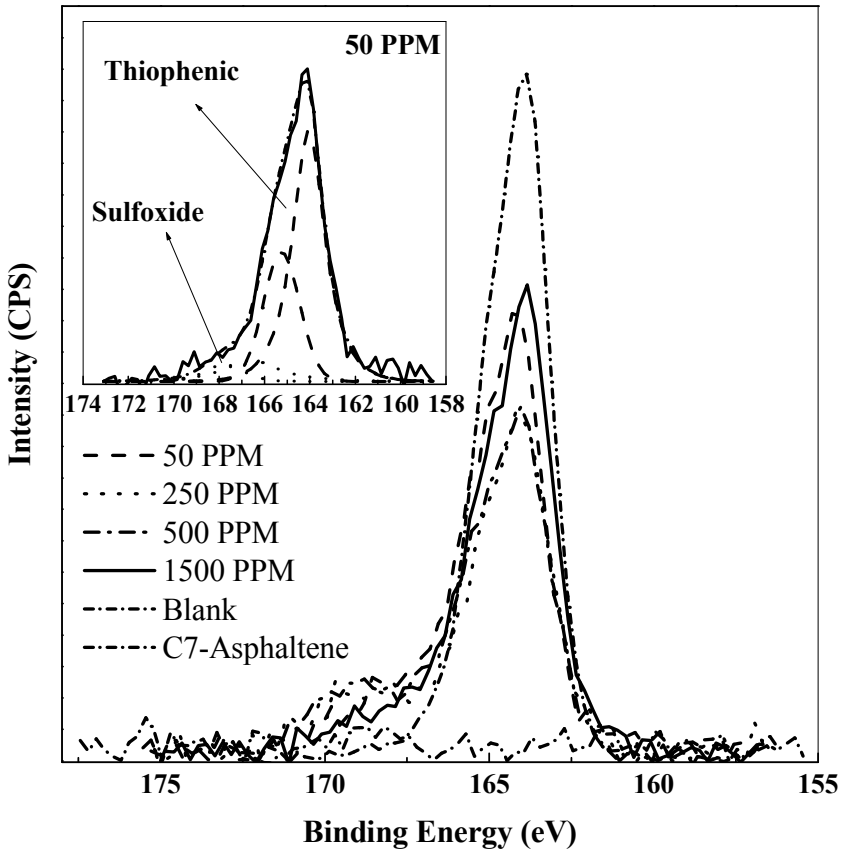

Figure 4.19 S 2p XPS spectra for blank stainless steel surface, adsorbed Cold Lake and bulk asphaltene sample. The inset graph presents the peak fitted features at 50 ppm

The sulfur 2p XPS spectral analysis of adsorbed asphaltene showed presence of thiophenic and sulfoxide species however the bulk asphaltene (C7) only indicated the presence of thiophenic species. The formation of sulfoxide species on stainless steel surface can simply be explained by interaction of sulfur with ferrous oxide film. The O 1s spectra analysis on stainless steel surface revealed the presence of ferrous oxide film. The

key distinguishing feature of S 2p XPS spectral analysis between gold and stainless steel surface was that gold surface indicated thiol species whereas the stainless steel surface showed sulfoxide species.

4.5.2.4 Nitrogen Spectra

The nitrogen 1s spectra for adsorbed Cold Lake asphaltene on stainless steel surface showed a significant noise making the quantitative analysis very difficult. Regardless the observed spectrum showed similar nature as seen on gold surface therefore indicating the presence of pyridinic and pyrrolic species.

Chapter 5

Conclusions and Recommendations

5.1 Conclusions

The overall objective of the thesis - investigation of asphaltene-metal interactions - was achieved via a combined QCM and XPS study for two different asphaltenes - Cold Lake and MD asphaltenes. The kinetics and equilibrium behaviour of asphaltene adsorption was investigated using QCM experimentation. The XPS analysis generated information on the functional groups for the adsorbed and bulk asphaltene.

There are several original contributions of this work. This is the first study that uses two very different techniques - QCM and XPS – concurrently to investigate asphaltene adsorption behaviour. Thus, the surface coverage of adsorbed asphaltene is assessed by two complementary techniques. The mathematical model developed to analyze XPS data for estimation of fractional surface coverage is not only the first one applied for asphaltene adsorption but also for any adsorption study. This work is the first study wherein the chemical speciation of adsorbed asphaltenes as a function of asphaltene concentration using XPS analysis has been carried out.

There are several specific findings of the experimental study. The kinetic study of the Cold Lake and MD asphaltene indicated that the adsorption process exhibits a rapid initial step followed by gradual increase in mass towards the equilibrium level. The

kinetic analysis of asphaltene adsorption data revealed that the process is diffusion controlled at initial times and follows first-order adsorption kinetics at longer times. The XPS spectrum analysis of the Cold Lake and MD asphaltene over carbon, oxygen, sulfur and nitrogen elements revealed presence of carboxylic, thiophenic, thiol, pyridinic and pyrrolic type functional groups. The fractional coverage data estimated from analyses of XPS and QCM experimental results followed a Langmuir type (Type-I) isotherm for Cold Lake and MD asphaltene. The MD asphaltene showed higher amounts of adsorption compared with Cold Lake asphaltene. This difference can be attributed to the higher association state of asphaltenes, over estimation resulted due to possibility of asphaltenes adsorbed loosely on metal surface or any viscoelastic losses and any variation in surface coverage or any interaction. The free energy estimated based on QCM and XPS data match well and was found to be -21.1 to -26.2 ±0.1 kJ/mol for Cold Lake and MD asphaltene. The thickness of adsorbed asphaltene varied over 8-12 nm range. Considering the asphaltene nano-aggregate model, it is proposed that the asphaltenes are oriented vertically when adsorbed.

The Cold Lake asphaltene adsorption study on stainless steel surface employing the QCM and XPS technique was also investigated. Although features of adsorption kinetics and nature of species were similar to that found for gold surface, the asphaltene adsorption on stainless steel surface showed no particular trend as a function of asphlatene concentration in solution. The XPS spectral analysis indicated presence of thiophenic, sulfoxide, ferrous oxide, pyrolic, pyridinic, C-H species in aromatic or aliphatic form and

carbon-oxygen bond species.

The XPS study on Heavy oil 2 asphaltene and its sub-fraction was conducted to investigate any differences in functional group when adsorbed at 500 ppm on gold surface. The XPS spectral analysis of heavy oil 2 asphaltene and its sub-fraction did not show any differences in species although small differences in intensity were observed.

5.2 Recommendations

The combined XPS and QCM study has offered several key insights - how fast the asphaltene adsorption on metal surfaces is, what the extent of asphaltene adsorption on metal surfaces is, and what the nature of asphaltene species interacting with the metal surfaces is. It is useful to emphasize that asphaltene are complex mixture of compounds. It is further proposed that asphaltenes to be fractionated in 4-5 sub-fractions and interaction of these individual fractions with metal surface be investigated with combined QCM and XPS study. This may help in investigating a particular fraction which shows high affinity or interaction with metal surface. This can help develop specific schemes for minimizing or mitigating the asphaltene deposition process.

It is also imperative to note that asphaltene deposition process involves several complex steps including asphaltene-asphaltene and resin-asphaltene interactions. It is proposed that asphaltene-asphaltene interactions to be studied by first adsorbing an initial layer of asphaltene on metal surface and then exposing this surface to a high concentration of asphaltene solution with a continuous monitoring of the mass change of the surface. Such

data can be generated by QCM experiments and will offer insights into asphaltene-asphaltene interactions. Similarly the asphaltene-resin interaction can also be studied to investigate the role of resins in asphaltene deposition mechanism.

References

Abdallah,W.A.; Taylor,S.D. Surface Characterization of Adsorbed Asphaltene on a Stainless Steel Surface. *Nuclear Instruments and Methods in Physics Research* **2007**, 258, 213-217.

Acevedo, S.; Ranaudo, M. A.; Garcia, C.; Castillo, J.; Fernandez, A.; Caetano, M.; Goncalvez, S. Importance of Asphaltene Aggregation in Solution in Determining the Adsorption of this Sample on Mineral Surfaces. *Colloids and Surfaces, A: Physicochemical and Engineering Aspects* **2000***, 166*, 145-152.

Acevedo, S.; Castillo, J.; Fernandez, A.; Goncalves, S.; Ranaudo, M. A. A Study of Multilayer Adsorption of Asphaltenes on Glass Surfaces by Photothermal Surface Deformation. Relation of this Adsorption to Aggregate Formation in Solution. *Energy Fuels* **1998***, 12*, 386-390.

Acevedo, S.; Ranaudo, M. A.; Garcia, C.; Castillo, J.; Fernandez, A. Adsorption of Asphaltenes at the Toluene-Silica Interface: A Kinetic Study. *Energy Fuels* **2002***, 17*, 257-261.

Acevedo, S.; Rodriguez, P. An Electron Microscopy Study of Crude oils and Maltenes. *Energy & Fuels* **2004**, 18, 1757-1763.

Acevedo, S.; Borges, B.; Quintero, F. Piscitelly, V.; Gutierrez, L. B. Asphaltenes and Other Natural Surfactants from Cerro Negro Crude Oil. Stepwise Adsorption at the Water/Toluene Interface: Film Formation and Hydrophobic Effects. *Energy & Fuels* **2005**, 19, 1948-1953.

Adamson, A. W. In Physical Chemistry of Surfaces; Wiley: New York, **1997**.

Alboudwarej, H. *Asphaltene Deposition in Flowing Systems*, The University of Calgary, Calgary, AB, Canada, **2003**.

Alboudwarej, H.; Pole, D.; Beck, J.; Svrcek, W. Y.; Yarranton, H. W. Adsorption of Asphaltenes on Metals. *Ind. Eng. Chem. Res.* **2005***, 44*, 5585-5592.

Altgelt, K.H.; Boduszynski M.M. *Composition and Analysis of Heavy Petroleum Fractions;* Marcel Dekker, Inc.: New York, **1994**.

Andersen, S. I.; Birdi, K. S. Aggregation of Asphaltenes as Determined by Calorimetry. *J. Colloid Interface Sci.* **1991***, 142*, 497-502.

Andersen, S. I.; Christensen, S. D. The Critical Micelle Concentration of Asphaltenes as Measured by Calorimetry. *Energy Fuels* **2000***, 14*, 38-42.

Andreatta, G.; Bostrom, N.; Mullins, O. C. High-Q Ultrasonic Determination of the Critical Nanoaggregate Concentration of Asphaltenes and the Critical Micelle Concentration of Standard Surfactants. *Langmuir : ACS journal of surfaces and colloids* **2005***, 21*, 2728-2736.

Aske, N. *Characterization of Crude Oil Component, Asphaltene Aggregation and Emulsion Stability by Means of Near Infrared Spectroscopy and Multivariate Analysis*, Norwegian University of Science and Technology ,Trondheim, **2002**.

Auflem, I.H. *Influence of Asphaltene Aggregation and Pressure on Crude Oil Emulsion Stability*, Norwegian University of Science and Technology ,Trondheim, **2002**.

Aung, K.M.; Ho, X.; Su, X. DNA Assembly on Straptavidin Modified Surface: A study using Quartz Crystal Microbalance with Dissipation or Resistance Measurements. *Sensors and Actuators* **2008**, B, 1-8

Bantignies,J.L.;Moulin,C.C.;Dexpert,H. Asphaltene Adsorption on Kaolinite Characterized by Infrared and X-ray Absorption Spectroscopies. *Journal of petroleum science and engineering* **1998**, 20, 233-237.

Beamson,G.;Briggs,D. High Resolution Monochromated X-ray Photoelectron Spectroscopy of Organic Polymers: A Comparison Between Solid State Data for Organic Polymers and Gas Phase Data for Small Molecules. *Molecular Physics*, **1991**, 76, 4, 919-936

Boduszynski, M. W. In *Chemistry of Asphaltenes;* Bunger, J. W., Li, N. C., Eds.; American Chemical Society: Washington, DC, **1984**; Vol. Chapter 7.

Briggs, D.; Seah, M.P.; *Practical Surface Analysis Vol 1: Auger and X-ray Photoelectron Spectroscopy, 2nd ed*.; Wiley and Sons, Inc.: New York, **1990**.

Brundle, C. R.; Evans, C.A.; Wilson, S. *Encyclopaedia of Material Characterization-Surfaces Iinterfaces,Tthin Films;* Elsevier, **1992**.

Buckley, J.S. Microscopic Investigation of the Onset of Asphaltene Precipitation. *Fuel science and technology international* **1996**, 14, 55-74.

Bunger, J.W.; Li, N.C. Chemistry of Asphaltenes. *American chemical society (Washington , DC)* **1981**

Calemma, V.; Rausa, R.; D'Antona, P.; Montanari, L. Characterization of Asphaltenes Molecular Structure. *Energy Fuels* **1998***, 12*, 422-428.

Cosultchi, A.; Rossbach, P.; Hernandez-Calderon, I. XPS Analysis of Petroleum Well Tubing Adherence. *Surface and Interface analysis* **2003**, 35, 239-245.

Cox, L.E.; Haire, R.G. X-ray-Photoemission-Spectroscopy Study of the Electronic Structure of Am Metal and AmH_x (for $x \square 2$). *Physical Review* **1992**, B 45, 13239 - 13243

Czandema, A. W.; Lu, C. In *Applications of Piezoelectnic Quartz Crystal Microbalances;* Lu, C., Czandema, A. W., Eds.; Elsevier: Amsterdam, **1984**; Vol. 7, pp 1.

Ekholm, P.; Blomberg, E.; Claesson, P.; Auflem, I. H.; Sjoblom, J.; Kornfeldt, A. A Quartz Crystal Microbalance Study of the Adsorption of Asphaltenes and Resins Onto a Hydrophilic Surface. *J. Colloid Interface Sci.* **2002***, 247*, 342-350.

Fuhr, B. J.; Cathrea, C.; Coates, L.; Kalra, H.; Majeed, A. I. Properties of Asphaltenes from a Waxy Crude. *Fuel* **1991***, 70*, 1293-1297.

Flewitt, P. E. J.; Wild, R. K., Physical Methods for Materials Characterization, 2nd Edition, Institute of Physics Publishing: Bristol, UK (2003).

Gafonova, O. V.; Yarranton, H. W. The Stabilization of Water-in-Hydrocarbon Emulsions by Asphaltenes and Resins. *J. Colloid Interface Sci.* **2001**, 241, 469-478.

Glasmastar, K.; Larsson, C.; Hook, F.; Kasemo, B. Protein Adsorption on Supported Phospholipid Bilayers. *Journal of Colliods and Interface Science* **2002,** 246, 40-47.

Gonzalez, G.; Moreira, M. B. C. The Wettability of Mineral Surfaces Containing Adsorbed Asphaltenes. *Colloids and Surfaces* **1991***, 58*, 293-302.

Groenzin, H.; Mullins, O. C. Molecular Size and Structure of Asphaltenes from various Sources. *Energy Fuels* **2000***, 14*, 677-684.

Hammami, A.; Phelps, C.H.; Monger-McClure, T.; Little, T.M. Asphaltene precipitation from Live oils: An experimental investigation of onset conditions and reversibility. *Energy and Fuel* **2000**, 14, 14-18.

Hiemenz, P.C.; Rajagopalan, R. *Principles of Colloid and SurfaceChemistry.* Marcel Dekker, Inc.: New York, **1997**.

Hirschberg, A.; DeJong, L. N. J.; Schipper, B. A.; Meijer, J. G. Influence of Temperature and Pressure on Asphaltene Flocculation. *SPEJ, Society of Petroleum Engineers Journal* **1984***, 24*, 283-293.

Institute of Petroleum (**1982**). Standard No. IP 143/82, London.

Jaroniec, M.; Madey, R. In *Adsorption on Heterogeneous Solids;* Elsevier: Amsterdam, **1988**; pp 351.

Jeribi, M.; Almir-Assad, B.; Langevin, D.; Henaut, I.; Argillier, J. F. Adsorption Kinetics

of Asphaltenes at Liquid Interfaces. *J. Colloid Interface Sci.* **2002***, 256*, 268-272.

Johnson, L. *Surface Studies of Potentially Corrosion Resistant Thin Film Coatings on Chromium and Type 316l stainless steel*, Kansas state university, Kansas, USA, **2006**.

Kanazawa, K. K.; Gordon, J. G. Frequency of a Quartz Microbalance in Contact with Liquid. *Anal. Chem.* **1985***, 57*, 1770-1771.

Karan, K.; Hammami, A.; Flannery, M.; Stankiewicz. A. B. Evaluation of Asphaltene Instability and a Chemical Control During Production of Live Oils. *Petroleum Science and Technology* **2003**, 21, 629-645.

Kawanaka, S.; Park, S. J.; Mansoori, G. A. Organic Deposition from Reservoir Fluids: A Thermodynamic Predictive Technique. *SPE Reservoir Engineering* **1991***, 6*, 185-192.

Kelemen, S. R.; Gorbaty, M. L.; Kwiatek, P. J. Quantification of Nitrogen Forms in Argonne Premium Coals. *Energy & Fuels* **1994**, 8(4), 896-906.

Kharrat, A.M. Oilphase DBR, Schelumberger, Personnel communication, 2007.

Koots, J.A.; Speight, J.C., Relation of Petroleum Resins to Asphaltenes, *Fuel*, **1975**, 54, 182-187.

Labrador, H.; Fernandez, Y.; Tovar, J.; Munoz, R.; Pereira J. Ellipsometry study of the adsorption of asphaltene films on glass surface. *Energy and Fuel* **2007**, 21, 1226-1230.

Laiho, T.; Lukkari, J.; Meretoja, M.; Laajalehto, K.; Kankare, J.; Leiro, J. Chemisorption of alkyl thiols and S-alkyl thiosulfates on Pt(1 1 1) and polycrystalline platinum surfaces. *Surface Science* **2005**, Issue 1, 83-89.

Leon, O.; Rogel, E.; Urbina, A.; Andujar, A.; Lucas, A. Study of the Adsorption of Alkyl Benzene-Derived Amphiphiles on Asphaltene Particles. *Langmuir* **1999**, *15*, 7653-7657

Liu, Y. Some consideration on the Langmuir isotherm equation. *Colloids and Surfaces* **2005**, 274, 34-36

Lopez-Linares, F.; Carbogani, L.; Sosa-Stull, C.; Pereira-Almao, P. Quinolin-65 and Violanthrone-79 as Model Molecules for the Kinetics of the Adsorption of C7 Athabasca Asphaltenes on Macroporous Solid Surfaces. *Energy and Fuel* **2006**, 20, 2748-2750.

Lucklum,R.; Behling,C.; Haupttmann, P. Gravimetric and non-gravimetric chemical quartz crystal resonators, *Seventh Technical Digest of the International Meeting for Chemical Sensors*, Beijing, China, July 27–30, **1998**, 121–123.

Marczewski, A. W.; Szymula, M. Adsorption of Asphaltenes from Toluene on Mineral

Surface. *Colloids and Surfaces, A: Physicochemical and Engineering Aspects* **2002**, *208*, 259-266.

Martin, S. J.; Granstaff, V. E.; Frye, G. C. Characterization of a Quartz Crystal Microbalance with Simultaneous Mass and Liquid Loading. *Anal. Chem.* **1991**, *63*, 2272-2281.

Miller, J. T.; Fisher, R. B.; Thiyagarajan, P.; Winans, R. E.; Hunt, J. E. Subfractionation and Characterization of Mayan Asphaltene. *Energy Fuels* **1998**, *12*, 1290-1298.

Morel, F.M.; Hering, J.P *Principles and Applications of Aquatic Chemistry*, Wiley, New York, 1993.

Mullins, O.C.; Sheu, E.Y.; Hammami, A.; Marshall, A. *Asphaltenes. Heavy oils, and petroleomics*. Springer, **2007**.

Naske, A. *Characterisation of Crude Oil Components, Asphaltene Aggregation and Emulsion Stability by means of Near Infrared Spectroscopy and Multivariate Analysis*, Norwegian University of Science and Technology ,Trondheim, **2002**.

Nellensteyn, F. J. The Colloidal Structure of Bitumens. *The Science of Petroleum* **1938**, *4*, 2760.

Nomura, T.;Okuhara, M. Frequency shifts of Piezoelectric Quartz Crystals Immersed in Organic Liquid. *Anal. Chim. Acta*. **1982**,142, 281-284.

Ostlund, J.-A.; Wattana, P.; Nyden, M.; Fogler, H. S. Characterization of Fractionated Asphaltenes by UV-vis and NMR Self-diffusion Spectroscopy. *J. Colloid Interface Sci.* **2004**, *271*, 372-380.

Ostlund, J.-A.; Wattana, P.; Nyden, M.; Fogler, H. S.; Holmberg, K Functional Groups in Fractionated Asphaltenes and the Adsorption of Amphiphilic Molecules. *Colloids and surfaces Interface*. 2004, 234, 95-102.

Papadimitriou, N. I.; Romanos, G. E.; Charalambopoulou, G. Ch.; Kainourgiakis, M. E.; Katsaros, F. K.; Stubos, A. K. Experimental Investigation of Asphaltene Deposition Mechanism During Oil Flow in Core Samples. *Journal of Petroleum Science & Engineering* **2007,** 57(3-4), 281-293.

Pernyeszi, T.; Patzko, A.; Berkesi, O.; Dekany, I. Asphaltene Adsorption on Clays and Crude Oil Reservoir Rocks. *Colloids and Surfaces, A: Physicochemical and Engineering Aspects* **1998**, *137*, 373-384.

Pfeiffer, J. P.; Saal, R. N. J. Asphaltic Bitumen as Colloid System. *J. Phys. Chem.* **1940**, *44*, 139-149.

Rajagopal, K.; Silva, S. M. C. An Experimental Study of Asphaltene Particles Sizes in n-heptane-toluene Mixtures by Light Scattering. *Brazilian Journal of Chemical Engineering* **2004**, 21, 601-609.

Ramos, A.; Harahuchi, L., Notrispe, F., Loh, W., Mohamed, R. Interfacial and Colloidal Behaviour of Asphaltenes Obtained From Brazilian Crude Oils. *Journal of Petroleum Science and Engineering* **2001**, 32, 201-216

Ravey, J. C.; Ducouret, G.; Espinat, D. Asphaltene Macrostructure by Small-angle Neutron Scattering. *Fuel* **1988**, *67*, 1560-1567.

Shedid, A.; Abbas, El Abbas A. Reversibility of Asphaltene Deposition under Dynamic Flow Conditions. *Petroleum Science and Technology* **2006**, 24(12), 1457-1467.

Sheu, E. Y.; Storm, D. A.; Shields, M. B. Adsorption Kinetics of Asphaltenes at toluene/acid Solution Interface. *Fuel* **1995***, 74*, 1475-1479.

Siegbahn, K. Atomic, Molecular and Solid State Studied by Means of Electron Spectroscopy, Nova Acta Regia. Sci., **1967,** IV, 20.

Sirota, E. Physical Structures of Asphaltenes. *Energy and Fuel* **2005**, 19, 1290-1296

Siskin, M.; Kelemen,S.R.; Eppig,C.P.; Brown, L.D.; Afeworki, M. Asphaltene Molecular Structure and Chemical Influence on the Morphology of Coke Produced in Delayed Coking. *Energy and Fuel* **2006**, 20, 1227-1234.

Speight, J. G. In *The Chemistry and Technology of Petroleum;* Marcel Dekker, Inc.: New York, **1991**.

Speight, J. G.; Moschopedis, S. E. In *Chemistry of Asphaltenes;* Bunger, J. W., Li, N. C., Eds.; American Chemical Society: Washington, DC, **1981**.

Strausz, O. P.; Mojelsky, T. W.; Lown, E. M. The Molecular Structure of Asphaltene: An Unfolding Story. *Fuel* **1992***, 71*, 1355-1363.

Sztukowski, D. M.; Jafari, M.; Alboudwarej, H.; Yarranton, H. W. Asphaltene Self-association and Water-in-hydrocarbon Emulsions. *J. Colloid Interfacial Sci.* **2003**, 265, 179-186.

Toulhoat, H.; Prayer, C.; Rouquet. G. Characterization by Atomic Force Microscopy of Adsorbed Asphaltenes. *Colloids and Surfaces A: Physiochemical and Engineering Aspects* **1994**, 91, 267-283.

Weber, W. J.; Morris, J. C. Kinetics of Adsorption on Carbon Solution. *Journal of the Sanitary Engineering Division, American Society of Civil Engineers* **1963**, 89, 31–39.

Xie, K.; Karan, K. Kinetics and Thermodynamics of Asphaltene Adsorption on Metal Surfaces: A Preliminary Study. *Energy & Fuels* **2005**, 19(4), 1252-1260.

Xie, K. *Asphaltene Adsorption on Metal Surfaces*, Queen's University, Canada, **2006**

Yarranton, H. W.; Alboudwarej, H.; Jakher, R. Investigation of Asphaltene Association with Vapor Pressure Osmometry and Interfacial Tension Measurements. *Ind Eng Chem Res* **2000***, 39*, 2916-2924.

Zhang,J.; Su, X.;O'Shea, J. Antibodyyantigen affinity behavior in liquid environment with electrical impedance analysis of quartz crystal microbalances. *Biophysical Chemistry* **2002**, 99, 31-41.

Appendix A

Troubleshooting the base line drift problem of QCM experimental Set-up

This section presents the erratic behaviour of base line observed during QCM experimentation and troubleshooting strategy employed to solve the problem. In the first part the base line drift problem is briefly been discussed followed by troubleshooting strategy and the experimental results obtained with a proper analysis is explained.

Base line drift problem of QCM

The frequency response obtained via QCM showed erratic behaviour in toluene medium. The Figure A.1 below shows typical QCM response received for air followed by toluene. As can be seen from the figure 4.3 that there was no sign of drift when the experiment was conducted in air whereas the delta frequency drifted by -18 Hz with toluene in less than an hour. The magnitude of the drift is a significant because the overall frequency change associated with asphaltene adsorption is in the order of 20-100 Hz.

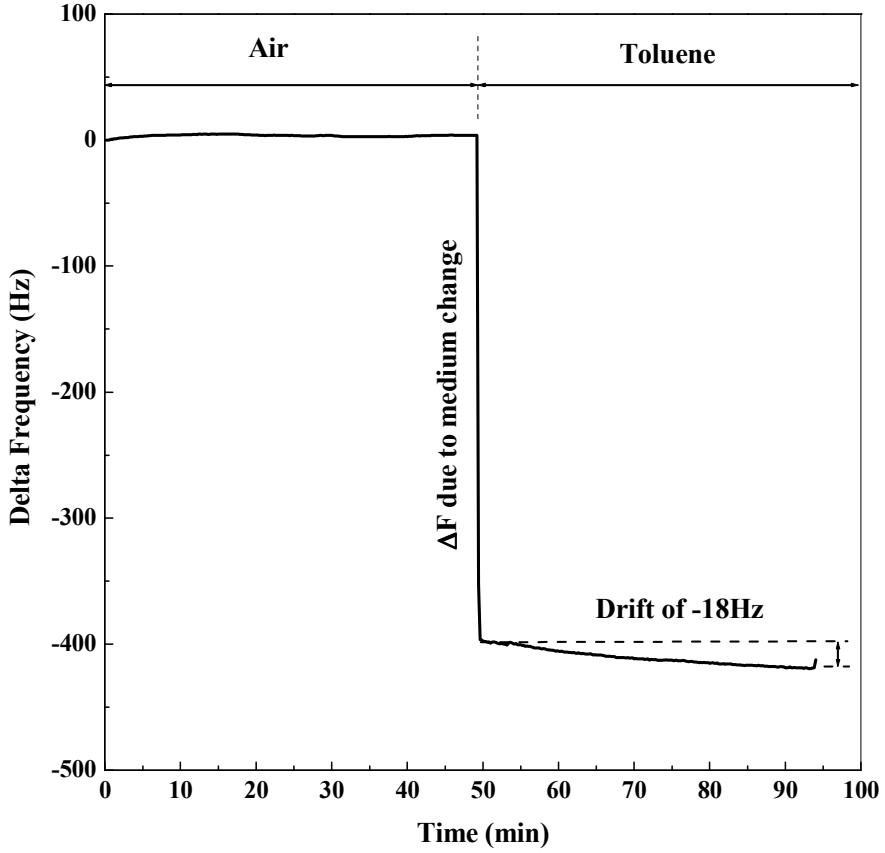

Figure A.1 Delta Frequency response for QCM exposed to air followed by toluene [25 ^{o}C; Toluene flow rate in the flow cell of 1 ml/min; gold surface].

Numerous experiments were carried out in toluene medium to investigate if any particular behavior can be observed and accounted for. The Figure A.2 presents delta frequency response of QCM with time exposed to toluene for three runs showing different behavior. The data obtained in air is not presented here in order to allow a detailed view of the drift in toluene. The run-1 and run-2 indicate that delta frequency can drift in upward or downward direction, the run-3 show trend of upward and downward

with a net effect in downward direction. On comparing runs 1, 2 and 3, it can be seen that the extent of drift is not same for three runs. If the extent and trend of the drift were similar for the different experiments, adsorption data could be corrected for all experiments via a universal equation accounting for the drift in the experiments. However, the erratic results obtained so far do not lend themselves to such a data correction strategy.

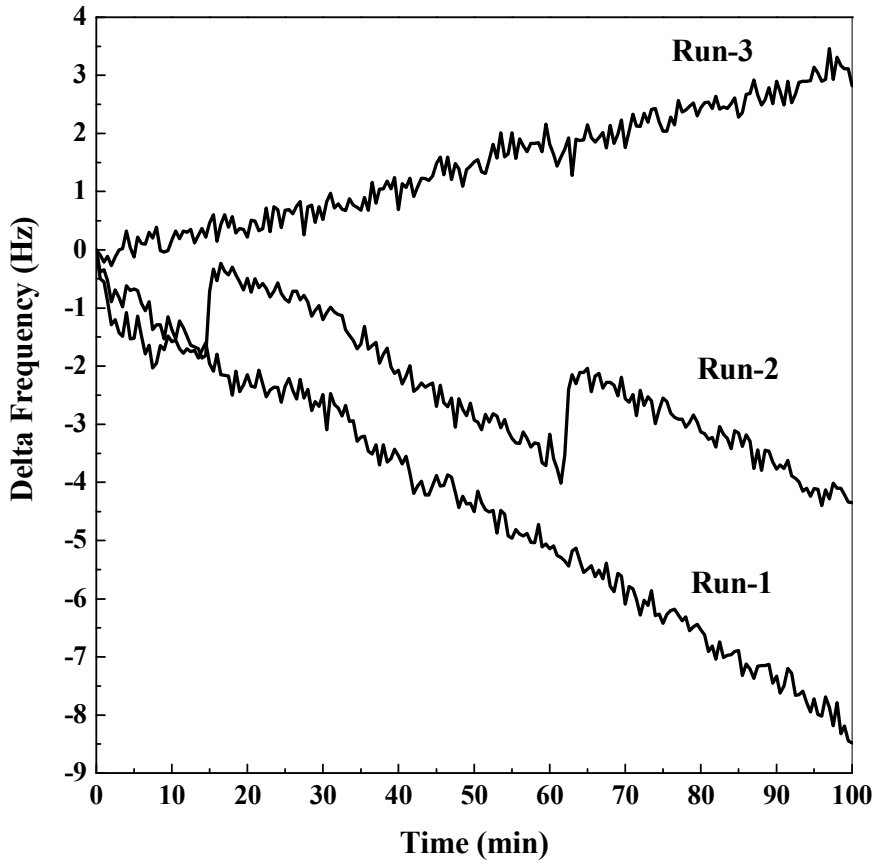

Figure A.2 Delta Frequency response for QCM exposed to toluene for three different runs on gold surface.

The experiments were also carried out in water medium to further investigate if this erratic behavior exhibits only in toluene medium. However the experiments in water showed similar drift problems.

Trouble shooting strategy

The erratic behaviour of QCM can be attributed to external factors and troubleshooting strategy was planned accordingly.

1. A new crystal holder and flow cell was employed, to check if the old crystal holder and flow cell were defective.
2. The cable connecting the RQCM to the holder was changed to rule out drift caused by faulty electronics.
3. The ambient room conditions were monitored to investigate any effect on RQCM electronics
4. The direction of the flow line was reversed to check for any pulsation effect due to the use of the peristaltic pump.
5. Static experiments were carried by eliminating the flow cell loop to check against any pump and tubing effect
6. The flow cell O ring was immersed in toluene for a week and experiments were carried out to investigate the effect of any O-ring swelling

A new crystal holder, flow cell and cable connecting RQCM to holder were employed but QCM continued to behave erratically. The other options are described in detail in the context of the experimental results in following subsections.

Investigation of effect of ambient conditions on RQCM electronics

The effect of ambient temperature and pressure was investigated by carefully monitoring the temperature and pressure along with the frequency response. The temperature of the room was monitored using a thermocouple. The experiments were carried out in similar fashion as described before except the additional monitoring of the temperature. The experimental results are provided in figure A.3 below.

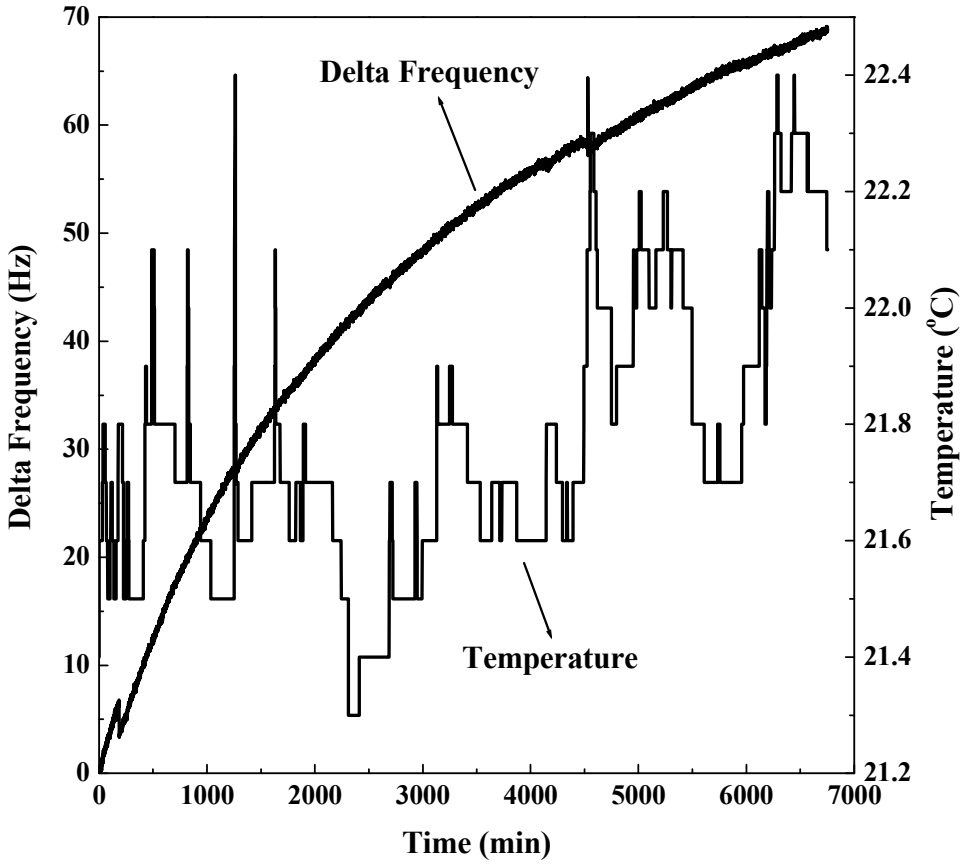

Figure A.3 Delta frequency data for toluene medium and temperature data of room for investigation of any temperature effect on frequency response.

The data in figure A.3 indicates that temperature of room does not have any effect on frequency response. The temperature of room fluctuated however the delta frequency continued to drift in upward direction. The atmospheric pressure data was obtained from weather network website. The experimental results are provided in figure A.4 below.

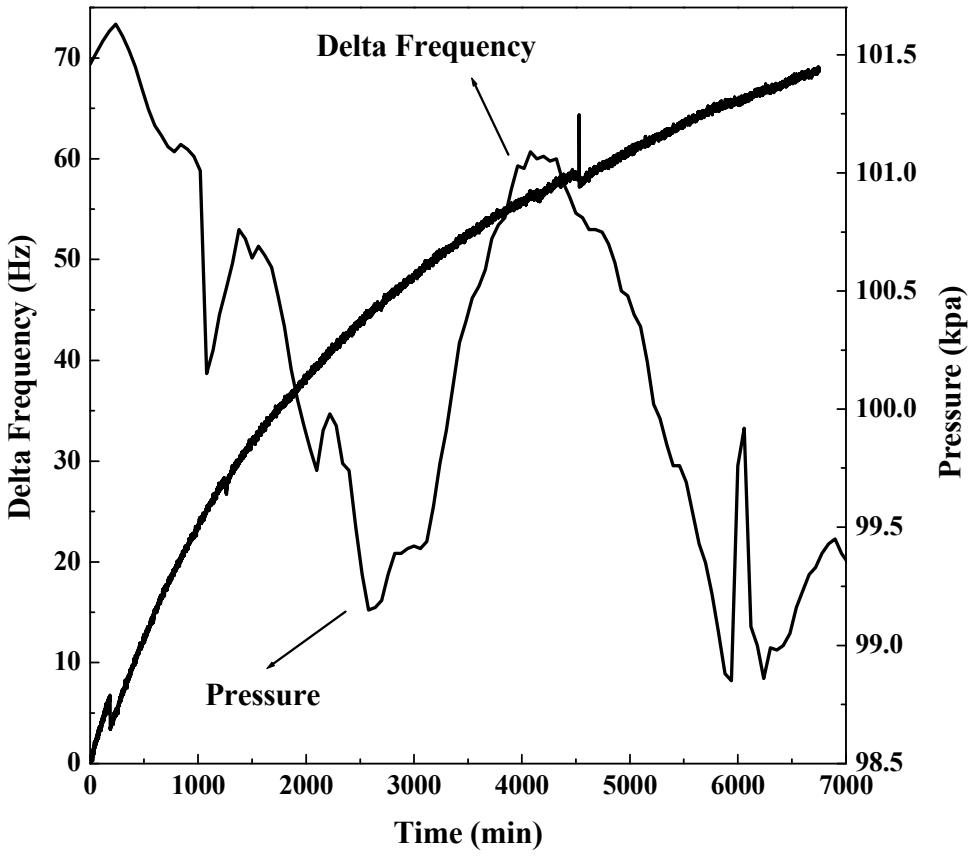

Figure A.4 Delta frequency data for toluene medium and pressure data of room for investigation of any pressure effect on frequency response.

The figure A.4 indicate that the atmospheric pressure dose not have any impact on

frequency response, the further investigations were continued.

Examination of any effect related to reversal of flow line direction on frequency response

The direction of flow line was reversed to check against any pulsation effects. The normal procedure employed was to pull the liquid from crystal surface, the reversal of flow line direction pushed liquid on crystal surface. The experimental results are outlined in figure A.5 below. The delta frequency drop observed was around -28 Hz in 165 min.

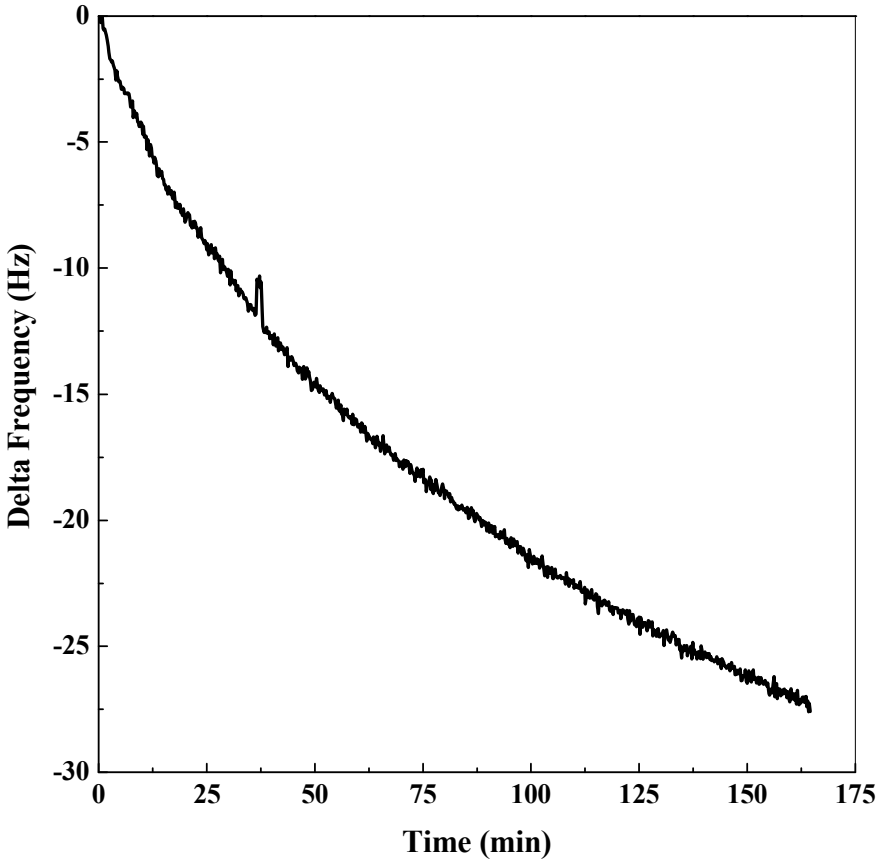

Figure A.5 Delta Frequency response for QCM exposed to toluene after direction of flow reversal.

The comparison of figure A.1 with A.3 clearly indicates that the problem of drift gets aggravated after the reversal of direction of flow. It is more likely that pulling of the liquid from flow cell provides pulse less flow when compared with pushing the liquid on crystal surface.

Static Experiments

The batch experiments were conducted by removing flow cell loop to check against any pump or tubing effect. The experiments were carried out in beaker immersed in temperature controlled water bath. The experimental results are provided in figure A.6 below. As can be seen from the figure that frequency drift problem continues even at longer time. The drift at initial times (0-60 min) can be anticipated due to the time required to reach thermal equilibrium. However at longer times the drift continues and is higher in magnitude than with flow cell and pump is use. These experiments realize the importance of employing the flow cell.

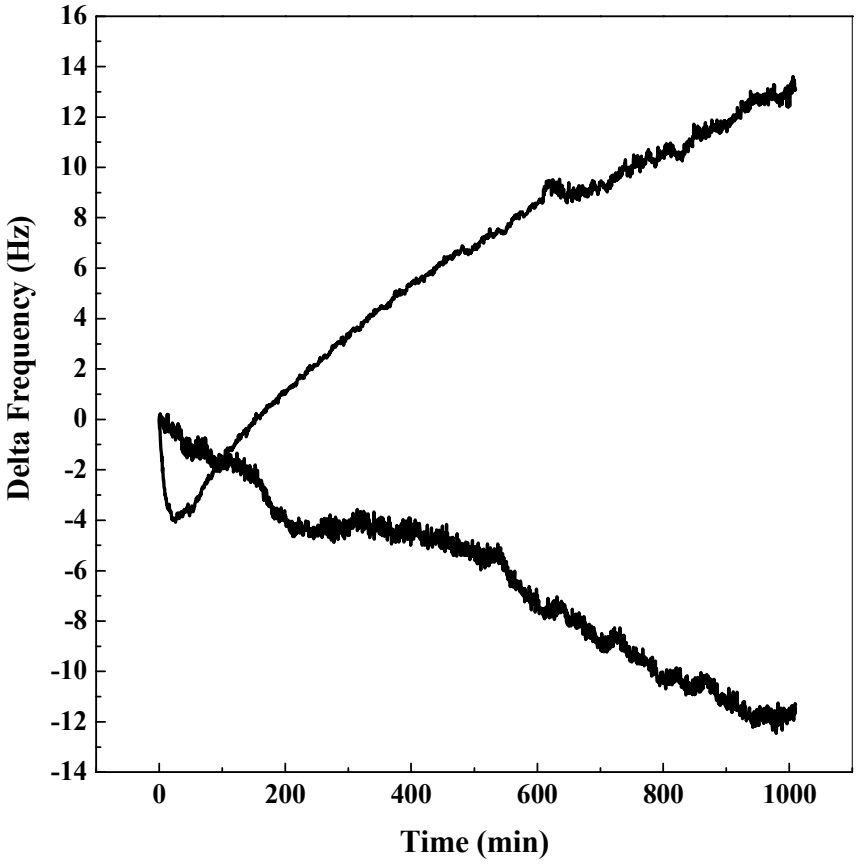

Figure A.6 Delta Frequency response for QCM exposed to toluene under static flow conditions

Examination of effect of O-ring swelling on frequency response

Toluene is considered as highly reactive material and it was hypothesized that toluene can cause swelling of the O-ring of flow cell. The swelling of O ring can put additional pressure or stress on crystal surface causing the frequency to drift. The flow cell was planned to be soaked in toluene for a week time followed by gentle blow dry in nitrogen.

The routine experimental procedures were carried out; the experimental results are presented in figure A.7 below.

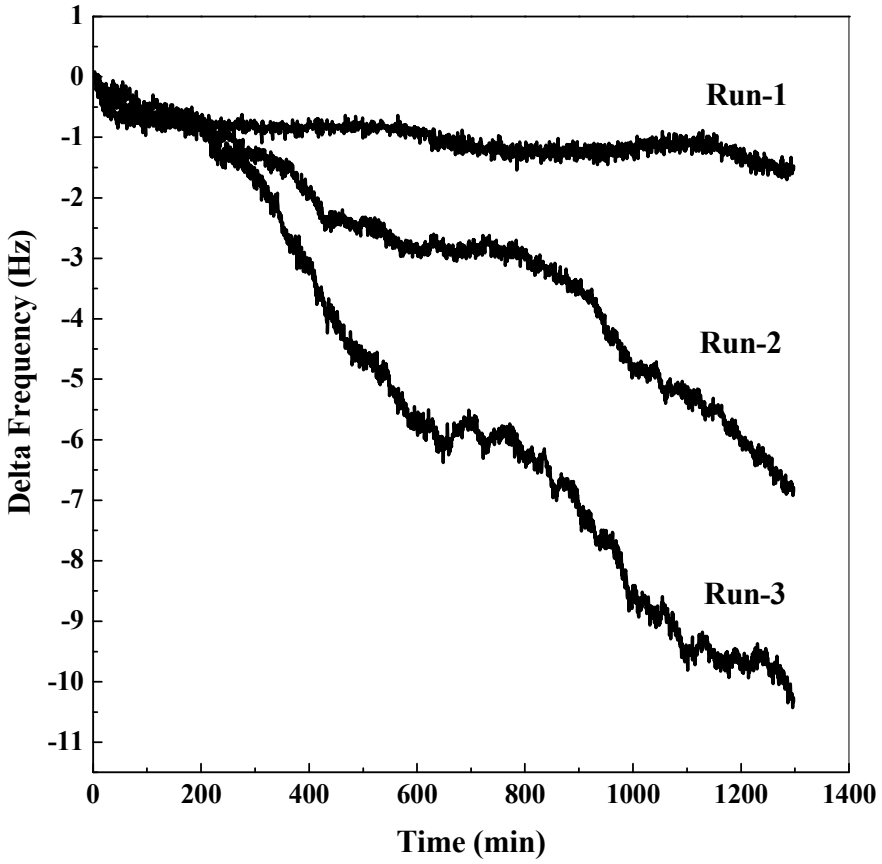

Figure A.7 Delta Frequency responses for QCM exposed to toluene after soaking the flow cell O-ring for a week in toluene.

Three different runs were conducted under similar conditions. The run-1 was very satisfactory with a drift of only -2 Hz in 1200 min, however run-2 and run-3 showed respectively higher drifts. The O-ring swelling can partly be seen as a reasonable

explanation for base line drift. The data for first 200 min for all the three runs showed a drift of less than -1 Hz. The adsorption experiments were planned to be carried out for 200 mins and modeled to obtain the equilibrium mass as described in more detail in chapter 5.

Appendix B

XPS Peak fit Parameters for Cold Lake asphaltene adsorption on Gold Surface

The peak fit parameters therefore binding energy and full width at half maximum (FWHM) for adsorbed Cold Lake asphaltene at varying concentration on gold surface is presented below:

Table B.1 Peak fitted parameters of C 1s for blank, adsorbed and bulk Cold Lake asphaltene on gold

Concentration (PPM)	Binding Energy (eV)	FWHM (eV)
50	284.8 286.3	1.7 2.2
100	284.8 286.4	1.6 2.4
250	284.8 286.0	1.6 2.3
500	284.8 286.5	1.7 2.5
1000	284.8 286.5	1.7 2.2
1500	284.8 286.3	1.6 2.2
Bulk	284.8 286.4	1.7 1.9
Blank	284.8 286.5	1.7 2.66

Table B.2 Peak fitted parameters of O 1s for blank, adsorbed and bulk Cold Lake asphaltene on gold

Concentration (PPM)	Binding Energy (eV)	FWHM (eV)
50	531.5	1.5
	532.7	2.0
100	531.6	2.2
	533	2.7
250	531.6	1.9
	533.0	2.3
500	531.0	1.5
	532.9	2.4
1000	530.9	1.8
	532.8	2.2
1500	531.6	1.6
	532.9	2.2
Bulk	531.3	1.9
	532.8	2.6
Blank	531.5	1.9
	532.9	2.1

Table B.3 Peak fitted parameters of S 2p for blank, adsorbed and bulk Cold Lake asphaltene on gold

Concentration (PPM)	Binding Energy (eV)	FWHM (eV)
50	161.8	2.0
	163.0	2.1
	164.0	1.8
	165.3	2.0
100	161.8	1.5
	163.0	0.9
	164.0	1.7
	165.2	1.8
250	161.8	1.3
	163.0	1.0
	164.0	1.3
	165.3	1.7
500	164.2	1.7
	165.4	1.8
1000	164.0	1.7
	165.2	1.9
1500	164.2	1.6
	165.4	1.5
Bulk	164.1	1.8
	164.2	1.2
Blank	161.2	1.4
	162.4	1.9

Table B.4 Peak fitted parameters of N 1s for bulk asphaltene

Concentration (PPM)	Binding Energy (eV)	FWHM (eV)
Bulk	398.7	1.47
	400.2	1.83

Appendix C

Kinetic data for MD Asphaltene Adsorption on Gold Surface

In the following section the kinetic data for MD asphaltene adsorption on gold surface is presented below. The equation 4.1 was used to extract the equilibrium mass from the kinetic data the quality of fit is also presented.

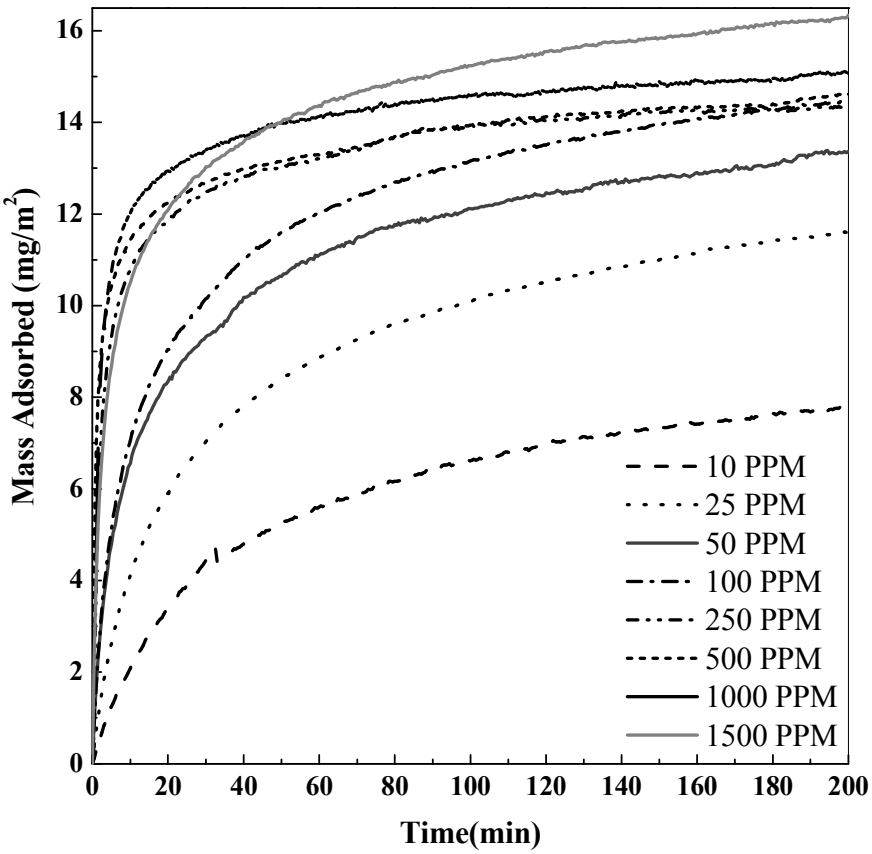

Figure C. 1 Kinetic data of MD asphaltene adsorption on Gold surface at 25^{o}C

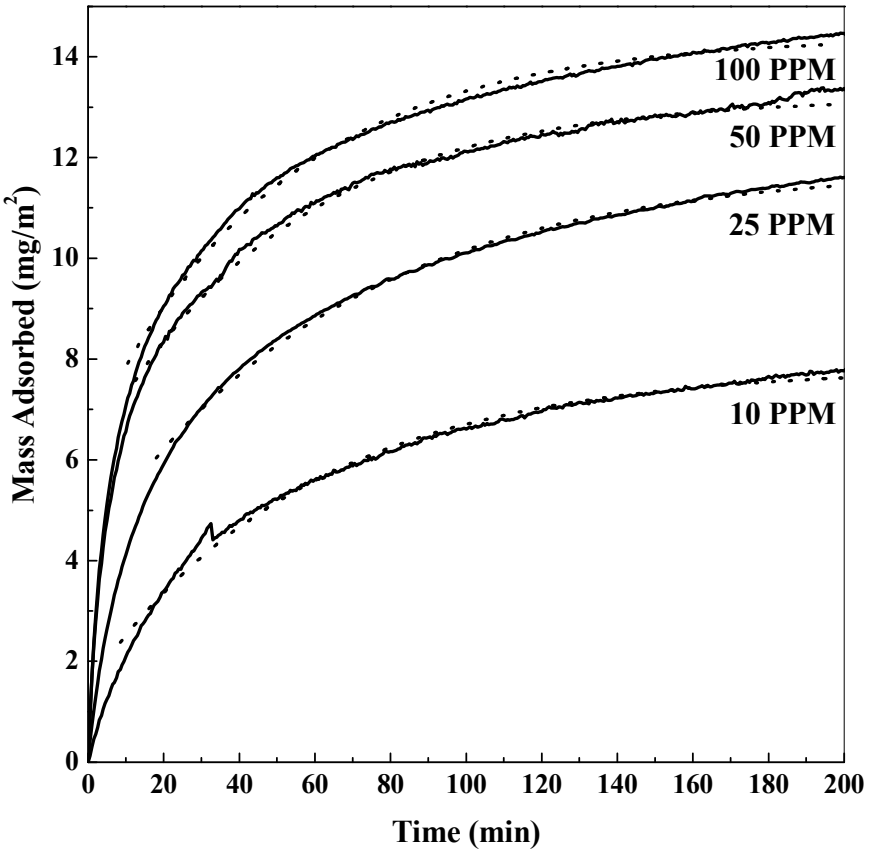

Figure C.2 Kinetic data of MD asphaltene adsorption fitted to equation 4.1, the dotted line shows the fit

Table C. 1 MD asphaltene adsorption data on gold surface

Concentration (PPM)	m_{eq} (mg/m^2)	m_o (mg/m^2)	τ (min)
10	7.82 ± 0.02	1.51 ± 0.03	57.8 ± 0.76
25	11.82 ± 0.01	4.17 ± 0.03	65.1 ± 0.68
50	13.20 ± 0.01	6.03 ± 0.04	50.7 ± 0.61
100	14.40 ± 0.02	6.38 ± 0.05	50.0 ± 0.60
250	14.31 ± 0.01	10.10 ± 0.03	41.7 ± 0.58
500	14.49 ± 0.01	10.94 ± 0.03	51.3 ± 0.94
1000	14.84 ± 0.01	10.78 ± 0.05	31.8 ± 0.67
1500	16.01 ± 0.02	8.96 ± 0.06	39.8 ± 0.71

Appendix D

XPS spectra for MD asphaltene and peak fit parameters

The XPS spectra acquired over Carbon 1s, Oxygen 1s, Sulfur 2p and Nitrogen 1s elements is presented below. The peak fit parameters is also tabulated.

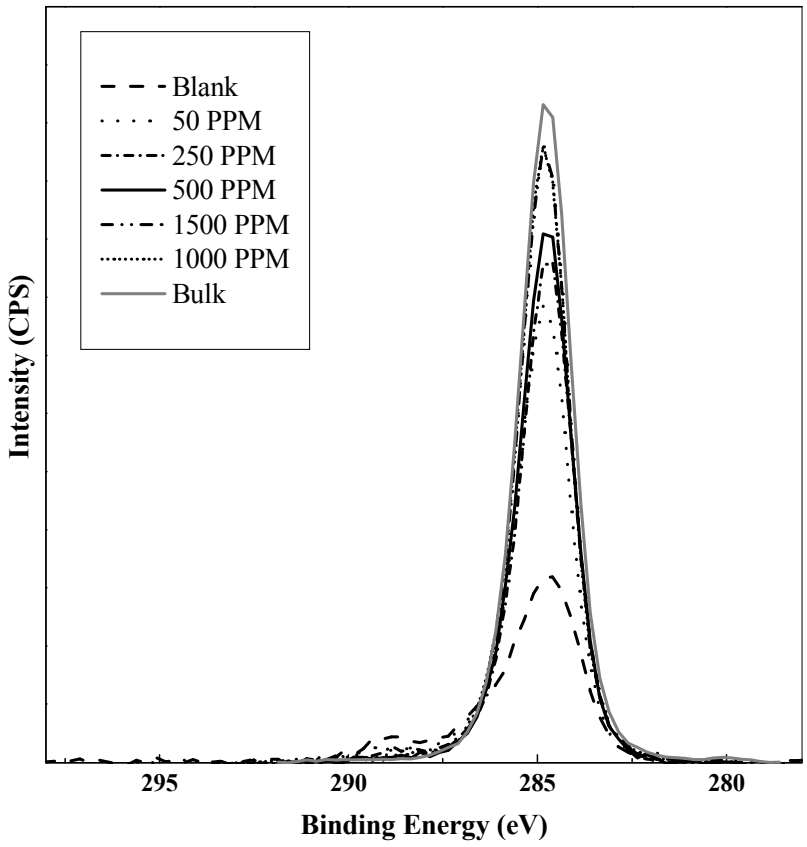

Figure D.1 C 1s XPS spectra for blank, adsorbed and bulk MD asphaltene on gold surface

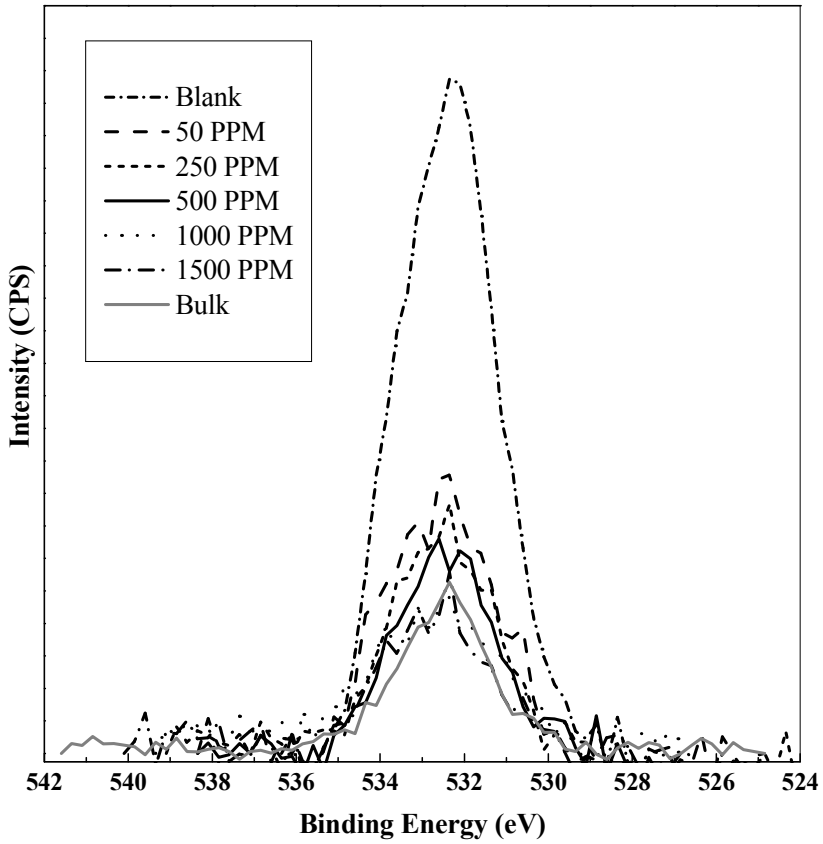

Figure D.2 O 1s XPS spectra for blank, adsorbed and bulk MD asphaltene on gold surface

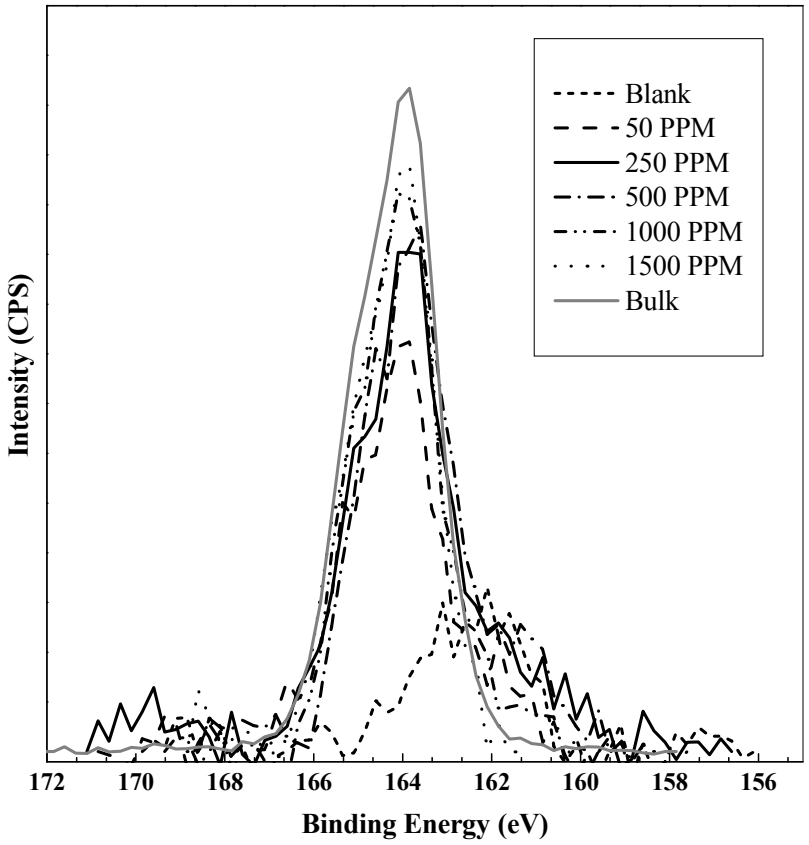

Figure D.3 S 2p XPS spectra for blank, adsorbed and bulk MD asphaltene on gold surface

Table D.1 Peak fitted parameters of C 1s for blank, adsorbed and bulk MD asphaltene on gold surface

Concentration PPM	BE eV	FWHM eV
50	284.8	1.56
	287.3	4.17
100	284.8	1.68
	286.4	2.57
250	284.8	1.55
	286.7	3.9
500	284.8	1.62
	286.2	1.99
1000	284.8	1.51
	286.4	2.24
1500	284.8	1.57
	286.5	2.01
Bulk	284.8	1.59
Blank	284.8	1.69
	286.5	2.71

Table D.2 Peak fitted parameters of O 1s for blank, adsorbed and bulk MD asphaltene on gold surface

Concentration PPM	BE eV	FWHM eV
50	531.7	2.15
	533.3	2.26
100	531.2	1.67
	532.5	2.03
250	531.6	1.72
	533	2.19
500	531.7	1.91
	532.8	2.38
1000	531.8	2.32
	533.3	2.61
1500	531.9	2.54
	533.2	2.45
Bulk	532.22	1.82
	533.3	1.96
Blank	531.5	1.90
	532.9	2.10

Table D. 3 Peak fitted parameters of S 2p for adsorbed asphaltene on gold

Concentration	BE (eV)	FWHM (eV)
50	162.1	1.51
	163.3	0.98
	164.0	1.36
	165.2	1.35
100	161.2	1.49
	162.4	0.82
	163.7	1.52
	164.9	1.46
250	161.4	2.22
	162.6	1.89
	163.8	1.48
	165.0	1.52
500	161.4	1.48
	162.6	0.83
	163.7	1.37
	164.9	1.28
1000	161.4	1.20
	162.6	0.72
	163.8	1.33
	165.0	1.21
1500	163.8	1.51
	165.0	1.45
Bulk	163.8	1.50
	165.0	1.44

Appendix E

Peak fit Parameters for Heavy Oil 2 Asphaltene Adsorbed on Gold Surface

The following table presents peak fit parameters for Heavy oil 2 asphaltene and its sub-fraction adsorbed on gold surface.

Table E. 1 Peak fit parameters for adsorbed heavy oil asphaltene and its sub-fraction at 500 ppm on gold surface

Asphaltene Type	Element	BE eV	FWHM eV
HO2-C_7	Carbon 1s	284.8	1.55
HO2-F_3		284.9	1.84
		286.2	1.91
HO2-F_7		284.9	1.56
		286.4	3.03
HO2-C_7	Oxygen 1s	532.9	2.77
HO2-F_3		532.0	2.11
		533.5	2.43
HO2-F_7		531.9	1.97
		533.1	2.38
HO2-C_7	Sulfur 2p	164.2	1.46
		165.4	1.33
HO2-F_3		164.2	1.67
		165.4	1.59
HO2-F_7		162.0	1.71
		163.2	1.14
		164.3	1.39
		165.5	1.52

Appendix F

Peak fit parameters for Cold Lake asphaltene on Stainless Steel surface

The peak fit parameters for Cold Lake asphaltene adsorption on Stainless Steel surface is tabulated below:

Table F. 1 Peak fit parameters of Carbon 1s for adsorbed Cold Lake asphaltene, bulk and blank samples on stainless steel surface

Concentration (PPM)	BE (eV)	FWHM (eV)
50	284.8	1.63
	286.1	2.93
100	284.8	1.59
	286.1	2.83
250	284.8	1.73
	286.6	2.78
500	284.8	1.68
	286.1	4.5
1000	284.8	1.61
	286.0	2.34
1500	284.8	1.63
	186.2	2.12
Bulk	284.8	1.67
	286.4	1.9
Blank	284.8	1.83
	287.7	3.53

Table F. 2 Peak fit parameters of Oxygen 1s for adsorbed Cold Lake asphaltene, bulk and blank samples on stainless steel surface

Concentration PPM	BE eV	FWHM eV
50	530.0	1.27
	531.6	3.00
100	530.4	1.90
	532.3	2.10
250	530.2	1.57
	531.7	3.00
500	530.0	2.05
	532.0	2.66
1000	530.2	1.79
	531.7	2.85
1500	530.2	2.09
	532.0	2.55
Bulk	531.3	2.73
	532.8	2.53
Blank	530.0	1.45
	530.9	2.73

Table F. 3Peak fit parameters of Sulfur 2p for adsorbed Cold Lake asphaltene, bulk and blank samples on stainless steel surface

Concentration (ppm)	BE (eV)	FWHM
50	164.3	1.72
	165.5	1.55
	167.0	3.26
	168.2	3.31
100	164.3	1.55
	165.5	1.51
	166.2	1.14
	167.4	0.94
250	164.2	1.72
	165.4	1.68
	167.8	2.00
	169	1.60
500	164.1	1.93
	165.3	1.90
	167.1	5.13
	168.3	4.32
1000	164.2	1.56
	165.4	1.45
	166.4	0.95
	167.6	1.13
1500	164.0	1.58
	165.2	1.54
	167.1	3.24
	168.3	3.63
Bulk	164.1	1.77
	164.2	1.19
Blank	168.1	1.77
	169.3	1.85